Czech University of Life Sciences Prague

Faculty of Environmental Sciences

Department of Water Resources and Environmental Modeling

Analysis of rainwater flow in snowpack

Diploma Thesis

Supervisor: Ing. Roman Juras, Ph.D.

Author: Bc. Veronika Čejková

CZECH UNIVERSITY OF LIFE SCIENCES PRAGUE

Faculty of Environmental Sciences

DIPLOMA THESIS ASSIGNMENT

Bc. Veronika Čejková

Environmental Modelling

Thesis title

Analysis of rainwater flow in snowpack

Objectives of thesis

The main goal of this work is to test snow transfer functions to analyse snowpack outflow data from the sprinkling experiments.
The student will focus on:
1. Creation of the dataset to be run in DRUtES
2. Sensitivity analysis of parameters for water flow in snow based on the literature review.
3. Modeling of outflow from different snowpack types and the effects of data uncertainty

Methodology

At first, the student will do a literature review to obtain suitable parameterisations for the retention curve and hydraulic conductivity curve in snow. Next, she will simulate snowpack outflow and test the sensitivity of the input data, especially snow grain size and snow density, on the parameterisation and resulting outflow and compare the results to measured data from sprinkling experiments.

The proposed extent of the thesis

min. 50 stran

Keywords

Rain-on-snow, snowmelt, experiments, water flow, modelling, DRUtES

Recommended information sources

D'Amboise, Christopher J. L., Karsten Müller, Laurent Oxarango, Samuel Morin, and Thomas V. Schuler. 2017. "Implementation of a Physically Based Water Percolation Routine in the Crocus/SURFEX (V7.3) Snowpack Model." Geoscientific Model Development 10 (9):3547–66.

Hirashima, Hiroyuki, Satoru Yamaguchi, and Takafumi Katsushima. 2014. "A Multi-Dimensional Water Transport Model to Reproduce Preferential Flow in the Snowpack." Cold Regions Science and Technology 108:80–90.

Juras, Roman, Sebastian Würzer, Jirka Pavlásek, Tomáš Vitvar, and Tobias Jonas. 2017. "Rainwater Propagation through Snowpack during Rain-on-Snow Sprinkling Experiments under Different Snow Conditions." Hydrology and Earth System Sciences 21 (9):4973–87.

SINGH, V P. – SINGH, P. *Snow and glacier hydrology.* Dortrecht: Kluwer Academic Publishers, 2001. ISBN 0-7923-6767-7.

Wever, N., C. Fierz, C. Mitterer, H. Hirashima, and M. Lehning. 2014. "Solving Richards Equation for Snow Improves Snowpack Meltwater Runoff Estimations in Detailed Multi-Layer Snowpack Model." The Cryosphere 8 (1):257–74.

Expected date of thesis defence

2018/19 SS – FES

The Diploma Thesis Supervisor

Ing. Roman Juras, Ph.D.

Supervising department

Katedra vodního hospodářství a environmentálního modelování

Advisor of thesis

Johanna Ruth Blöcher

Electronic approval: 29. 1. 2018

doc. Ing. Martin Hanel, Ph.D.

Vedoucí katedry

Electronic approval: 30. 1. 2018

prof. RNDr. Vladimír Bejček, CSc.

Děkan

Prague on 18. 04. 2019

Declaration

I declare that I have worked on my master thesis titled "Analysis of rainwater flow in snowpack" by myself and I have used only the sources mentioned at the end of the thesis. As the author of the master thesis, I declare that the thesis does not break copyrights of any their person.

In Prague on 16. 4. 2019 _____

Acknowledgement

I would like to thank Ing. Roman Juras, Ph.D. and Ing. Johanna Ruth Blöcher, for their advice and support during my work on this thesis.

Abstrakt

Diplomová práce se zabývá modelováním proudění vody sněhovou pokrývkou. Cílem je zlepšit odhad odtoku v důsledku dešťových událostí (ROS). Práce využívá modely pro popis proudění vody půdou a porovnává výsledky parametrů, které byly navrženy pro sněhovou pokrývku s měřenými daty odtoků při umělém zadešťování pokrývky. Jako model proudění je použita Richardsova rovnice, a pro určení hydraulických vlastností van Genuchtenův model, jehož parametrizace je testována. Simulace byly počítány pomocí software DRUtES ©. Práce následně provádí analýzu citlivosti parametrizace a porovnává reakce výstupů na změny ve vstupních hodnotách.

Klíčová slova: Sníh, ROS events, van Genuchtenův model, Richardsova rovnice, DRUtES.

Abstract

The thesis is focused on modelling of liquid water flow in the snow. The aim is to improve outflow prediction that arises due to rain-on-snow events. (ROS). The thesis employs a model for soil water flow and compares parameters' performance, that was created for snow description with measured data from artificial sprinkling experiment conducted on real snowpack. As flow model the Richards equation was used and for determination of hydraulic properties the van Genuchten model was used whose parametrization were tested. Simulations were computed with the software DRUtES ©. Then, a sensitivity analysis was conducted to compare the reaction of results on the change of input values.

Keywords: Snow, ROS events, van Genuchten model, Richards equation, DRUtES

Table of content

1 Introduction

Rain on snow (ROS) events can cause floods that may result in material or life losses. Singh et al., (1997) stated that ROS events have a bigger potential to cause floods than regular snowmelt in spring season. Presence of liquid water in snowpack during and after ROS also has an impact on the mechanical strength of the whole snow cover and increases the risk of wet avalanches and slush flows (Jaedicke et al., 2008; Smart et al., 2000). In order to prevent tragic consequences, it is needed to better understand processes that may cause such disasters.

This thesis is focused on a specific approach of modelling outflow from snowpack. It is assumed that liquid water flow through snowpack can be most precisely described by the Richards equation (Wever et al., 2014), which describes unsaturated water flow in soils so for purpose of this thesis the Richards equation was chosen as an appropriate flow model. To determine the hydraulic properties of the porous medium van Genuchten model was used with empirical parametrization that makes it suitable for snow. Parametrization using grain size and density of snowpack that can be easily obtained from field measurement. This approach is a major simplification and could cause uncertainties.

The goal of this thesis is to examine the performance and limits of validity of suggested parametrization on different natural snowpacks under artificial ROS event represented by sprinkling experiments. Software DRUtES was used for modeling, which is a powerful tool for solving unsaturated flow with the Richards equation. The data for modeling were used from sprinkling experiments published by Juras et al., (2017). The dataset contains information about snow profile, inflow and outflow logs from 10 experiments, nevertheless only 3 experiments were modeled in this thesis.

Snow is a complex medium with still ongoing processes that have an influence on hydraulic properties and because of this complexity, simplification is used. More variables raise not only better precision, but even higher uncertainties. For the purpose of this thesis was used 1D model that simplifies outflow from snowpack in order to reduce computational complexity. Also, it is not possible to obtain spatial differentiation of snow hydraulic properties from the measured data. On the other hand, it needs to be considered that simplification neglected some processes that have an influence on measured data, but

the model does not account for them. This thesis includes a description of these processes to be able to explain the possible deviation of model output from measured data. These processes are described in the literature review.

2 Goals

The main goal of this thesis is to answer the following questions:

1. Can we model snowpack outflow based on easily established properties (local water content, grain size, density) of snowpack?
2. Is the parametrization of van Genuchten model working on real layered snowpack?
3. How the measurement uncertainties influence the outflow modeling?
4. There is a proven contribution of meltwater and liquid water content on the total outflow. Can be this phenomenon neglected by simple model or can it cause an inaccuracy?

3 List of abbreviations and symbols

SWE	Snow water equivalent [L^3]
LWC	Liquid water content [%]
PDE	Partial derivative equation
RE	Richards equation
SSA	Specific surface area [L^2M^{-1}]
NS	Nash – Sutcliff coefficient of efficiency
RMSE	Root mean squared error
MSE	Mean squared error
ρ	Bulk density [ML^{-3}]
k	Intrinsic permeability [L^2]
ϕ	Porosity [-]
θ	Volumetric water content [-]
θ_s	Saturated water content [-]
θ_r	Residual water content [-]
θ_e	Effective water content [-]
h	Pressure head [L]
K_s	Saturated hydraulic conductivity [LT^{-1}]
K_r	Relative hydraulic conductivity [LT^{-1}]
d	Grain diameter [L]

4 Literature review

4.1 Snowpack characteristic

Snowpack is a complex medium. Its properties are changing in time by the influence of temperature, pressure, wind, and precipitation during a season (De Michele et al., 2013). This process is called snow metamorphism. The snowpack can be uniform or consists of different layers that originate from different snow events. Layers have different textural therefore hydraulic properties and can retain a different volume of liquid water (Singh et al., 1997). Spatial evolving of snow cover depend on topography, vegetation, and meteorology (Liston and Elder, 2006). To estimate outflow from the snowpack is needed to know its characteristics at least saturated, residual and initial liquid water content (LWC), grain size and bulk density for every layer. The major issue with snow is that the changes must be tracked and included to the model for long-term forecasting and hindcasting. Unlike soil, in snowpack densification and textural changes caused by grain growth due to temperature changes or dissolution of grain clusters due to melting can be observed. Homogenization of snowpack properties within layers is called ripening. Ripe snowpack is the term for snowpack that is isothermal at 0°C and liquid water can be observed within entire profile. The process of ripening starts with air temperatures above the freezing point. Snow-pack is getting warmer until it reaches the melting point (Singh, 2011). This process is connected to the creation of the preferential flow paths network. The snowpack can contain ice layers and present liquid water is mostly retained by capillary forces (Kattelmann and Dozier, 1999).

Physicals properties that are commonly measured for further research are snow depth (SD), bulk density (ρ), snow water equivalent (SWE), specific surface area (SSA), liquid water content (LWC), porosity (ϕ), temperature (T) and thermal conductivity (λ) (Kinar and Pomeroy, 2015).

Snowpack consists of ice particles, liquid water (with 0°C temperatures), and air. The density of snowpack is determined as the ratio of the weight of snow to its volume and

grows linearly with time (Kattelmann and Dozier, 1999). Snow dry density can be considered as bulk dry density due to small values of liquid water content in the snow. LWC is usually 0% - 10% of snow mass (Coléou and Lesaffre, 1998). LWC is free liquid water that occupies pores in the snow and porosity is the ratio of pore volume to total volume. It can be determined from the equation:

$$\phi = 1 - \frac{\rho_s}{\rho_i}, \quad (1)$$

ρ_s is the dry density of snow and ρ_i is the density of ice = 917 kg.m^{-3}. This relation shows the dependency of porosity on the density of snow. Liquid water is linearly dependent on the ratio of pore volume to ice volume (Coléou and Lesaffre, 1998).

SWE is the function of density and snow depth. It is computed as follows:

$$SWE = h\frac{\rho_b}{\rho_w}, \quad (2)$$

where h [L]is depth, ρ_b [ML^{-3}]is the bulk density of and ρ_w [ML^{-3}]is the density of water close to 0°C. This property of snow is important to estimate water resources in snowpack because SWE essentially means the depth of water resulting from melting the entire snowpack (Sturm et al., 2010).

Permeability depends on grain size and pore size. The same approach is applied to snow, but snow grains are not stable. Their size and shape are constantly influenced by metamorphism driven by temperature (melting and refreezing), LWC, wind, precipitation, and settling of the snowpack. Generally, snow grains metamorphism is characterized for wet snow (grain clusters, melt-freeze particles, and slush) and dry snow (faceted or rounded) (Colbeck, 1986). Metamorphism can be simplified to processes in wet and dry snow. Dry snow particles growth rate decreases with increasing snow density but increases with a temperature gradient (Colbeck, 1983). Temperature gradient in snow depends on air temperature and ground temperature. Snowpack works as insulation layer, so the temperature of the snowpack bottom is close to 0 °C, because the soil underneath is often unfrozen. In dry snowpack with temperatures just below melting point are grains rounded due to vapor sublimation on the surface. Water molecules in vapor settle on

vacant sites of grains. Small temperature gradient causes small and slow growth rates of grains that lead to sintering of grains. Particles are well bonded and form stable snowpack. With large temperature gradient (10 - 20 °C.m^{-1}) come large growth and rounded particles recrystallize in faceted forms because vapor transfer is quicker than within snowpack with the smaller temperature gradient. With large temperature gradient grains grow into faceted forms and bonds between particles weaken. Metamorphism of particles within wet snow highly depends on water content. Low water contents (0 – 3 %) cause grain clusters with strong bonds because of lowering surface energy on the liquid to solid, vapor to solid and liquid to vapor interfaces. Clusters of grains have weak bonds between each other and snowpack is less stable. There is no temperature gradient in wet snowpack along profile but between particles. Smaller grains have a lower temperature that causes heat flow between bigger and smaller grains. Heat flow cause melting of smaller grains that are later consumed by bigger grains. Grain growth is slow down by grow process. With large water content (around 7%) bonds between and within the grain clusters decrease drastically and compact snow pack turns into slush (Colbeck, 1983).

Grain size is a very important parameter for computing intrinsic permeability. Simple models uses diameter or radius, but if permeability is measured it is proven that varies with size and shape of grains and pore size (Colbeck, 1979). Examples of grain types are depicted in Fig. 1.

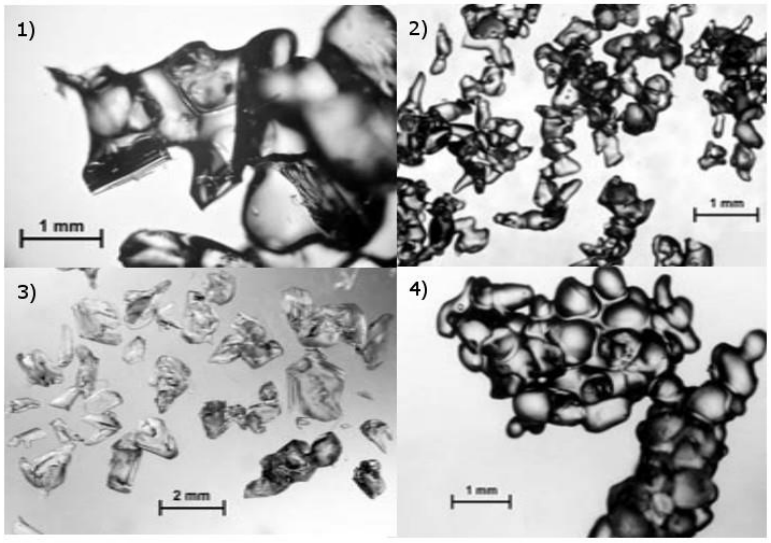

Fig. 1 – Photos of grain types taken from Fierz et al., (2009). Pic. 1) melt freeze crust, 2) rounded grains, 3) faceted particles, 4) clustered rounded grains.

4.2 Snow profile analysis

For measuring snowpack properties that are used as input for modelling is used snow profile analysis. First, a hole has to be dug in the snow that reaches from top to ground. Than the excavated snow wall is flattened. The profile is measured by a ruler that is stabilized at one place and is used for measuring for whole analysis. Temperature is needs to be measured every 5 cm to obtain a temperature gradient along profile. On cut profile can be seen the layering. After the layers are determined profile is examined in more detail usually every 5 or 10 cm. Grain size is measured on the special crystal card with a millimeter scale. Grains are examined under magnificent glass. For snow grain types is commonly used international classification for seasonal snow by Fierz et al., (2009) that includes symbols for grain types that will be used later in this thesis.

Tab. 1 - Snow classification according to Fierz et al., (2009)

Class	Symbol
Precipitation particles	+
Machine made snow	◎
Decomposing and fragmented precipitation particles	/
Rounded grains	●
Faceted crystals	□
Dept hoar	∧
Surface hoar	∨
Melt forms	○
Ice Formations	■

Measuring crystal card has to be cold so it does not cause melt of grains. Grains are usually in clusters and it is hard to estimate size and type. For this task is needed person with the trained eye but still, the determination of grain types can be subjective.

Next task is LWC that is measured by Denoth meter that measured the dielectric constant of snow at radio frequencies. (Denoth, 1994) This device can measure LWC and density. The traditional way of measuring density is to sample undisturbed snow into metal cylinder or block that is without top and bottom and very carefully cut redundant snow on both sides. Snow should fill the whole space of measuring tool and should not be denser due to manipulation. Than is weighted and the weight of measuring tool is subtracted. This technique is hard to perform on coarse or ice layers. Due to the volume of measuring

tool is density averaged along bigger ranges of snow depth and thin layers (e.g. ice layers) cannot be measured. The last measurement is the value of SWE. For this purpose, is used a tube with a centimeter scale that is perpendicularly put into the snow. After assuring that tube reaches ground snow height is measured and snow inside tube is densified. The tube is lifted from snowpack and weighted with the whole amount of dense snow.

4.3 Water propagation through the snowpack

Rainwater could initiate fast outflow from snowpack (Kattelmann et al., 1985). There are two types of flow in snowpack; preferential and matrix flow. Matrix flow appears at top homogenous layers of snowpack and is spatially evenly distributed. Little macroscopic heterogeneities and lower water content with small hydraulic gradient cause distributed flow that behaves like the classic unsaturated flow that can be described by Darcy – Buckingham law:

$$q_z = -K(\theta)\frac{\partial h}{\partial z}, \tag{3}$$

where q_z [LT^{-1}] is a flux, $K(\theta)$ [LT^{-1}] is hydraulic conductivity as a function of liquid water content, h [L] is pressure head and z [L] is the vertical coordinate.

Preferential flow tends to differ spatially and arise in heterogeneous layers. Paths arise on microstructure discrepancies and create wetted zones (Schneebeli, 1995; Waldner et al., 2004). Water flow through preferential paths is usually faster than matrix flow (Kattelmann et al., 1985), but it is often slowed down by capillary barriers on snow layer interfaces. During ROS events is the outflow through preferential paths much faster than outflow from regular melting (Singh et al., 1997).

Unsaturated flow in a porous medium is driven by capillary forces and gravity and its velocity depend on hydraulic properties of the layer. Snowpack layering when finer grains occur over coarser grains can cause the capillary barrier (Waldner et al., 2004). These barriers caused ponding of water. Avanzi et al., (2016) states that LWC on these barriers raises from regular 10 % up to 33 – 36 %. Higher water content changes the hydraulic properties of the layer above the capillary barrier. On capillary barriers, water changes

direction and distribute horizontally along the barrier (Avanzi et al., 2016). This behavior is described as lateral flow. Direction change of flow can be also caused by structural discrepancies or even by ice lenses that occurs in the snowpack (Colbeck, 1972). Under freezing condition ponding water freeze and create ice layer with lower permeability than regular layer (Wever et al., 2016). Capillary barriers, ice layers, ice lens, and discrepancies cause time lag in the outflow. Liquid water flows through ways with the smallest resistance, therefore, follow the established pattern of preferential flow paths Since the flow path system is developed in the snowpack the outflow is much faster (Würzer et al., 2016). The velocity of the wetting front of percolating water through preferential path is close to the velocity of saturated gravity flow (Waldner et al., 2004).

4.4 Flow model

Flow model is represented by Richards equation (RE) in this thesis. RE is used to describe gas and water movement in the porous medium where gas movement is neglected due to large differences in mobility between gas and water (Farthing and Ogden, 2017). This equation is derived from the Darcy Buckingham law and the continuity equation (Richards, 1931). The Darcy-Buckingham law describes water flow for unsaturated conditions and depends on unsaturated hydraulic conductivity and the volumetric water content of the medium.

RE can be expressed as pressure head *(h)* form, water content *(θ)* form or mixed form a combination of both. (Celia et al., 1990). In this thesis were used *h* based form:

$$C(h)\frac{\partial h}{\partial t} - \nabla \cdot K(h)\nabla h - \frac{\partial K}{\partial z} = 0\,, \qquad (4)$$

where *z* is positive downward coordinate [L], *t* is the time [T], *h* is pressure head [L], *K(h)* is unsaturated hydraulic conductivity [LT^{-1}] and $C(h) = d\theta/dh$ is specific moisture capacity function [L^{-1}].

RE has no analytical solution for the whole porous medium. For numerical solution can be used finite element, finite volume or finite difference method. Software DRUtES (Kuráž et al., n.d.) is employed in this thesis. The software uses the finite element method that is based on the approximation of results between nods of mesh that covers the whole profile. It is important to choose the right density of mesh. Computational time and accuracy of results has to be balanced; the denser the mesh means the longer computational time is needed. The mesh does not need to be uniform, it can be variable. This solution is better for media with discrepancies. Mesh can be denser and more precise around irregular areas. Another type of discretization that can be used is adaptive. Mesh become denser when a number of iterations rise to fulfill precision criterion (Ho-Le, 1988). RE solution includes results not just in spatial terms but even in time. Time steps have the same importance for accuracy as spatial mesh and it can be defined by the same discretization approaches. Loose time steps can cause overshooting of best result (Ginting, 2012).

To start RE calculation boundary and initial conditions needs to be established. Boundary condition describes a known state on edges of the medium. These conditions can be stationary (Dirichlet boundary condition), non-stationary (Neumann condition) or a combination of both. The stationary condition is e.g. free drainage which means stable pressure head that represents free water level above medium. Non-stationary condition means flux that can be e.g. prescribed by precipitation data. Commonly is used Neumann condition with zero flux (Arendt and Warma, 2003). Initial state describing hydraulic properties of medium or every layer in medium if there are any differences.

4.5 Hydraulic properties

This thesis uses the van Genuchten model for determination of hydraulic properties of the porous medium. This model introduces an analytical expression of relative hydraulic conductivity K_r [LT^{-1}], based on Mualem´s theory (Mualem, 1976) of deriving K_r from the water retention curve (WRC). WRC shows the relationship between water content and pressure head of unsaturated porous medium that is derived from the capillary suction

model. The porous medium is represented by a bundle of capillary tubes that are filled according to the water content in the system. Pressure head in tubes is changing due to the different diameter of tubes, therefore, the size of capillary suction. With pressure head on the y-axis and given water content can be constructed a curve that describes the distribution of pore size in the medium. Cumulative distribution range on the interval (0,1). van Genuchten, (1980) introduced equivalent water content θ_e [-] which fulfill this condition:

$$\theta_e = \frac{\theta - \theta r}{\theta s - \theta r}, \tag{5}$$

where θ_r [-] is the residual water content, θ is the water content [-], θ_e [-] is the equivalent water content and θ_s [-] is the saturated water content. Both values are limits for water content on the water retention curve. To link equivalent water content to pressure head van Genuchten (1980) introduced function:

$$\theta_e = \frac{1}{(1 + (\alpha|h|)^n)^m}, \tag{6}$$

α [L^{-1}], n [-] and m [-] are parameters that have an influence on shape and slope of water retention curve. van Genuchten (1980) expressed unsaturated hydraulic conductivity K_r (based on Mualem´s model (Mualem, 1976)), as a function of θ_e:

$$K_r(\theta_e) = K_s\, \theta^{\frac{1}{2}}[1 - (1 - \theta^{\frac{1}{m}})^m]^2 \tag{7}$$

$$(0 < m < 1), \left(m = 1 - \frac{1}{n}\right). \tag{8}$$

K_s [LT^{-1}] is saturated hydraulic conductivity which is a constant value. Parameter α influences shape and parameter n influence the slope of the WRC. Bigger values of α result in more curvy shapes whereas bigger n means the smaller slope of the curve. Characteristics of soil can be assumed from WRC. Bigger n (smaller slope on water retention curve smaller slope on cumulative distribution of grain size) can tell that soil has more distributed grain sizes in the bigger range of pore sizes, therefore, it could be assumed that water does not discharge so quickly, and it is easier to reach saturation. S-shape of curve influenced by α that shows a big drop on start tells that grain size is uniform

grains are big and water flows more easily through soil. WRC of three materials can be seen in Fig 2. Sand has coarse and grain, therefore smaller retention ability in comparison to clay that is known for his big retention ability due to high pore distribution.

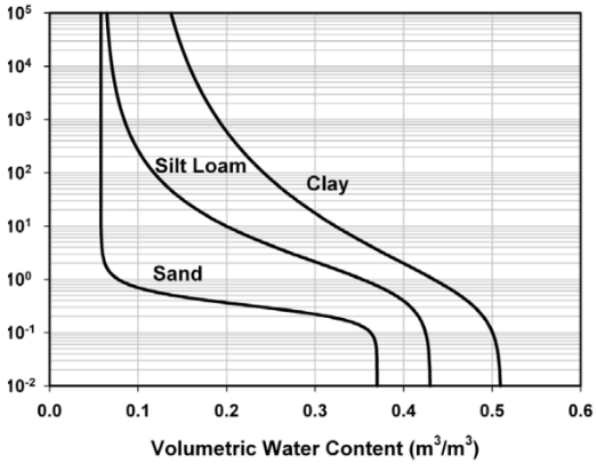

Fig 2 – Example of WRC of three soils with different retention ability taken from (Tessin, 2016)

For plotting, the probability density distribution of pore size can be used the derivative of WRC. From peak and shape of WRC derivative can be seen the ability of matrix to retain water based on the idea that more uniform and bigger pores retain less water than smaller and well-distributed pores. Saturated and residual water content are limits of WRC, so curve remain in the same shape but can be lengthened or shorten. If residual water content raises it means that the smallest pores are filled with water and fewer pores participate in water transport. Retention ability is not smaller, but pores distribution is restricted between θ_r and θ_s.

Cumulative frequencies of pore distribution can be obtained from van Genuchten θ_e [-] and height of meniscus h_c in a capillary tube with a given radius that represent pores of the same radius.

$$h_C = \frac{2\sigma \cos\gamma}{\rho_w g r}, \tag{9}$$

where r [L] is radius of capillary tube, h_c [L] is height of meniscus, ρ_w is density of water near 0 °C that is 1000 kg.m^{-3}, σ is liquid-air surface tension that is 0.0072 N.m^{-1} for clear water and $cos\ \gamma$ is a contact angle that is neglected.

4.6 Parametrization of van Genuchten model

This chapter introduces parameters that were used for modelling in this thesis. Parameters conducted by Calonne et al., (2012), Hirashima et al., (2010) and Yamaguchi et al., (2012, 2010) needs only one or two information about the snowpack (grain size or density and grain size). This approach is a major simplification of snowpack properties, basically, it means that pore size distribution can be determined from average grain size or average grain size and density. Calonne et al., (2012), Hirashima et al., (2010) and Yamaguchi et al., (2012, 2010) have developed equations to determine these parameters under certain conditions so it can be determined limits of their empirical approach based on the comparison of measured outflow data with results of the simple model using described parametrization.

Yamaguchi et al., (2010) express the relationship between parameters α, n, and grain size. The experiment shows strong dependency α and n on grain size. Air entry suction decreases with increasing grain size it means that α increases with increasing grain size whereas n decreases with increasing grain size. Based on experiment Yamaguchi et al., (2010) introduced empirical equations for computing α and n where grain diameter d mm is the only variable:

$$\alpha = 7.3d + 1.9 \quad (10)$$

$$n = -3.3d + 14.4. \quad (11)$$

According to Yamaguchi et al., (2010) equations for α and n reach values which are depicted in Fig. 3.

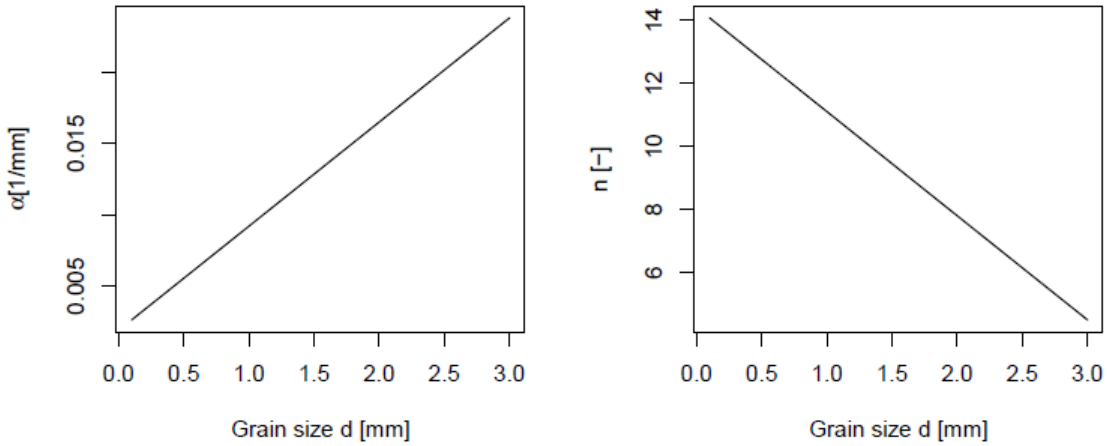

Fig. 3– Values of α and n related to grain size diameter d according to Yamaguchi et al. (2010) equation.

Experiment of Yamaguchi et al. (2010) was conducted on snow with densities closely around 550 kg.m^{-3} and differs only with grain size. Grain shape was not considered.

Tab. 2 – Densities and grain sizes of samples used in Yamaguchi et al. (2010) experiment to determine α and n values for the van Genuchten model.

Density [kg.m^{-3}]	553	549	548	545	550
Grain size [mm]	0.5	1.1	1.5	2.1	3.1

Hirashima et al., (2010) reviewed Yamaguchi et al., (2010) and find out that the equation for n have a limitation because n cannot acquire values below 1 in van Genuchten model and this equation is not valid for d larger than 4 mm. Hirashima et al., (2010) suggested a new equation for n:

$$n = 15.68 \exp(-0.46d) + 1. \qquad (12)$$

According to Hirashima et al., (2010) equation for α and n reach values which are depicted in Fig. 4.

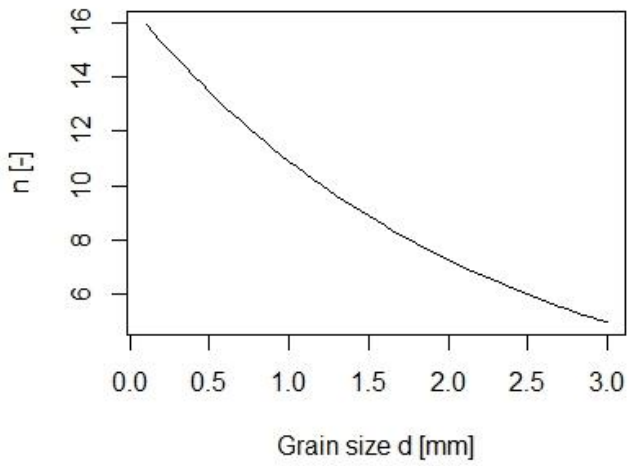

Fig. 4 -Values of *n* related to grain size diameter *d* according to Hirashima et al. (2010) equation.

Hirashima et al., (2010) used Yamaguchi et al., (2010) measured data but used different regression curve for a description of their behavior to expand limits of validity. Values of *n* for grains that differ in size from experiment samples are in both cases forecasted by regression curve. There is no physical evidence that both approaches (Eq. 10, 11, 12) can be used on snow with different densities or grain types.

Yamaguchi et al., (2012) suggested a new equation for α and *n* that includes density because he found out that α can be established from density and grain size. So he took a model of air entry suction where Coléou and Lesaffre, (1998) introduce parameter d/ρ and applied it to the equations for both parameters. Yamaguchi et al., (2012) concludes that van Genuchten parameters strongly depends on ρ/d and α decreases as quickly as ρ/d decreased whereas *n* increases with ρ/d. The equations for α and *n* are as follows where variables are grain size *d* [m] and density of snow ρ [kg.m^{-3}]

$$n = 1 + 2.7 * 10^{-3} \left(\frac{\rho}{d}\right)^{0.61} \quad (13)$$

$$\alpha = 4.4 * 10^{6} \left(\frac{\rho}{d}\right)^{-0.98}. \quad (14)$$

The relationship between of parameters α and ρ/d is depicted in Fig. 5.

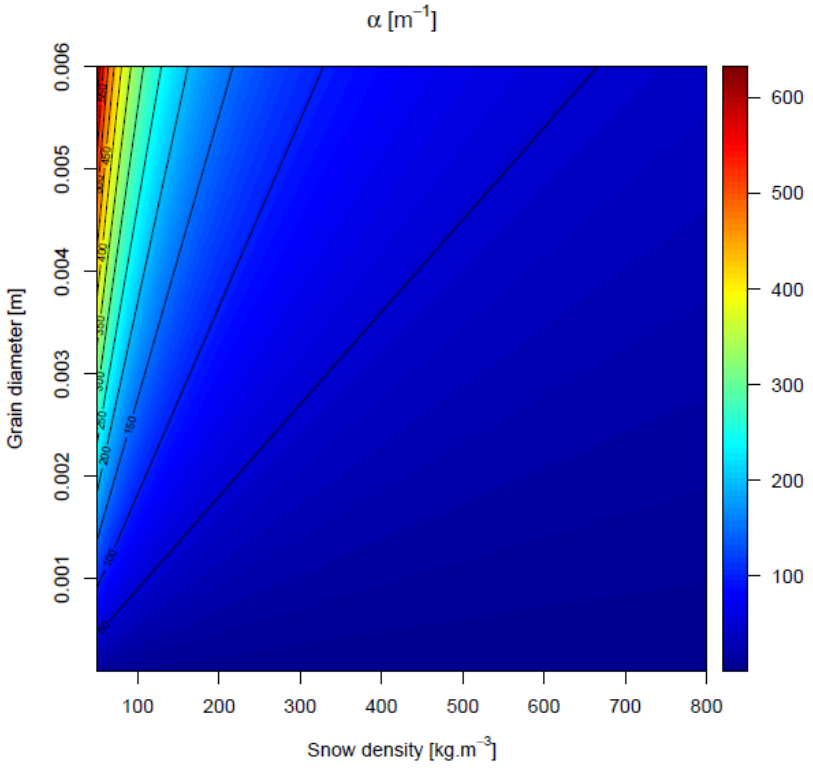

Fig. 5 – Values of α m^{-1} according to Yamaguchi et al. (2012) equation (12).

Lower densities and higher *d* result in higher *α* and therefore it shows the inability to retain water just like it can be expected. A laboratory experiment was in this case made on samples with variable densities and these samples were divided by 3 grain types; melted forms, refrozen melted forms and rounded forms. With this approach could Yamaguchi estimate if there is any significant influence of grain shape on values of *α*. Yamaguchi et. al, (2012) described that approach with grain size and density works for both cases; snow with different grain size and same density and snow with the same grain size but different density. Regression (Eq. 13, 14) was made on melted forms and refrozen melted forms that have a spherical shape. Uncertainty arises with different grain type. Rounded forms that create clusters of irregular shapes shows weaker relation between computed *α*, *n* and *ρ/d*. Yamaguchi et. al, (2012) states that Eq. 13 and 14 cannot be used for rounded grains. Basically, when Eq. (13, 14) are used, grain shape in whole profile is considered as melt forms or refrozen melt forms and grain size distribution is determined from 1 grain size and density of snow.

Tab. 3 - Grain size, densities and uniformity coefficient (UC) of samples that were used on the determination of equation for α and n by Yamaguchi et al., (2012).

Melt form			Refrozen melt form			Rounded grains		
Grain size [mm]	UC	Densities [kg.m^{-3}]	Grain size [mm]	UC	Densities [kg.m^{-3}]	Grain size [mm]	UC	Densities [kg.m^{-3}]
2.2 ± 0.7	1.7	431/ 488/ 631	0.5 ± 0.0	1.5	502/ 555	0.4 ± 0.1	1.8	381/ 480/ 508
1.1 ± 0.4	1.7	421/ 492/ 575	1.1 ± 0.3	1.7	523/ 548/ 594	0.9 ± 0.4	1.8	366/ 618
1.8 ± 0.6	1.8	361/ 621	1.5 ± 0.4	1.7	502/ 519/ 550	0.3 ± 0.1	1.8	363/ 431
2.0 ± 0.7	1.8	458/ 608	2.1 ± 0.4	1.4	500/ 547	0.3 ± 0.2	1.9	390/ 401
2.1 ± 0.7	1.8	396/ 508/ 377	3.1 ± 0.3	1.3	497/ 550	0.4 ± 0.1	1.9	309/ 363/ 483
1.6 ± 0.6	1.8	378/ 478/ 636	3.9 ± 0.5	1.1	456/ 476/ 502			
4.1 ± 1.6	1.8	370/ 551	4.6 ± 0.6	1.2	456/ 501			
2.2 ± 0.7	1.8	613/ 635	5.8 ± 0.9	1.2	500/ 424/ 456			
1.4 ± 0.5	1.8	399/ 462/ 489/ 590						
1.8 ± 0.6	1.8	461/ 463						
2.0 ± 0.7	2	565						
0.4 ± 0.1	2	388/ 509/607						

Uniformity coefficient (UC) is the ratio of grain diameter below which are 60 % of particles from the whole sample and grain diameter below which are 10 % of particles from the whole sample. This tool is used for determination of grain size distribution in soil. When the uniformity coefficient equals 1 all soil particles have the same size. Well distributed soil has a uniformity coefficient between 4 and 6. All the snow samples that were used in Yamaguchi et al., (2012) experiment have a quite small uniformity coefficient, therefore, the grain size is mostly uniform.

Saturated hydraulic conductivity K_s [LT^{-1}] is can be obtained from the equation:

$$K_s = \frac{k\rho g}{\mu}, \tag{15}$$

where k [L^2] is intrinsic permeability describing properties of the porous medium that is fully saturated, ρ [ML^{-3}] is the density of the material, g [LT^{-2}] is gravitational acceleration and μ [ML^{-1}T^{-1}] is dynamic viscosity of liquid water. Dynamic viscosity of liquid water at 0 °C is 1.787*10^{-3} N.s.m^{-2} Several approaches to estimate k of snow were developed.

Calonne et al., (2012) developed an equation based on computer tomography (CT) images. This equation gives the best results in comparison with older equation and is not affected by the anisotropy of intrinsic permeability (Calonne et al., 2012). Intrinsic permeability is computed according to Calonne as follows:

$$k = (3.0 \pm 0.3) r^2 \exp\left((-0.0130 \pm 0.0003)\rho_s\right), \qquad (16)$$

where r [L] is grain size radius and ρ_s [ML^{-3}] is snow density.

Intrinsic permeability is higher with lower temperatures when grains grow and create bigger clusters. This behavior can be observed on dry snowpack (Conway and Abrahamson, 1984). Lower permeability could be seen with a melting process that has a destructive influence on grain structures.

Samples for Calonne´s et al., (2012) determination of intrinsic permeability was collected for research of thermal conductivity of snow conducted by Calonne et al., (2011). In both papers is either not mentioned grain size nor densities of samples. Calonne et al., (2011) only state the range of densities that is between 103 – 544 kg.m^{-3} and grain types. Calonne et al., (2012) worked with representative elementary volume from which he computed specific surface area and porosity. Porosity was used for determination of density. He used snow with properties that were estimated based on Calonne et al., (2012) papers. Tab. 4 describes 35 samples in total.

Tab. 4 - Estimation of samples properties that was used for determination of equation 14 for intrinsic permeability that is conducted by Calonne et al., (2012)

Grain types	Density [kg.m^{-3}]	Porosity [-]
Precipitation particles	100 - 140	0.9 - 0.85
Decomposing and fragmented snow	140 - 160	0.85 - 0.88
Rounded grains	160 - 430	0.88 - 0.57
Faceted crystals	230 - 290	0.74 - 0.7
Depth hoar	270 - 370	0.71 - 0.61
Melt forms	470 - 550	0.51 - 0.41

5 Methods

5.1 Numerical solver

For modelling of outflow is used dual Richards unsaturated equation solver (DRUtES ©) (Kuráž et al., n.d.). The software uses the Richards equation (RE) to compute the pressure head in observation points and times in a porous medium. To do that it needs to be established relative hydraulic conductivity curve *K(h)* and capacity term *C(h)*. Both of these functions are based on Mualem - van Genuchten model (van Genuchten, 1980) that is implemented in computation so input values for DRUtES are parameters of this model. The software numeric is described in detail Kuráž et al., (2013b). DRUtES offer many options to describe a situation that is modeled with different levels of complexity. This thesis employs 1D modelling and does not include other processes than flow through homogenous layers. This means that preferential flow is neglected. According to Colbeck, (1972) 1D modelling can be used at the domain that is large enough so the inhomogeneities can be averaged. Domains that represents natural snowpack properties used in this thesis are considered homogenous and grains shape are considered as spherical. Mesh in 1D is created by an internal mesh generator, but it is needed to describe layering of the snowpack profile. Layers must be ordered from bottom to top where the bottom starts at zero and top ends with a total height of profile. Every layer has id number and the density of the mesh have to be stable along whole computation.

Hydraulic properties of every layer are described by van Genuchten parameters α, n, m, residual water content θ_r, saturated water content θ_s and specific storage S. Initial condition can be prescribed by water content θ or pressure head h. The last parameter is hydraulic conductivity K. Since modelling is in 1D, K represents only downward direction and anisotropy is neglected.

Boundary condition can be chosen from Dirichlet, Neumann, seepage face, free drainage, and atmospheric boundary. DRUtES allow adding files with inflow logs as Neumann condition. The file must contain time logs and inflow in units that are defined in the configuration files. Seepage face is a boundary condition that can switch between Neumann and Dirichlet. When conditions on this boundary reach saturated state, the

boundary is set up to Dirichlet condition of zero pressure head otherwise is used Neumann condition (Kuráž et al., 2011).

The configuration of the whole simulation contains its duration, choosing observation points and times, choosing minimum and maximum of time step and number of iteration and length of *h* criterion for the Picard method, which represents the error iteration criterion of the pressure head.

To obtain the reliable result in reasonable computational time, size of the time step, iteration criterion and mesh density must be balanced. RE is a partial differential equation (PDE) which describes changes in a porous medium in time and space. DRUtES solves PDE for a medium with a finite element method. This method is based on an approximation of the result between two computational nods. These nods creating computational matrix and closer they are to each other the results are more precise in terms of describing the state of the whole medium in one discrete time step or in one spatial coordinate in time. The first unknown in RE is a change of relative hydraulic conductivity in space and the second unknown is a change of water content in time. Both solutions are dependent on each other because water content influences relative hydraulic conductivity (Eq. 7) and in another way, conductivity has an influence on the flux rate along the whole medium. The whole system is described by a large matrix of linear equations that describe the rate of change between computational nods. These functions are approximated so closer the nods are the more precise the approximation is. Based on estimated discrete values, iterations are conducted to obtain pressure head *h* value. Standard Picard method was used to finds a solution by linearization of non-linear products. (Kuraz et al., 2013a). DRUtES allows the user to choose Picard criterion that determines when should iteration stop based on the required similarity of iteration result for pressure head in $h_{(t+1)}$ and $h_{(t)}$. Difference between those two steps must be smaller than the chosen criterion. (Kuraz et al., 2013a) A number of iterations can be limited by the determination of the maximum number of iterations. When the Picard method criterion is too small and a maximum number of iterations is also small, then convergence error can occur.

Inaccuracy in numerical solution arise with large computational steps but also with small steps. In order to avoid mistakes, it is needed to conduct more simulations with a different setup and compare results between each other. If the simulations do not differ, regardless

of the decreasing computational step, the result can be determined. In this thesis was used the approach with decreasing time step and decreasing Picard criterion to reach stable solutions. Lowest values of the time step, Picard criterion and mesh density were limited by computational time.

5.2 Input data processing and set up of numerical solver

Profile information of three different profiles from the study of Juras et al., (2017) were processed. All hydraulics properties, measured characteristics of the environment, outflow volume and it´s artificial rainwater contribution will be described in the following chapters named after the location where sprinkling experiment was conducted.

The snowpack profiles in Juras et al., (2017) were characterised by different layers identified by hand hardness test and visual assessment of grain size and type. Density and LWC were measured every 5 cm of snow profile depth. For the purpose of modelling, every layer had to have established hydraulic properties so when a thick layer with one measured grain size and hardness have changing values of LWC or density it was divided to keep homogeneity of hydraulic properties along the layer.

Configuration files must be set up to start DRUtES simulations of runoff. Hydraulic properties of every layer of snowpack were filled in the *matrix.conf* file (see appendix Fig. 24). The first input is a number of layers. Every further hydraulic property description must have the same number of rows as the number of layers. Parameters for the van Genuchten model were computed based on Eq. 10, 11, 12, 13, 14, 15 and 16. For every simulation was one set of parameters taken. Six different combination of parameter used in this work are listed in Tab. 6. For better readers clarity abbreviations for each combination are introduced.

Tab. 5 – Combination of van Genuchten parameters obtained from different studies (Eq: 10, 11, 12, 13, 15, 16).

Combinations of used parameters				Abbreviations
1	Yamaguchi 2012 (α)	Yamaguchi 2012 (n)	Calonne 2012 (k)	Yam.12
2	Yamaguchi 2010 (α)	Yamaguchi 2010 (n)	Calonne 2012 (k)	Yam.10
3	Yamaguchi 2012 (α)	Yamaguchi 2010 (n)	Calonne 2012 (k)	Yam.12-Yam.10
4	Yamaguchi 2012 (α)	Hirashima 2010 (n)	Calonne 2012 (k)	Yam.12-Hir.10
5	Yamaguchi 2010 (α)	Yamaguchi 2012 (n)	Calonne 2012 (k)	Yam.10-Yam.12
6	Yamaguchi 2010 (α)	Hirashima 2010 (n)	Calonne 2012 (k)	Yam.10-Hir.10

Grain size obtained from in situ measurement is not always uniform. In some cases, varies between two values. For the first simulation was taken the mean of these two values in further simulations were these ranges used for sensitivity analysis.

Parameter m was computed according to Eq. 8, from n value. Residual water content θ_r [-] was set up as 0. This is only assessed value because θ_r [-] is hard to established and there is no accredited method on how to do it. Saturated water content θ_s [-] was established as porosity ϕ [-] that was computed by Eq. 1 from measured layer density and ice density. Specific storage was set to 0 because it is not expected that snow reaches full saturation during simulation time. Because of 1D modelling and neglected anisotropy angle was set to 0 and K was computed from Eq. 15 that used Eq. 16 to obtain k. As initial condition was used LWC from Denoth meter that was recalculated from percentage to volumetric water content θ [-] by dividing it with 100. Set up have orientation from bottom to top therefore the first boundary was chosen seepage face and second was Neumann condition that uses a text file with inflow logs. This file must be named after boundary number e.g. *102.bc* and must be placed with the *matrix.conf* file into the *water.conf* folder.

The computational mesh is implemented in DRUtES for 1D modelling but it is needed to be set up. File containing DRUtES Set-up is called drumes1d.conf (see appendix Fig. *26*) and it is located in mesh folder. In the next step can be set up different mesh density for every layer that is defined by depth from bottom to top. Then the number of materials that have to correspond with the number of layers in matrix.conf. Every layer is identified with id number and is defined by depth from bottom to top.

Last configuration file that was edited was global.conf (see appendix Fig. 25). DRUtES offers a solution for 1 to 3 dimensions problem. This thesis using the 1D description of

the snowpack. To apply an internal mesh generator option 1 should be set. Rest of options are error criteria and time step. Some of these options were constantly changed with every simulation to obtain reliable results. A maximum number of iterations were constantly set to 10 to keep a reasonable number of iterations. Iteration criterion was at loosest point set up to 1e-2 and with a tightened criterion to 1e-5. Lower values lengthened the computational time. The initial and minimum time step was set on low values according to computation demand. This number sets the lowest time step to which calculation can decrease. Too low values could cause a computational problem. Decreasing time step indicates some problem with an approximation. Maximum time step must be small enough to keep precision of computation but big enough to keep computational time in reasonable ranges. Also, the output file with low time step can reach over a hundred million logs and result in big files. Described set up and its limitations are suitable for problems in this thesis.

5.3 Experimental design

Experimental data used in this thesis has been chosen from Juras et al., (2017) for comparison of measured and modeled outflow. Deuterium-enriched water was sprinkled on snowpack during winter in the vicinity of Davos, Switzerland, to separate artificial rain from melt snow in the outflow. All experiment was conducted on flat terrains at elevations between 1850 and 2050 m a.s.l.

Metal plate (1 m^2) was inserted into the snowpack and inclined around 6%. Natural and undisturbed snow on metal plate was insulated from three sides to prevent artificial sprinkled water to a runoff in other directions than the monitored side. Runoff was caught and measured by tipping bucket with 100 ml volume of the tip. The tipping bucket is connected to a logger where the data were stored.

Insulated snowpack was sprinkled by artificial water from a calibrated nozzle under pressure of 2 bar that was stable during sprinkling. volume of sprinkled water was estimated. From the pressure values. The nozzle is attached to the tent construction and is 160 cm above the center of the metal lysimeter. This height was optimal for equal

distribution of sprinkled water on snowpack in measured 1 m^2 range. Other meteorological parameters like air temperature or humidity were recorded during the experiments. The tent has side covers to prevent wind influencing sprinkled water direction. These sides are after sprinkling periods removed to prevent great temperature increase inside the tent. Sprinkling was conducted four times in 30 min periods with rain intensity of 10.25 $mm.h^{-1}$. Between every sprinkling pulse were 30 min pauses. Sprinkled water temperature varies between 4.3 to 7.5 °C that fulfill the standard temperature of rain in the winter season.
Based on isotopic signature of outflow samples contribution of pre-event water (melted snow + LWC) was distinguished in runoff. On the site of the experiment, few snow pits for snow profile analysis were excavated. Snow pit analysis was conducted. All this information was put together and were averaged to describe sprinkled snow cover that cannot be disturbed before sprinkling. The first centimeter on the top of the snow profile could not be measured due to measurement limitations and was neglected in the computation. This layer had a large pore size and very small density, so it has a small influence on complete runoff.

5.4 Data

5.4.1 Dischma

For the first attempt to simulate outflow from snowpack experiment from Dischma valley in Switzerland, Davos municipality. Sprinkling experiment was performed 1. 5. 2015 in Dischma valley (elevation 2000 m a.s.l.). The weather was windy and cloudy with light rain. The air temperature was during the whole experiment between 8 °C and 15 °C inside the tent and from 8 °C to 10 °C was measured by meteo station panel outside the tent. Profile description is in Fig. 6.

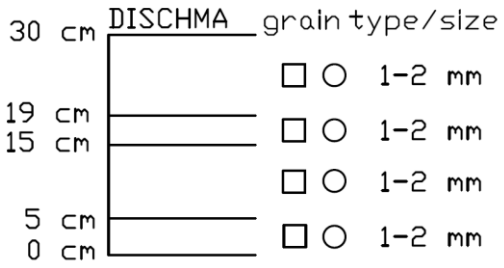

Fig. 6 – Dischma snow profile analysis obtain from Juras et al., (unpublished) data.

Dischma snowpack contained couple of layers with the same grain size that was measured between 1 and 2 mm and grain shape that was established as a mix of faceted grains and melted forms. From this information can be assumed that grains were not uniform, because of shape differences and size range. Averaged properties of snowpack before the experiment is in Tab. 6.

Tab. 6 – Averaged values for the whole snowpack determined from profile analysis of 3 reference profiles with standard deviations of measured values.

State	Temp.	LWC	LWC sd	Density	Density sd	Snow Depth	Snow depth sd
ripped	0 °C	3.8 %	0.3 %	403 kg.m^{-3}	33 kg.m^{-3}	28.1 cm	2.5 cm

Total averaged LWC was 3.8 % which is defined by Fierz et al., (2009) as wet snowpack. Wetness was relatively uniform along the profile. The hardness of the first layer from the top is between 2 and 3, the second layer is 2 and the rest of layers have hardness again between 2 and 3. Snow is dense and according to hardness test is snowpack well bonded. As can be seen, there is a difference between compactness of layers although key values for parametrization of the van Genuchten model is similar.

Juras et al., (2017) described in detail the outflow and its parts that can be used for another analysis of snowpack properties. Information is divided by sprinkling period that is 30 min pulse of artificial sprinkling. By rain is mean artificial sprinkling and non-rain out is a combination of melt snow and LWC outflow.

Tab. 7 – Information about total outflow, separated rain outflow and non-rain outflow from Dischma experiment conducted 1. 5. 2015 by Juras. The table is taken from Juras et al., (2017)

Sprinkling period	Input [mm]	LWC deficit [mm]	Total out [mm]	Rain out [mm]	Rain out [%]	Non-rain out [mm]	Volume rain stored [mm]	Volume rain stored [%]
1	10.39	0	7.20	1.58	21.89	5.62	8.81	84.83
2	10.39	0.25	10.44	5.14	49.21	5.30	5.25	50.55
3	10.39	4.98	11.14	6.41	57.55	4.73	3.98	38.30
4	10.39	11.55	16.22	9.64	59.46	6.58	0.75	7.17
Total	41.56	-	45.00	22.77	50.60	22.23	14.25	45.21

As can be seen in Tab. 7 total outflow is bigger than input which confirms that melt and initial LWC is participating on the outflow. At ripped snowpack can be seen that non-rain outflow is relatively stable at every peak, but rainwater contributes significantly lower at first sprinkling period. After introducing artificial rainwater into snowpack piston flow occurs (Feng et al., 2001; Juras et al., 2017). LWC is pushed out from snowpack with the contribution of melt and its place is taken by rainwater as can be seen at Tab. 7. Snowpack became more saturated during sprinkling and rainwater is conducted faster. Total outflow is raising after every sprinkling period and with it raising the contribution of non-rain outflow. As can be seen at Tab. 7 LWC deficit increasing with every sprinkling period so non-rain water contribution is created by melt (Juras et al., 2017).

Tab. 8 - Information about the time lag between input and total outflow and lag between input and separated rain outflow from Dischma experiment conducted 1. 5. 2015 by Juras. The table is taken from Juras et al., (2017)

Sprinkling period	Time lag total [min]	Time lag rain [min]	Peak time total [min]	Peak time rain [min]
1	13	26	33	36
2	9	9	29	34
3	11	11	28	31
4	9	9	27	27

As can be seen in Tab. 8 rainwater in outflow occurs 13 min after event outflow appears. Peak time shows that separated rain contribution to outflow have shifted peaks and takes longer to appear. Last sprinkling period shows the same peak time as total outflow. The process of reduction of lag times during sprinkling shows how saturation have an

influence on water conductivity in the snowpack. Last period shows that rainwater has the fastest transport and contributes to total outflow by the larger volume.

To be able to rely on parametrization it is required to try how results change with changing input values that is information about grain size and density. Dischma snowpack measured *d* of all layers that varies between 1 mm to 2 mm. Distributed grains have better ability to retain water than a uniformly distributed ones, but bigger pores conduct liquid water faster. All that are factors that have an influence on the total outflow (see appendix Fig.10 and Fig. 11).

Combination of parameter α with Hirashima et al., (2010) *n* is close to Yamaguchi et al., (2010) *n* in this range of grain size, therefore, is not necessary to plot the distribution of pore size for both cases. Densities that were used as input values for parametrization to compute pore size distribution were rounded into two numbers, 420 $kg.m^{-3}$ that represents second and third layer from the bottom and 450 $kg.m^{-3}$ that represent first and fourth layer from the bottom of Dischma snowpack. Yam.10 in Fig.10 (see appendix) shows that with bigger grains becomes pores more distributed and therefore grows retention ability of layer. This trend seems quite rapid with bigger grains is Yam.10 *n* smaller and pores became well distributed, α is not able to balance this growth because it is not connected to density.

The Yam.12 frequency of pore distribution curve reacts not even to grain size but also to density. With comparison to Yam.10 pores are distributed in smaller ranges with growing density. From observation in real conditions layers with 1 mm grains can be compressed, denser and therefore have smaller pores unlike of e.g. top layers with same grain size that are not compressed and have smaller density, therefore, more air must be present in one volume unit. With small densities becomes pore size more distributed, pores ranges in bigger values of pore size e.g. 1 mm grains with 200 $kg.m^{-3}$ have distribution as can be seen in Tab. 9 while Yam.10 layers with *d* of 1mm generalize pore distribution between 0.2 and 0.4 mm of pore diameter.

Tab. 9 – Pore distribution of layer with density of 200 kg.m^{-3} and d = 1 mm according to Yam.12

Pore diameter [mm]	0 - 0.4	0.4 - 0.6	0.6 - 0.8	0.8 - 1	1 - 1.2	1.2 - 1.4
Percentage representation [%]	5	15	38	22	10	10

Yam.12-Yam.10 shows less variability with pore distribution. All grains sizes keep relatively same slope, therefore the same range of distribution caused by n that is not influenced by density. Density only has an impact on α that controls the shape of the curve. With higher densities are curves of different grain size shifted closer together with smaller pore ranges but the distance ratio between curves remains.

Yam.10-Yam.12 (see appendix Fig. 28) have smaller sensitivity to density changes than Yam.12 and Yam.12-Yam.10, As can be expected curves remain in the same range with changing density only the slope is influenced but with minor impact (see appendix Fig. 28).

Frequency curve can tell that best possible reaction to change of values should be obtained with the application of Yam.12-Yam.10 or Yam.12-Hir.10 because of stable pores distribution with different grain size and that these parameters show a sensitive reaction to density. To be able to confirm this consideration all combinations of parametrization with input value d of 1 mm (simulation 2) and 2 mm (simulation 3) were tested on whole snowpack and were compared with measured outflow and first simulated outflow with d of 1.5 mm (simulation 1).

Conductivity ranges between saturated state when the conductivity of snowpack is on its maximum and state of residual water content when the conductivity of snowpack is on its minimum, but this relationship is not linear it is influenced by pore size. With small volumetric water content more distributed and smaller pores allow water to stay in contact and flow continuously.

For the same sets of parameters with input d =1.5 mm were computed relative hydraulic conductivities according to initial volumetric water content that can be seen on Table 10.

Table 10- Relative hydraulic conductivities K_r [cm.h^{-1}] computed for initial water content in both layer densities

K_r [cm.h^{-1}]	Yam.12	Yam.12 - Yam.10	Yam.12 - Hir.10	Yam.10	Yam.10 - Hir.10	Yam.10 - Yam.12
420 kg.m^{-3}	1.99	4.37	4.76	3.11	2.91	3.11
450 kg.m^{-3}	1.42	2.96	3.22	2.11	1.96	2.11

Relative conductivities that was computed for both densities (see appendix Fig. 29 and Fig. 30). Residual water content θ_r was set to 0 [-] and saturated water content θ_s was set to 0.5 [-] with density 450 kg.m^{-3} and 0.54 [-] with density 420 kg.m^{-3}.

Parameters influence hydraulic properties that are described only by density and by grain diameter. Yam.12 – Yam.10 and Yam.12 – Hir.10 show small retention ability, therefore, conductivity stays with raising θ [-] on low rates but when snowpack reaches breaking point between moist and wet, conductivity starts rising fast. Rest of parameters simulate some retention ability, therefore, raising of conductivity is slower and steady. In model can conductivities of snow with small retention ability cause depletion in consequence of initial water content. Conductivities reach high values even with 0.05 [-] water content. Water from shallow snowpack could be depleted fast with continuous inflow or leave snowpack without initial water content before inflow occurs. Yam.12 and Yam.12-Yam.10 start to conduct water with higher volumetric water content than Yam.10 and Yam10.-Yam.12. When snowpack reaches θ [-] than leads to raising conductivity, and K_r quickly gains great values and outflow will be much faster with parametrization that gives snowpack smaller retention ability. To be closer to real condition because of the draining of water at the beginning of the simulation, the last sensitivity test was suggested. Simulation 4 resulted in reduced densities by 20 [kg.m^{-3}] and rain diameter remains on 1.5 mm.

In Tab. 24, Tab. 25, Tab. 26 and Tab. 27 (see appendix) can be seen as input values for DRUtES of four simulations. Computations were stable with reliable results on the same setup for all four simulations. Used setup for the *global.conf* file is described in Tab. 9

Tab. 11 – Computational setup of DRUtES that is the same for all four simulations. Simulation 1 for d = 1.5 mm, simulation 2 for d = 1 mm, simulation 3 for d = 2 mm and simulation 4 for reduced density. A number of iteration and h tolerance is a restriction of the Picard method.

Simulation 1/2/3/4	Yam.10	Yam.12	Yam.12-Yam10	Yam.12-Hir.10	Yam.10-Yam.12	Yam.10-Hir.10
Max. n. of iteration	10	10	10	10	10	10
h tolerance	1e-5	1e-5	1e-5	1e-5	1e-5	1e-5
Max. time step	1e-5	1e-5	1e-5	1e-5	1e-5	1e-5
Min. time step	1e-7	1e-7	1e-7	1e-7	1e-7	1e-7
Density of mesh	0.3	0.3	0.3	0.3	0.3	0.3

For each simulation was used small time step and strict *h* Picard criterion. This setup lengthens computation time on 6 min and creates big files. But with less strict setup keeps occurs overshooting of results in one peak. Minimum time step stabilized computation, therefore, no slow convergence warning occurs. Computation has space to tighten time step if approximation getting less precise. Bottom boundary condition is set to seepage face and top boundary condition is Neumann with measured inflow logs.

5.4.2 Flüela

Second attempt of outflow simulation from snowpack was also based on the experimental data from Juras et al., (2017) experiment from Flüelapass (elevation 2150 m a.s.l.). Sprinkling experiment was performed 7. 5. 2015. The weather was sunny with a very gentle breeze. The air temperature was during the whole experiment between 9 °C and 16 °C inside the simulator. Profile description is depicted in Fig. 7.

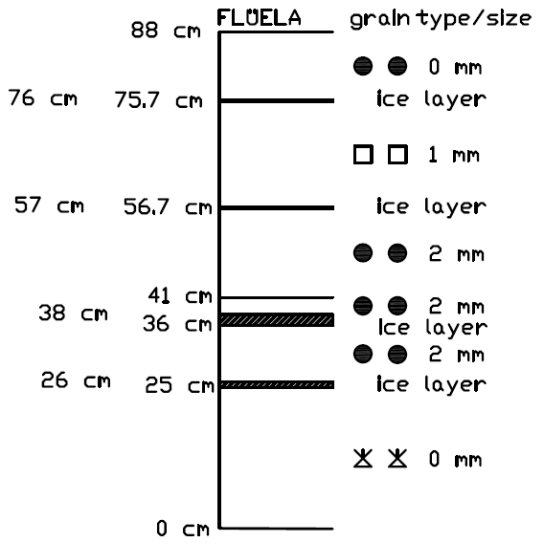

Fig. 7 – Flüela snowpack profile according to Juras et al., (unpublished) data.

Flüela snowpack was ripped, isothermal and wet. Unlike Dischma snowpack, Flüela snowpack was three times deeper and different layering can be observed. As can be seen in Tab. 12 averaged profile is denser with slightly less volumetric LWC than Dischma snowpack.

Tab. 12 – Averaged values for the whole snowpack determined from profile analysis of 3 reference profiles with standard deviations of measured values. Temp. mean temperature of snowpack

State	Temp.	LWC	LWC sd	Density	Density sd	Snow depth	Snow depth sd
ripped	0 °C	3.5 %	0.5 %	477 kg.m^{-3}	21 kg.m^{-3}	88.4 cm	2.1 cm

Whole profile has hardness 2 that mean soft except ice layers that have a hardness between 5 and 6. Snowpack is from moist to wet according to Fierz et al., (2009) and measured wetness is between 4 and 3 % along the profile. In comparison with Dischma snowpack, Flüela is less compact, less wetted but even with grains of diameter 2 mm have a density around 500 kg.m^{-3}. This observation confirms the influence of grain types on snowpack hydraulic properties.

Description of measured outflow can be found in Tab. 13.

Tab. 13 - Information about total outflow, separated rain outflow and non-rain outflow from Flüela experiment conducted 7. 5. 2015 by Juras. The table is taken from Juras et al., (2017)

Sprinkling period	Input [mm]	LWC deficit [mm]	Total out [mm]	Rain out [mm]	Rain out [%]	Non-rain out [mm]	Volume rain stored [mm]	Volume rain stored [%]
1	10.39	0	4.62	0	0	4.62	10.39	100
2	10.39	0	12.38	1.89	15.28	10.49	8.50	81.76
3	10.39	0	12.08	3.16	26.14	8.92	7.23	69.61
4	10.39	16.13	28.40	7.60	26.75	20.80	2.79	26.87
Total	41.56	-	57.48	12.56	22.00	44.83	28.91	69.57

Flüela snowpack shows big retention capacity according to the stored volume of rain and no LWC deficit until third sprinkling period. Total outflow after first sprinkling period is dominated by non-rain outflow resulting from piston flow. Sprinkled water contribution to total outflow is smaller than non-rain outflow. Total outflow exceeds input by 38 %. This increase can be credited to initial wetness and melt. Stored rain decreases over the whole sprinkling whereas rain outflow increase. Measured values are proportional and bonded but non-rain contribution increases sharply at the fourth sprinkling period. This can be explained by the melting process because even if the last period seems as high peak, it does not exceed the velocity of two previous peaks, it only takes longer until outflow ends.

Tab. 14 - Information about the time lag between input and total outflow and lag between input and separated rain outflow from Flüela experiment conducted 7. 5. 2015 by Juras. Values is used from Juras et al., (2017)

Sprinkling period	Time lag total [min]	Time lag rain [min]	Peak time total [min]	Peak time rain [min]
1	27	-	50	-
2	27	27	47	49
3	27	27	46	53
4	32	32	47	51

Peaks show expected behavior, longer lag after the first sprinkling period and after rise of conductivity, outflow answered similarly to the following sprinkling period. Total time

lag with fourth sprinkling period can be explained by LWC deficit that has to be filled first.

For first set up it is needed to determine how to describe ice layers. In profile were identified two 0.3 cm thick ice layers (1 and 2), one 1 cm thick layer (4) and one 2 cm thick (3). Numbers are given from top to bottom of profile. Even if first three layers are described straight forward as compact ice that cannot be penetrated even with knife blade they cannot be setup for the model as layers with a density of ice (917 $kg.m^{-3}$). The first problem would raise with θ_s that according to Eq. 1 will be equal zero and the second problem is that the model could not simulate melt that occurs during sprinkling and made layers permeable. Comparison to profile analysis after experiment shows that 0.3 cm layers became thicker but with preserved hardness. Thickness of 2 cm ice layer dissolute into the coarse layer. But this observation can be misleading due to the long lag between sprinkling and profile analysis after the experiment. Wever et al., (2016) proposes that the ice layer exceeds 700 $kg.m^{-3}$. According to previous pores distribution analysis (see appendix Fig. 27 and Fig. 28), smaller grain with bigger densities results in bigger retention ability but the question is how that big density changes conductivity. It is needed to decide what grain size should ice layers have and how it affects the result of the simulation (see appendix Fig. 31, Fig. 32, Fig. 33, Fig. 34, Fig. 35 and Fig. 36)

With introducing density into WRC conductivity increases in saturated state and decrease with bigger grains in low θ [-] state. Yam.12 with ρ_s = 800 $kg.m^{-3}$ shows that grains d = 0.5 mm have with 0.01 m pressure heads θ = 0.1 [-] while rest as of grain diameters depleted to θ_r [-]. Increase of conductivity (see appendix Fig. 35) due to the ability of Yam.12 -Yam.10 describe the uniform pore distribution of snow with big grains and high density. Conductivity reaches higher values than with parameters before. Bigger grains shows increase of conductivity with smaller water contents. This breaking point is essential because conductivity became very sensitive to volumetric water content. All parameters behave similar smaller grains start to conduct faster than big grain and are less sensitive to volumetric water content change. Yam.12, Yam.12 Hir.10 and Yam.12 – Yam.10 have reached bigger conductivities than the rest of parameters Layers with smaller grains slow down the water flow. They faster reaches a state of saturation when they are able to conduct water but in slower rates. Bigger grains slow down outflow but

only to the breaking point of saturation and than depleting quickly. To be closer to real conditions smaller grains seems to be better for describing ice layers. Yam.12, Yam.12 – Hir.10 and Yam.12 – Yam.10 shows bigger θ [-] with smaller pressure head, therefore, bigger retention ability. It also reacts to density with increasing pressure head to θ [-], unlike Yam.10, Yam.10 – Hir.10 and Yam.10 – Yam.12. Coarser grains cause that retention curves became similar with all parameters (see appendix Fig. 37 and Fig. 38). Slow flux from top layer could cause that ice layer with big grains will reach volumetric water content that is needed for depletion very slowly and in meantime will conduct water in smaller rates than layers with smaller grains.

Four simulations were carried out. Simulation 1 and 2 have density of 700 kg.m^{-3} and *d* of 0.5 mm and 1.5 mm. First, two simulation have a top and bottom layer with a measured grain size of 0.5 mm. Simulation 3 and 4 have this layer set to 1 mm diameter and ice layers with 0.5 mm. Simulation 3 have ice layer density 700 kg.m^{-3} and simulation 4 have 800 kg.m^{-3}. For the ice layer 3 were used *d* increased by 0.5 mm with every simulation. It needs to be said that this description can be far from real properties of ice layer but due to inability to measure grain size, density and wetness of ice layer is this part more about the ability to represent ice layer in modeled snowpack using suggested parametrization.

It is considered that the ice layer has no initial wetness due to their compactness, but this initial state raises the problem with 0.5 mm grains. According to WRC when wetness approaches zero volumetric water content became infinitely small and that causes computation problem. Therefore, is better to use pressure head as an initial condition. Its values were computed according to Eq. 5 and Eq. 6.

Tab. 15 – Initial condition of ice layers for DRUtES computed from wetness close to 0 [-].

Layer start [cm]	Layer end [cm]	Initial *h* [cm] Yam.10		Initial *h* [cm] Yam.12 - Yam10		Initial *h* [cm] Yam.12		Initial *h* [cm] Yam.10 - Yam.12		Initial *h* [cm] Yam.10 - Hir.10		Initial *h* [cm] Yam.12 - Hir.10	
-	-	700 kg.m^{-3}	800 kg.m^{-3}	700 kg.m^{-3}	800 kg.m^{-3}	700 kg.m^{-3}	800 kg.m^{-3}	700 kg.m^{-3}	800 kg.m^{-3}	700 kg.m^{-3}	800 kg.m^{-3}	700 kg.m^{-3}	800 kg.m^{-3}
25	26	42.5	40.3	56.5	61.1	46.6	48.6	35.0	32.0	40.4	38.5	53.8	58.4
36	38	29.5	27.7	32.9	35.3	33.5	33.3	30.0	26.1	30.1	28.2	33.6	36.0
56.7	57	42.5	40.3	56.5	61.1	46.6	48.6	35.0	32.0	40.4	38.5	53.8	58.4
75.7	76	42.5	40.3	56.5	61.1	46.6	48.6	35.0	32.0	40.4	38.5	53.8	58.4
25	26	42.5	40.3	56.5	61.1	46.6	48.6	35.0	32.0	40.4	38.5	53.8	58.4

Input values for DRUtES can be found in appendix in Tab. 28, Tab. 29, Tab. 30 and Tab. 31.

Computations were stable with reliable results on the same setup for all four simulations. Used setup for the *global.conf* file is described in Tab. 16

Tab. 16 – Computational setup of DRUtES for all four simulations. A number of iteration and *h* tolerance is a restriction of the Picard method.

Simulation 1/2/3/4	Yam.10	Yam.12	Yam.12-Yam10	Yam.12-Hir.10	Yam.10-Yam.12	Yam.10-Hir.10
Max. n. of iteration	10	10	10	10	10	10
h tolerance	1e-5	1e-5	1e-5	1e-5	1e-5	1e-5
Max. time step	1e-5	1e-5	1e-5	1e-5	1e-5	1e-5
Min. time step	1e-9	1e-9	1e-9	1e-9	1e-9	1e-9
Density of mesh	0.8	0.8	0.8	0.8	0.8	0.8

The minimum time step is lower than with Dischma snowpack because of slow convergence on the beginning of computation. The initial time step was set to same value as a minimum time step. Bottom boundary condition is set to seepage face and top boundary condition is Neumann with measured inflow logs.

5.4.3 Sertig

Second attempt of outflow simulation from snowpack was also based on the experimental data from Juras et al., (2017) experiment from Sertig (elevation 1850 m a.s.l.) in Switzerland. Sprinkling experiment was performed 17. - 19. 3. 2015. The weather was windy with light rain and snow precipitation. The air temperature was during the whole experiment between 0 °C and 10 °C inside the simulator. Profile description is depicted in Fig. 8.

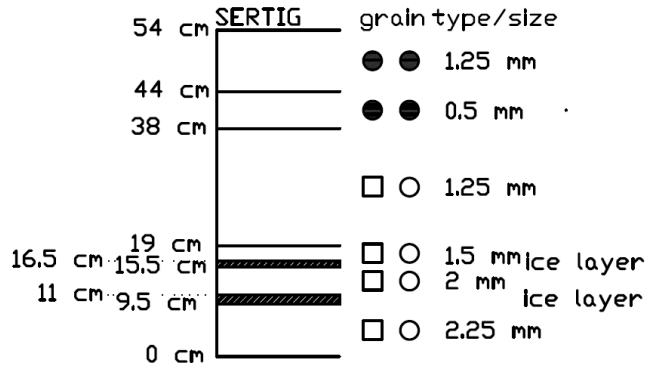

Fig. 8 – Sertig snowpack profile according to Juras et al., (2017) data.

Sertig snowpack was not fully ripped. Its temperature was below zero with small LWC. According to Fierz et al., (2009) 5 of 8 layers are dry. Density ranges between 250 – 350 kg.m^{-3}. Averaged values with standard deviation for the whole profile can be seen in Tab. 17.

Tab. 17– Averaged values for the whole snowpack determined from profile analysis of 3 reference profiles with standard deviations of measured values.

State	Mean temp.	LWC	LWC sd	Density	Density sd	Snow depth	Snow depth sd
Not ripped	-1 °C	0.2 %	1.1 %	247 kg.m^{-3}	4 kg.m^{-3}	54.4 cm	3.7 cm

Layers hardness ranged between 1 and 2 so they were not compact. On top of the snowpack occurs rounded grains and rest is combination of faceted and melt forms. An ice layer of 1.5 cm thick and 6 hardness was observed at a depth of 44 cm and a second 1 cm thick layer of ice with a hardness between 3 and 4 was above it. Snowpack was not completely dry there was some occurrence of liquid water on top and bottom of the snowpack. These two layers were closer to 0 °C unlike others that reaches -2 °C in minimum. That causes temperature gradient. With dry snowpack comes different outflow conditions. In natural condition water in dry snowpack tends more likely to flow in preferential paths. With higher rates of inflow water in preferential paths can reach a velocity of saturated flow and it can make outflow fast (Waldner et al., 2004a). Measured values of outflow can be seen in Tab. 18.

Tab. 18 - Information about total outflow, separated rain outflow and non-rain outflow from Sertig experiment conducted 18. 3. 2015 by Juras et al., (2017).

Sprinkling period	Input [mm]	LWC deficit [mm]	Total out [mm]	Rain out [mm]	Rain out [%]	Non-rain out [mm]	Volume rain stored [mm]	Volume rain stored [%]
1	10.39	3.17	8.14	4.04	49.65	4.10	6.35	61.10
2	10.39	5.36	11.48	9.29	80.95	2.19	1.10	10.56
3	10.39	6.87	10.52	9.01	85.62	1.51	1.38	13.31
4	10.39	9.15	12.53	10.26	81.85	2.27	0.13	1.29
Total	41.56	-	42.67	32.60	76.40	10.07	8.96	21.56

Sertig snowpack outflow exceeds by only 3 % because of low melt due to low temperatures. It can be assumed that non-rain contribution is mainly from the melt, because of lacking initial LWC. Compared to Dischma snowpack Sertig stored less volume of rain despite that profile is 20 cm deeper. Lower density and relatively coarse grains caused a decrease in retention capacity. About 80 % rain outflow from second to fourth sprinkling period suggest the presence of preferential paths. Time lags between inflow and outflow were given in Tab. 19.

Tab. 19 - Information about the time lag between input and total outflow and a lag between input and separated rain outflow from Sertig experiment conducted 18. 3. 2015 by Juras et al., (2017)

Sprinkling period	Time lag total [min]	Time lag rain [min]	Peak time total [min]	Peak time rain [min]
1	10	16	27	33
2	4	4	22	27
3	4	4	20	27
4	5	5	25	25

Despite the presence of ice layers time lags are smaller than those measured on shallow Dischma snowpack. Short time lag shows a quick reaction to inflow and according to the lag between total and rain peak that is small, inflow depleted quickly from snowpack with small additional melt contribution.

From the pore size distribution can be seen how parameters will interpret hydraulic properties of snow with small densities (see appendix Fig. 39). Parameters with Hirashima

et al., (2010) *n* is not depicted because of similarity with Yamaguchi et al., (2010) *n* in used grain sizes. Yam.12 shows a big increase of pore distribution with an increase of *d*, but with low density pores became big so influence on retention ability of snowpack by this parametrization should be minor. Yam.12-Yam.10 lowering distribution influence and only shift curves on pore diameter axis by grain size. This fulfills the idea of heterogenous uncompressed snow with uniform grain size. All parameters except Yam.10 are influenced by density so pore distribution is shifted to bigger pores. In Fig. 39, Fig. 40, Fig. 41 and Fig. 42 (see appendix) can be seen big influence that have density on parametrization.

Because there is no major delay of artificial rain outflow due to ice layers their model setup should make them more permeable. Simulation 1 was set up as it is measured with an ice layer density of 700 $kg.m^{-3}$ and grains diameter of 1.5 mm. Snowpack has small density and relatively big grain, so it should conduct water quickly. With small densities conductivity increases but it will last longer till layer reaches enough volumetric water content to conduct water in high rates. Parametrization tends to create layers with bigger grain and lower densities more distributed, therefore snowpack could retain more water. In order to assess the sensitivity of relatively dry snowpack on grain size, simulation 2 and simulation 3 were suggested. Simulation 2 had all grain size reduced by 0.5 mm and simulation 3 had all grain enlarged by 0.5 mm. Input values of all simulation for DRUtES can be seen in Tab. 32, Tab. 33 and Tab. 34 (see appendix).

Computations were stable with reliable results on the same setup for all four simulations. Used setup for the *global.conf* file is described in Tab. 20.

Table 20 – Computational setup of DRUtES for all four simulations. A number of iteration and h tolerance is a restriction of the Picard method.

Simulation 1/2/3/4	Yam.10	Yam.12	Yam.12-Yam10	Yam.12-Hir.10	Yam.10-Yam.12	Yam.10-Hir.10
Max. n. of iteration	10	10	10	10	10	10
h tolerance	1e-5	1e-5	1e-5	1e-5	1e-5	1e-5
Max. time step	1e-4	1e-4	1e-4	1e-4	1e-5	1e-4
Min. time step	1e-8	1e-8	1e-8	1e-8	1e-8	1e-8
Density of mesh	0.4	0.4	0.4	0.4	0.4	0.4

The minimum time step is lower compared to Dischma snowpack simulation, because of slow convergence on the beginning of computation. The initial time step was set to same value as a minimum time step. The maximum time step was looser than with previous computations. This setup gives a good result with computational time under 2 min. Bottom boundary condition is set to seepage face and top boundary condition is Neumann with measured inflow logs.

5.5 Error criteria

Performance of simulated outflow with every suggested parametrization was evaluated by listed error criterions:

RMSE – root mean square error computes differences between modeled and measured values. It takes into account variance by penalizing bigger error with bigger weight (Chai and Draxler, 2014). RMSE values are in range ⟨0, ∞) and with lower error (RMSE ≈0) the simulation reached better results. The equation for RMSE is as follows:

$$RMSE = \sqrt{\frac{1}{N}\sum_{t=1}^{N}(OBS[i] - SIM[i])^2}, \tag{17}$$

where *OBS* is observed value, *SIM* is modeled value both in *i* interval and *N* is a number of measured values (Máca, 2015).

MSE – mean squared error calculated error between measured and modeled values and gives all of them same weight (Chai and Draxler, 2014). MSE values are in range ⟨0, ∞) and with lower error is MSE ≈0. The equation for MSE is as follows:

$$MSE = \frac{1}{N}\sum_{t=1}^{N}(OBS[i] - SIM[i])^2, \tag{18}$$

where symbols represent the same as Eq. 17.

NS - Nash-Sutcliff coefficient of efficiency is the criterion that compares two models. One of them is an arithmetic mean of measured values and the other one is tested. Arithmetic mean is a simple and robust model. If is NS < 0, the tested model has bigger residual dispersion than the arithmetic mean. NS values are in range (-∞, 1⟩ and the ideal value of NS ≈1. The equation for NS is as follows:

$$NS = 1 - \frac{\sum_{t=1}^{N}(OBS[i] - SIM[i])^2}{\sum_{t=1}^{N}(OBS[i] - \overline{OBS})^2} \quad (19)$$

where $\overline{OBS}$ is arithmetic mean of observed values (Máca, 2015).

6 Results and discussion

6.1 Dischma results

First simulation uses input values that were measured on an experimental site, so the main goal is to see how reliable the results are of every parametrization. Recapitulation of simulations is as follows:

- Simulation 1 – measured d = 1.5 mm and ρ
- Simulation 2 – reduced d = 1 mm and measured ρ
- Simulation 3 – enlarged d = 2 mm and measured ρ
- Simulation 4 – measured d = 1.5 mm and ρ is reduced by 20 kg.m^{-3}

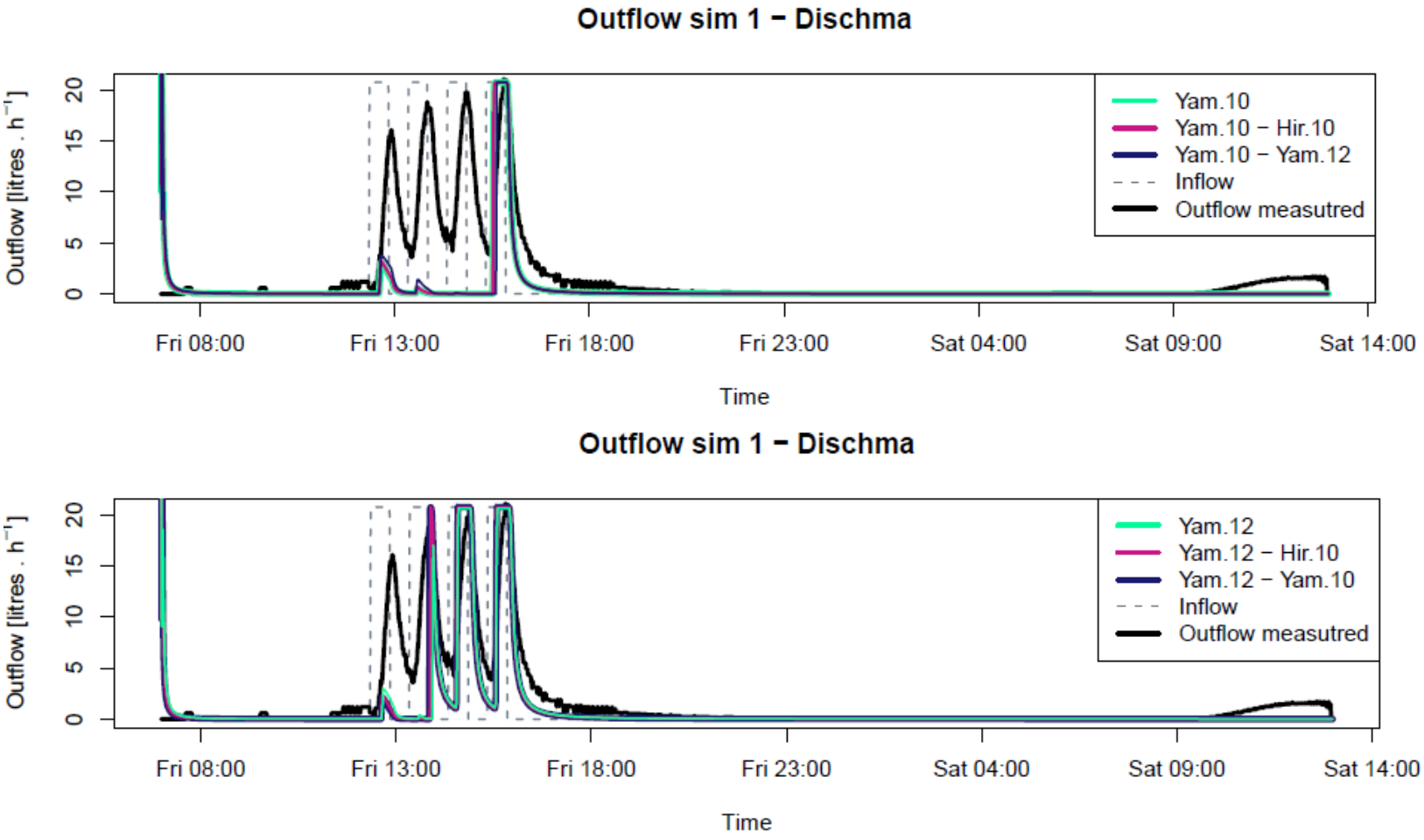

Fig. 9 – Simulated outflow with every parameter combination by DRUtES with profile description that can be seen on Tab. 24 (see appendix) and compared to measured inflow and total outflow.

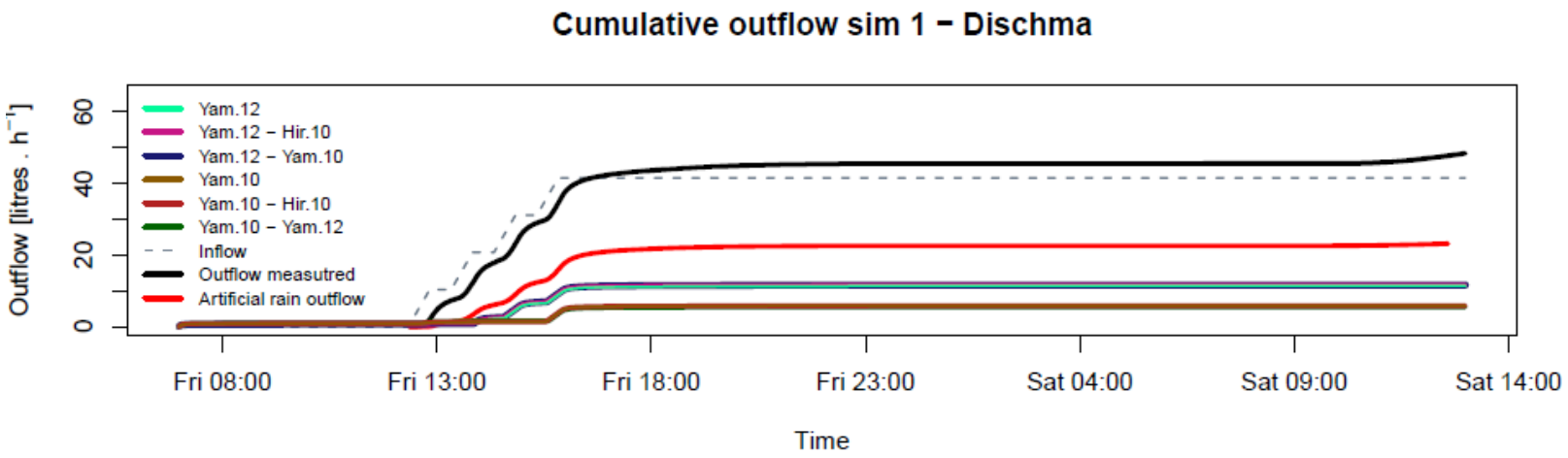

Fig. 10- Simulated cumulative outflow with every parameter combination by DRUtES with profile description that can be seen on Tab. 24 (see appendix) and compared to measured inflow, artificial rain that is separated only rain outflow and total outflow that is rain plus non rain water contribution.

Artificial rain outflow (Fig. 10) is closer to simulated outflow by its volume because there is no additional melt but the model, as it was designed, should simulate total outflow. In Dischma profile could be seen that parameters were not able to simulate artificial rain neither total outflow

On the start of simulation occurs outflow that was expected based on hydraulic conductivity analysis (see appendix Fig. 29). Snowpack depleted first because of high conductivities from initial wetness. This depletion was included in initialization on the beginning of simulation that results in the high outflow. To improve readability of figures this outflow was neglected. After the start of sprinkling snowpack have to reach a state when is able to conduct liquid water first. In this case, can be tell that parameter *n* plays a minor role in outflow because same α parameters combination behaves similarly. Yam.10 reaches bigger values of volumetric water content along profile because paramet rization describes more distributed layers that can retain more water than Yam.12 profiles. There is no continuous progress of wetting front with Yam.12. When snowpack reaches wet state, whole inflow depleted as can be seen in Fig. 9. Last peaks gain shapes of inflow periods. After reaching the breaking point of saturation, water starts depleted quickly. In Yam.10 occurs wetting front that move forward continuously. That suggests that Yam.10 have better retention ability than Yam.12 because Yam.12 wetting front switch between two positions of θ [-] Fig. 9 also shows that Yam.10 snowpack holds almost ¾ of the whole inflow.

Error criterion NS shows that best result has Yam.12, RMSE and MSE gives best result for Yam.12.

Tab. 21 – Computed error criteria between Dischma measured outflow and simulation 1.

Parameters	NS	RMSE	MSE
Yam.12	0.443	2.950	8.707
Yam.10	-0.019	3.995	15.957
Yam.10 - Yam.12	0.073	3.807	14.496
Yam.10 - Hir.10	-0.019	3.995	15.959
Yam.12 - Yam.10	0.397	3.071	9.425
Yam.12 - Hir.10	0.399	3.066	9.401

For sensitivity analysis was used trimmed outflow curves for better clarity. All simulations deplete on begging and.

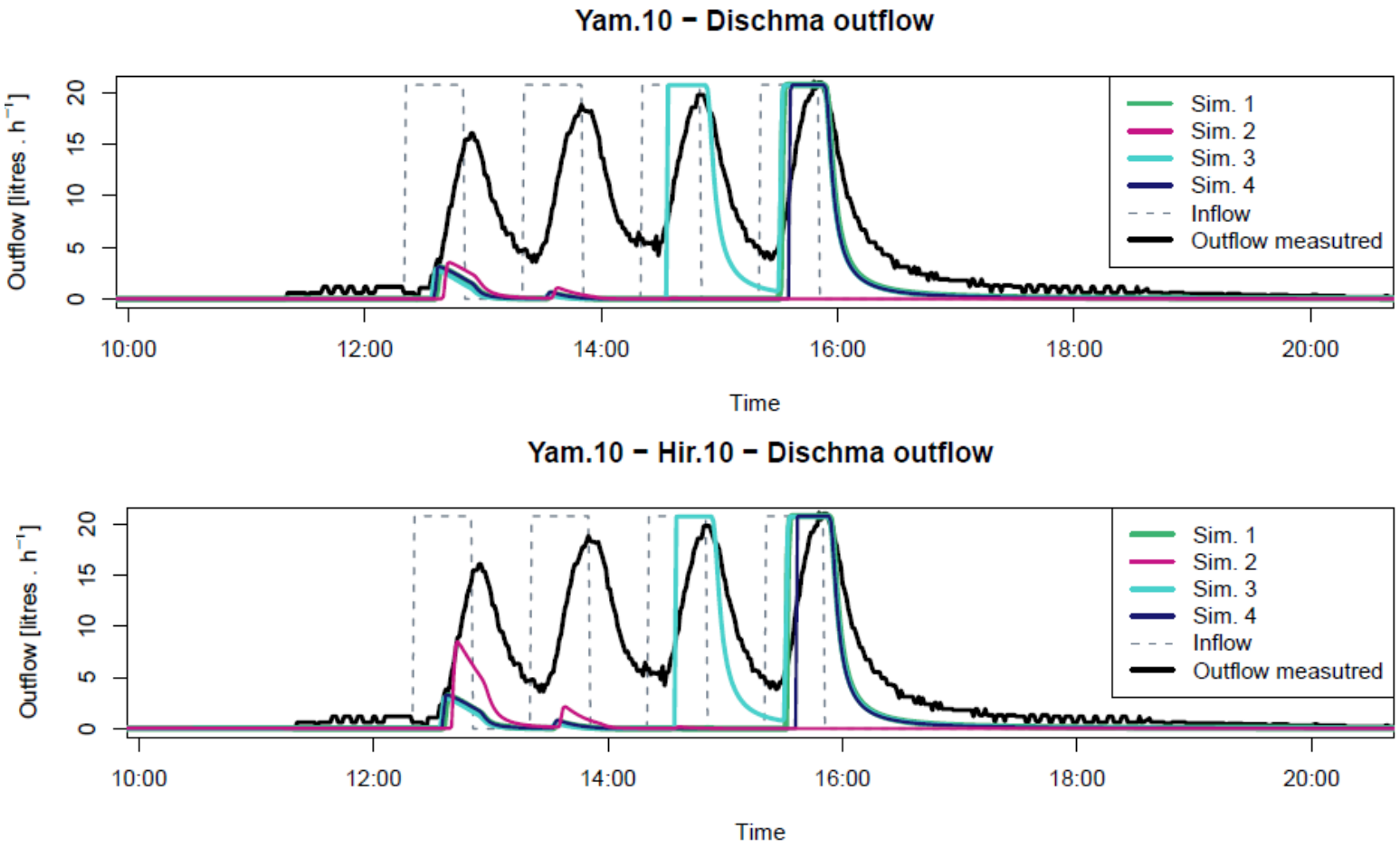

Fig. 11 – Sensitivity analysis with used setup from Tab. 24, Tab. 25, Tab. 26 and Tab. 27 (see appendix). Sim.1 have grain dimeter 1.5 mm, Sim.2 have d = 1mm, Sim.3 have d =2 mm and Sim.4 have d =1.5 mm and density reduced by 20 kg.m^{-3}.

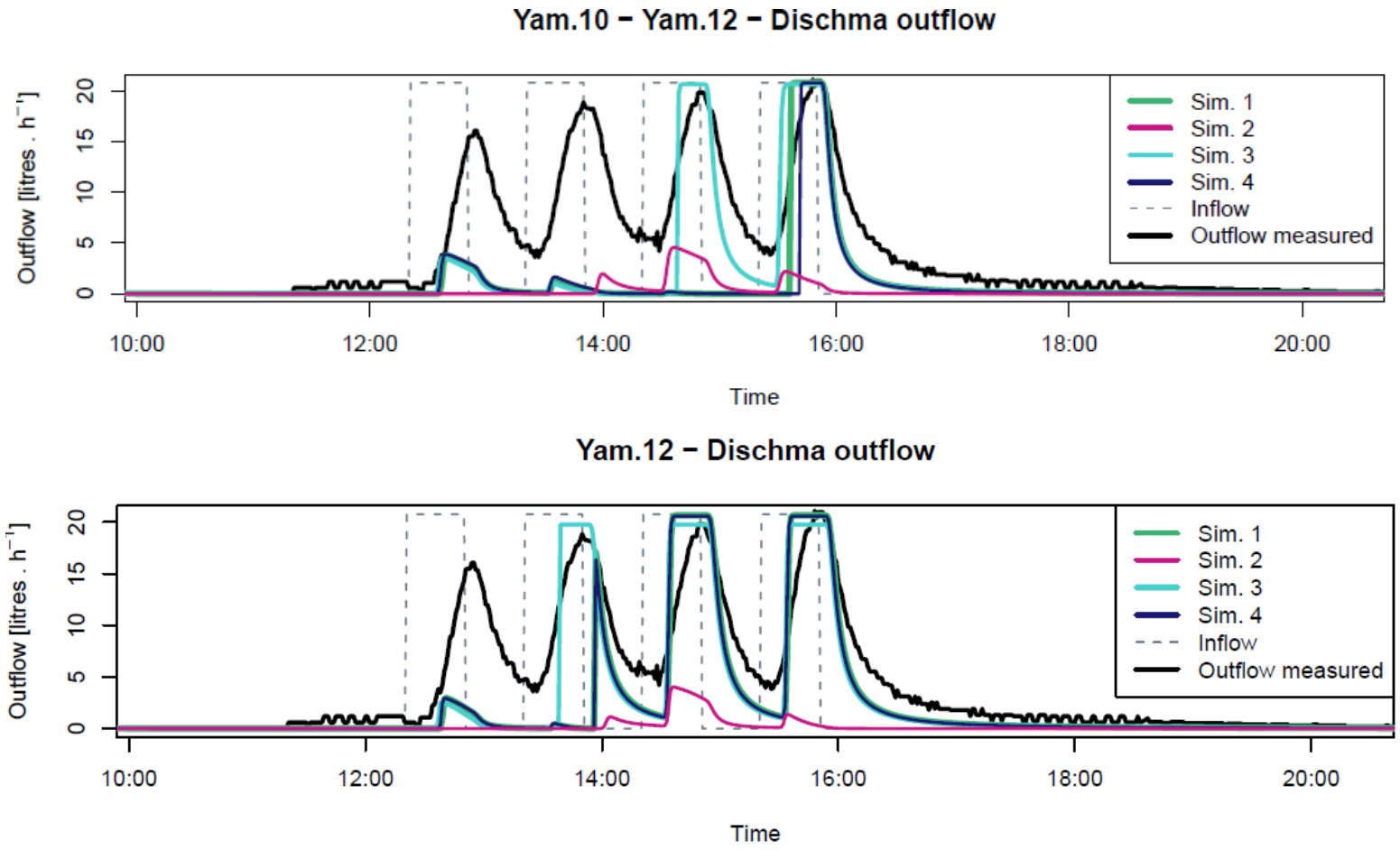

Fig. 12 - Sensitivity analysis with used setup from Tab. 24, Tab. 25, Tab. 26 and Tab. 27 (see appendix). Sim.1 have grain dimeter 1.5 mm, Sim.2 have d = 1mm, Sim.3 have d =2 mm and Sim.4 have d =1.5 mm and density reduced by 20 kg.m^{-3}.

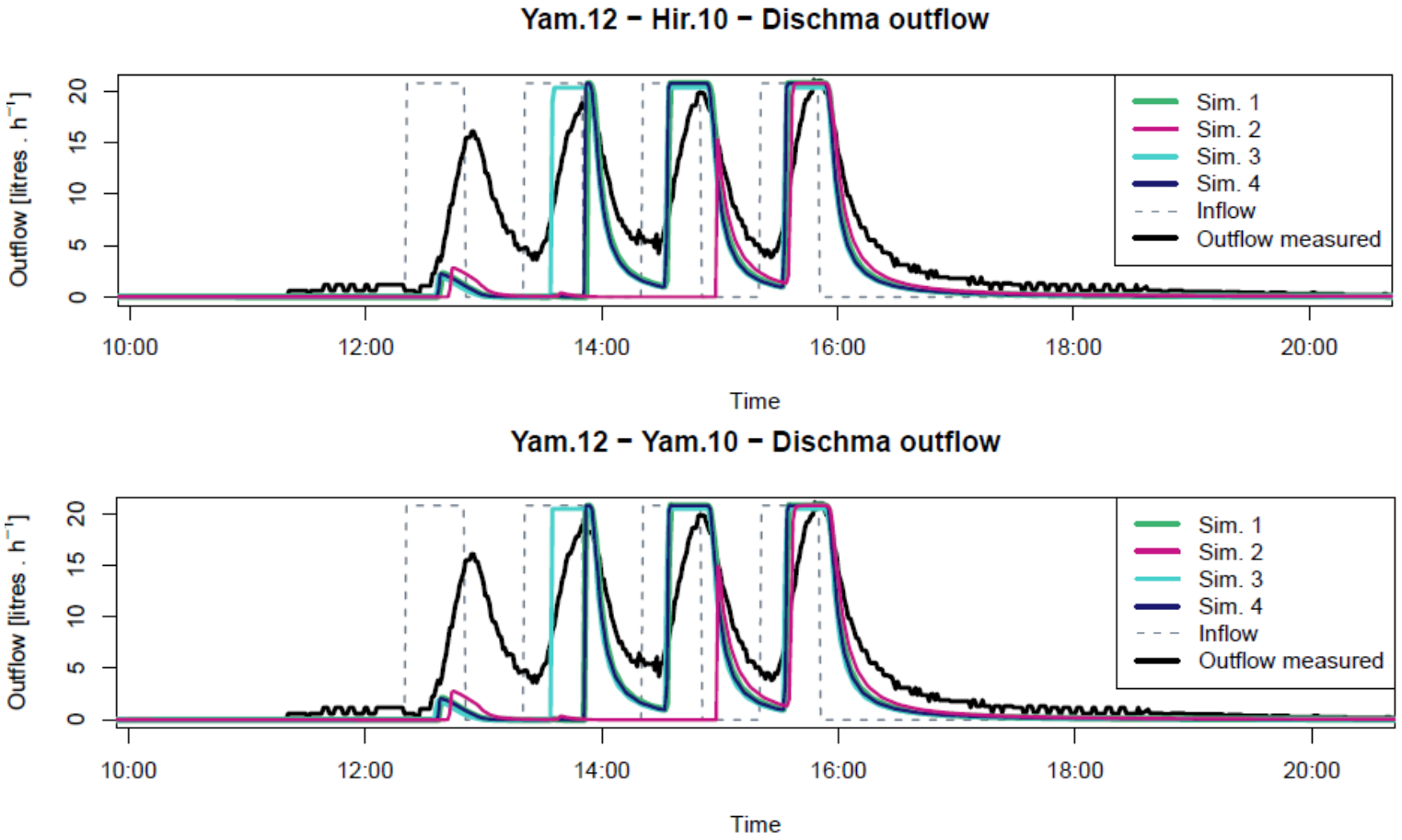

Fig. 13 - Sensitivity analysis with used setup from Tab. 24, Tab. 25, Tab. 26 and Tab. 27 (see appendix). Sim.1 have grain dimeter 1.5 mm, Sim.2 have d = 1mm, Sim.3 have d =2 mm and Sim.4 have d =1.5 mm and density reduced by 20 kg.m^{-3}.

Yam.10 shows small lag time with bigger density but only during the fourth sprinkling period. That is a consequence of the bigger conductivity that reacts to density. Grains with d = 1 mm cause inability to simulate outflow. Sim.2 shows outflow that acts similarly on beginning as sim.1, sim.3, and sim.4 but no more outflow occurs after the third and fourth sprinkling period. Flux along profile grows with wetting front and slows down when sprinkling stops. Conductivity of Yam.10 is much smaller with small grains and outflow is very sensitive to water content. When even minor volume of water depleted bottom, layer became less conductive and is not able to create more outflow. Because of low conductivity, the profile is not fully dry at the beginning of sprinkling. That cause outflow after first sprinkling period. Yam.10 shows sensitivity on grain size and even if it shows the same behavior on the beginning of outflow as other simulation breaking point of conductivity increase occurs with smaller water content and after the second inflow peak with the sim. 3 start profile depleted all volume of inflow. Sim. 1 with 1.5 mm depletes after the third peak of inflow. Yam.10 – Hir.10 shows similar behavior but retain more initial water content than Yam.10 before conductivity breaking point, therefore, bigger outflow occurs after the start of sprinkling. Yam.10 – Yam.12 shows a response with lower density same as Yam.10 and Yam.10 – Hir.10 but sim.1 shows bigger lag that can be linked to n parameter that include density. Sim.2 with d = 1mm shows different behavior than Yam. 10 that is also linked to n parameter. Yam.10 – Yam.12 flux slow down between layers and because water content before sprinkling is smaller than with Yam.10 water first fill free capacity and starts to percolate at end of third inflow peak.

Yam.12 scenario initiated greater outflow than Yam.10 – Yam.12 but the difference between the same grains and different density disappear. Sim.1 and sim.4 behaved almost the same. This is a consequence of α parameter that with changing density shifts pore distribution curves in suitable ranges. Differences should appear with smaller densities and bigger grains. Yam.12 also shows bigger outflow with the sim. 1, sim. 3 and sim. 4. despite fact that sim. 2 is similar to Yam.10 – Yam.12., Yam.12 scenario is more sensitive to coarser grains. Pores are more distributed, but in wider ranges, whereas Yam.10 – Yam.12 change with density only slope. Yam.12 – Yam.10 and Yam.12 - Hir.10 behaves similarly to every simulation. Because of the uniform change in pore distribution parametrization creates big outflow rates. With higher densities, pores distribution has the

same slope but in smaller pore diameter range. In *Fig. 13* - Fig. 13 can be seen big sensitivity on d =2 mm. Grains are able to simulate three inflow periods but, it can be seen that outflow gain shape of inflow periods. That is the influence of significant breaking point of conductivity that with given volumetric water content switch from small values to unrealistic high values.

6.2 Flüela results

Flüela simulation 1 has no initial outflow that was created by computational initialization so the result is not trimmed, but as can be seen on the beginning occurs outflow resulting from initial conditions of the snowpack. According to simulations, snowpack is not able to hold measured wetness and depleted in rates 5 – 10 [litres.h^{-1}]. Recapitulation of simulation is as follows:

- Simulation 1 – measured state with ice layers: d = 0.5, ρ = 700 kg.m^{-3}
- Simulation 2 – measured state with ice layers: d = 1.5, ρ = 700 kg.m^{-3}
- Simulation 3 – top and bottom layers enlarged d = 1 mm with ice layers: d = 0.5, ρ = 700 kg.m^{-3}
- Simulation 4 – top and bottom layers enlarged d = 1 mm with ice layers: d = 0.5, ρ = 800 kg.m^{-3}

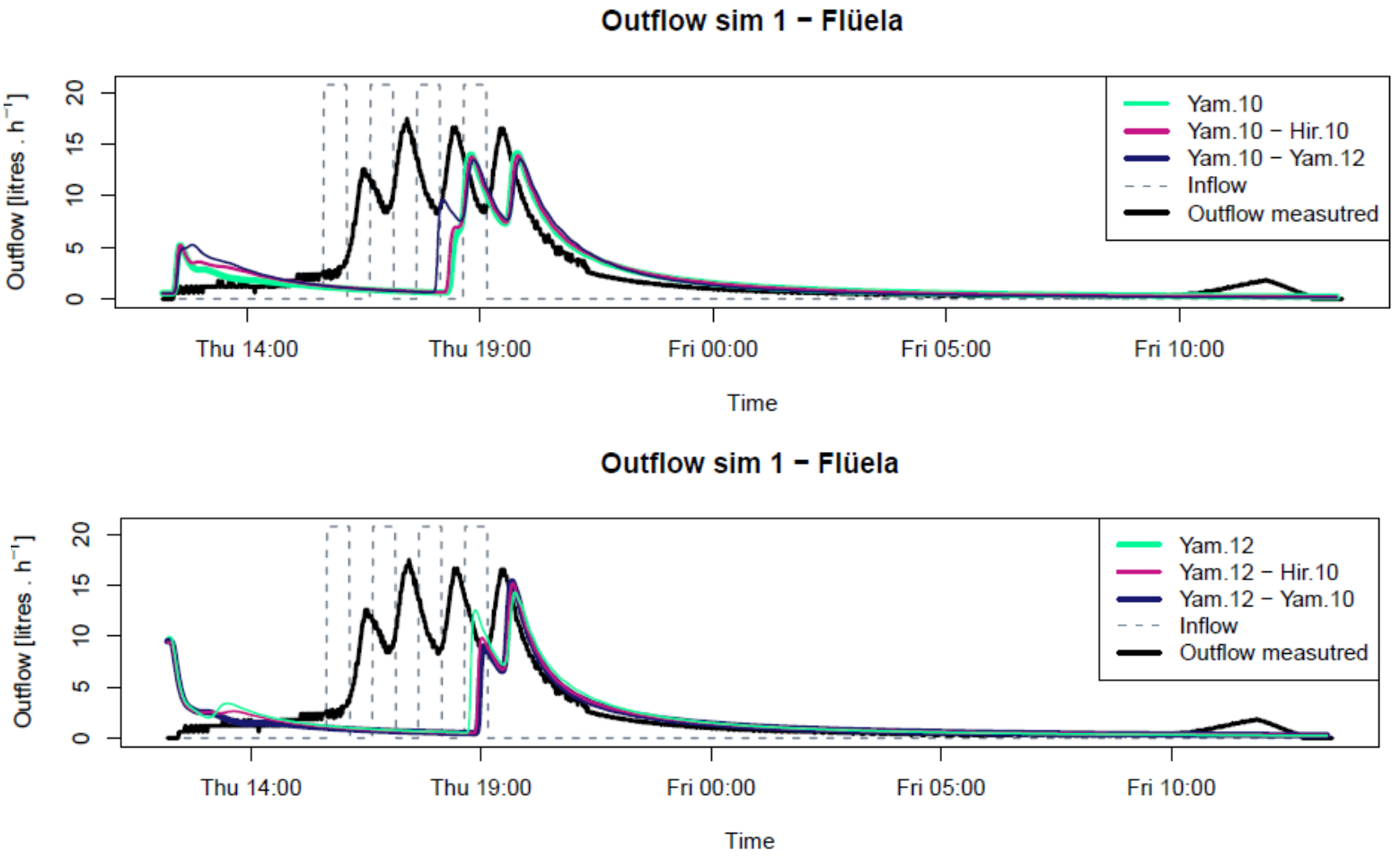

Fig. 14 - Simulated outflow with every parameter combination by DRUtES with profile description that can be seen on Tab. 28 (see appendix) and compared to measured inflow and total outflow.

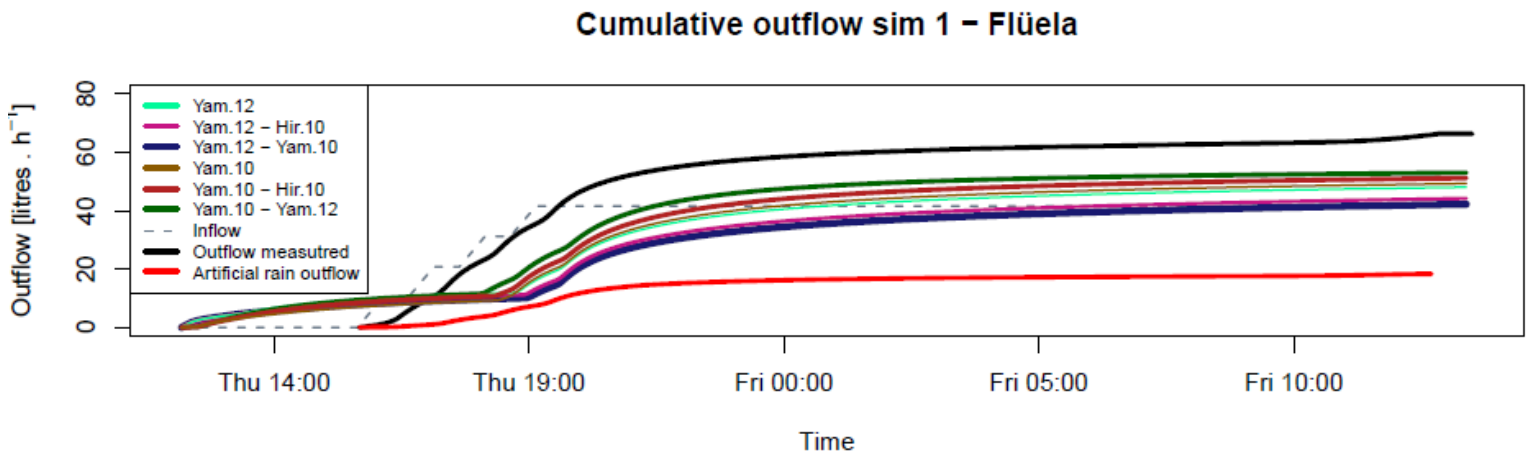

Fig. 15 - Simulated cumulative outflow with every parameter combination by DRUtES with profile description that can be seen on Tab. 28 (see appendix) and compared to measured inflow, artificial rain that is separated only rain outflow and total outflow that is rain plus non rain water contribution.

Combination of parameters looks again similar for parameter α but unlike in Dischma simulations, group with Yamaguchi et al., (2010) α shows a better result. In Flüela snowpack was the contribution of artificial rain outflow relatively small because of initial LWC that was pushed out from snowpack first. Rain took place after LWC and outflow are balanced. In Fig. 15 seems a simulated volume of outflow strange because it exceeded inflow. Flüela cumulative outflow seems to be closer to reality but from the wrong reasons. Parametrization describes snowpack that is not able to hold initial water content.

Yam.10 shows less θ [-] above the ice layers which suggest higher permeability compared to Yam.12 parametrisation. Therefore Yam.10 shows bigger total outflow. Yam.10 ice layers with 0.5 mm grain conduct water in higher rates than Yam.12 and vice versa with the coarser grains. Bottom layer with initial water content 0.04 [-] depleted immediately after the start of simulation with Yam.12 but with Yam.10 was reaction slower. This is a consequence of not including density into parametrization. On the other hand, with extreme densities is this approach unreliable

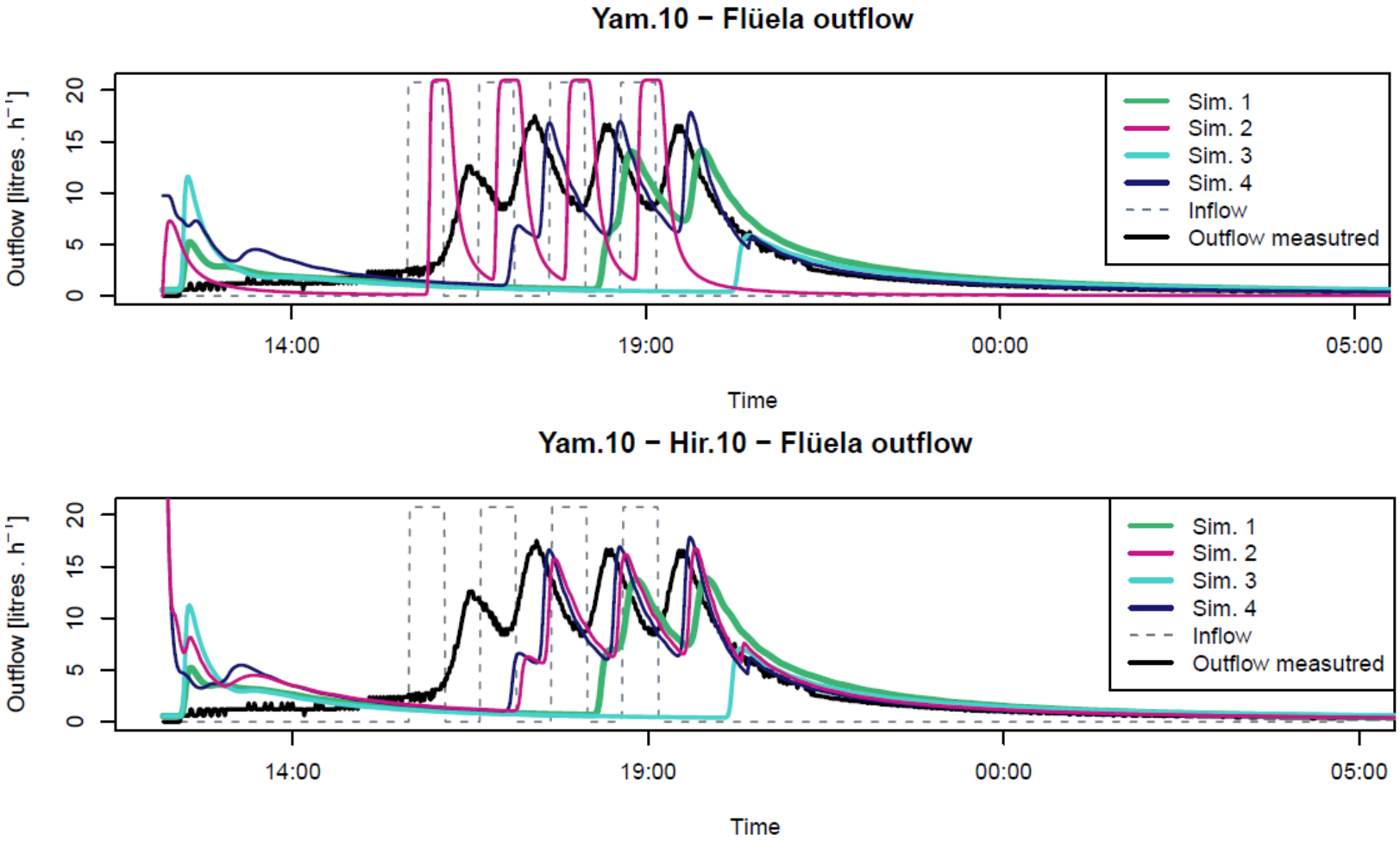

Fig. 16 - Sensitivity analysis for Yam.10 and Yam.10 – Hir.10 parameters on Flüela snowpack. Sim. 1 describe the measured state of snowpack and ice layers with d = 0.5 mm and density of 700 kg.m^{-3}. Sim. 2 is with ice layers of 1.5 mm and 700 kg.m^{-3}. Sim. 3 is with top and bottom layer set to 1 mm grains and ice layers with d = 0.5 mm and density of 700 kg.m^{-3}. Sim. 4 is the same as a sim. 3 but ice layers d = 0.5 mm and density of 800 kg.m^{-3}. Input values for all sim. can be found in Tab. 28, Tab. 29, Tab. 30 and Tab. 31 (see appendix).

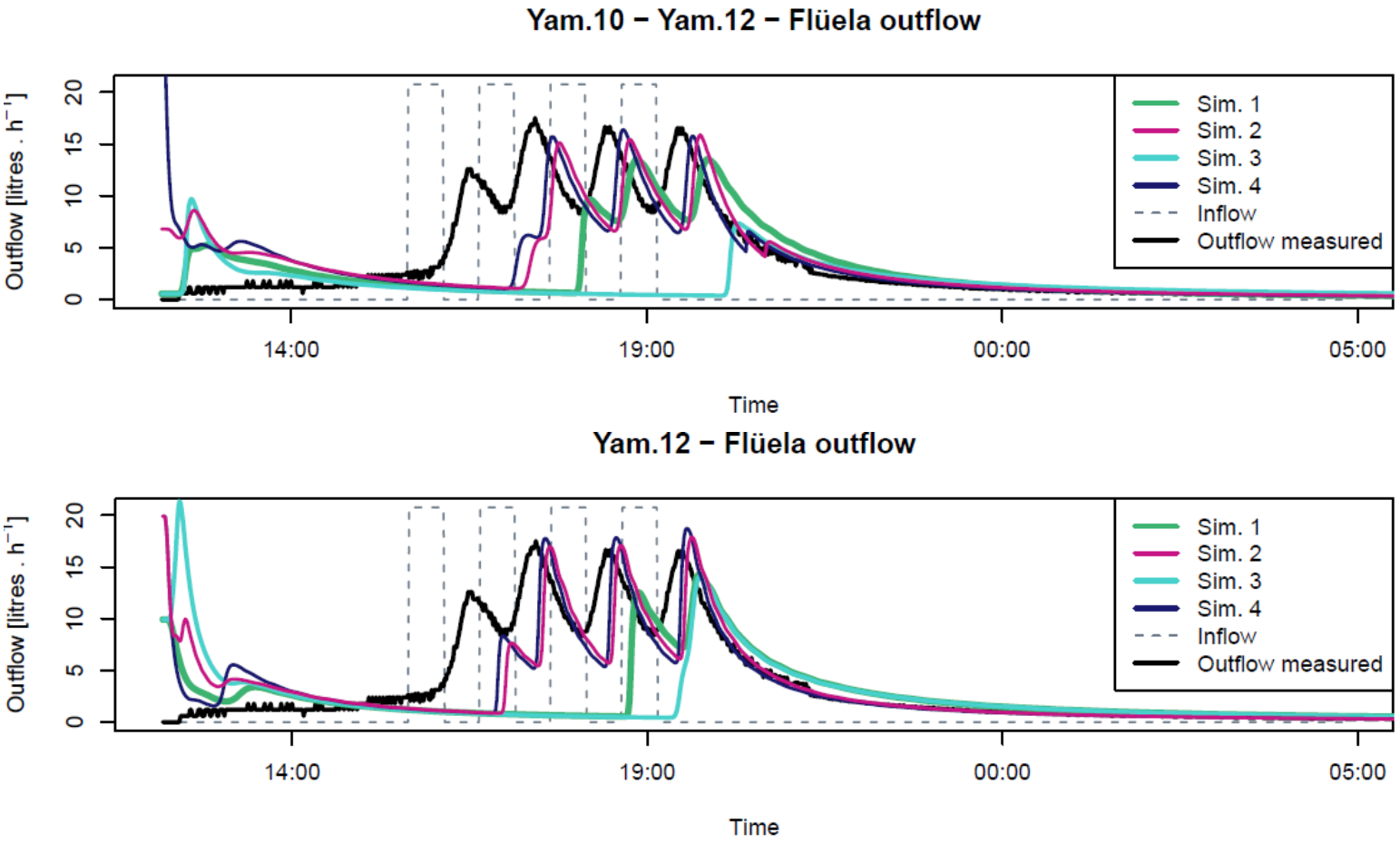

Fig. 17 - Result of sensitivity analysis for Yam.10 -Yam.12 and Yam.12 parameter on Flüela snowpack. Sim. 1 describe the measured state of snowpack and ice layers with *d* 0.5 mm and density of 700 kg.m^{-3}. Sim. 2 is with ice layers of 1.5 mm and 700 kg.m^{-3}. Sim. 3 is with top and bottom layer set to 1 mm grains and ice layers with *d* 0.5 mm and density of 700 kg.m^{-3}. Sim. 4 is the same as a sim. 3 but ice layers *d* is 0.5 mm and density of 800 kg.m^{-3}. Input values for all sim. can be found in Tab. 28, Tab. 29, Tab. 30 and Tab. 31 (see appendix).

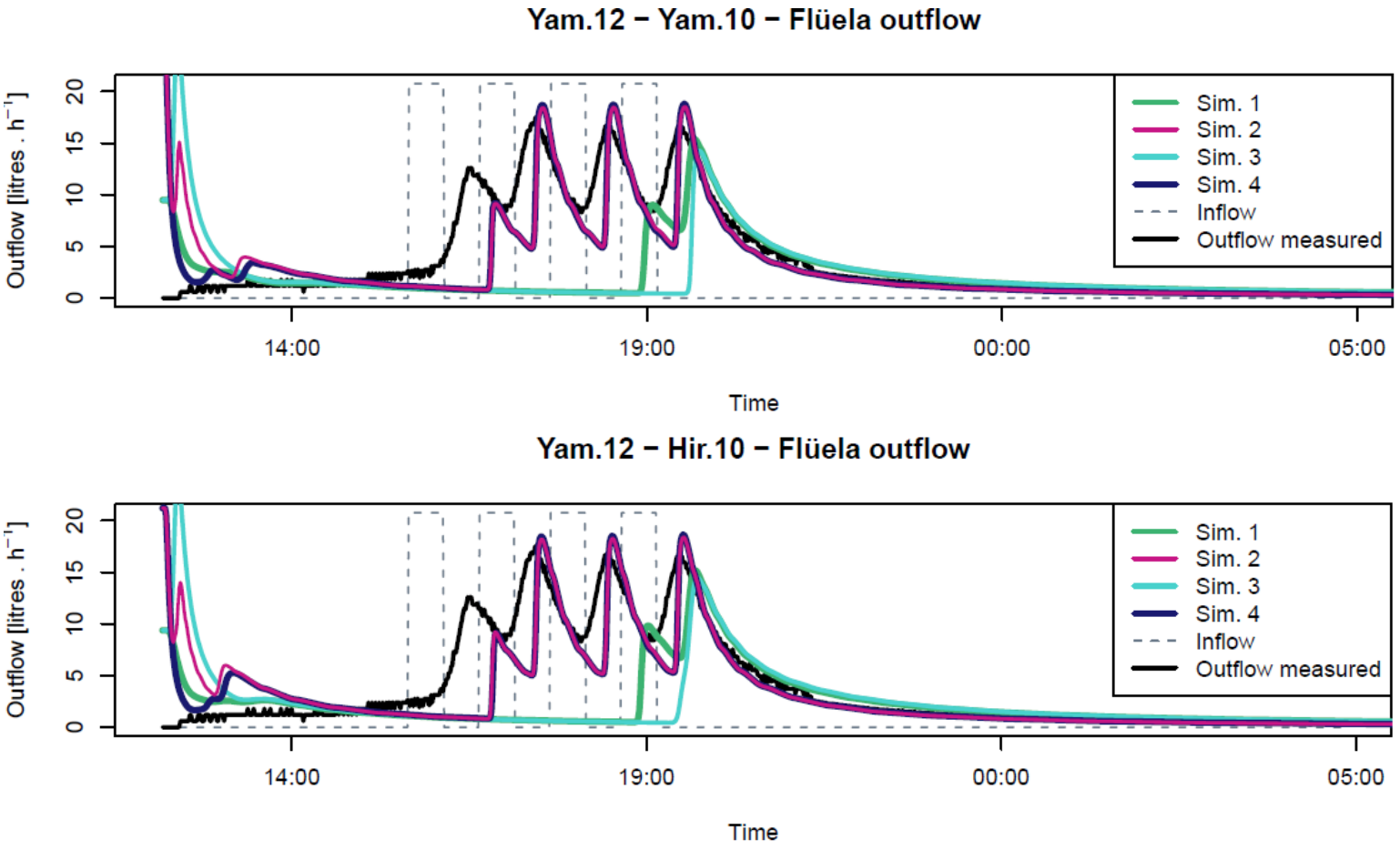

Fig. 18 - Result of sensitivity analysis for Yam.10 -Yam.12 and Yam.12 parameter on Flüela snowpack. Sim. 1 describe the measured state of snowpack and ice layers with *d* 0.5 mm and density of 700 kg.m^{-3}. Sim. 2 is with ice layers of 1.5 mm and 700 kg.m^{-3}. Sim. 3 is with top and bottom layer set to 1 mm grains and ice layers with *d* 0.5 mm and density of 700 kg.m^{-3}. Sim. 4 is the same as a sim. 3 but ice layers *d* is 0.5 mm and density of 800 kg.m^{-3}. Input values for all sim. can be found in Tab. 28, Tab. 29, Tab. 30 and Tab. 31 (see appendix).

Outflow from initialization of computation reaches high values. For better visualization of sensitivity analysis was this outflow trimmed. Yam. 10 overshoot conductivity of ice layers even with the sim. 2. Outflow is with small lag equal to inflow with a comparison to Yam.10 – Hir.10 have Yam.10 bigger retention and is able to conduct water without supplementation of initial water content. Yam.10 -Hir.10 adjust the *n* behavior not only for coarse grains but even for smaller ones. As can be seen in Fig. 4 unlike Yamaguchi et al., (2010) *n*, the curve is nonlinear. Sim. 2 with Yam.10 is similar to Dischma snowpack when outflow was fast enough to copy the inflow curve. Sim.3 that should help snowpack depleted faster with same ice layer setup as a sim. 1 but with bigger grains on the top and bottom layer do the exact opposite. Due to high conductivities of the top and bottom layer sim. 3 lost more water from initial water content and because the flux is slowdown by ice layers it took longer to fill loses. First, two ice layers from the top are 0.3 cm thick so their influence is smaller than bottom ice layer that is 1 cm thick. The second layer from the bottom was due to smaller hardness set to bigger grains, therefore, is more permeable.

Sim. 3 resulted in the smallest outflow from all simulation with every parameter because initial loss has the same influence on all of them. Quite a good result show sim. 2 with bigger grains are ice layers more permeable. Unlike with Dischma snowpack combination of ice layers and small grains in the top and bottom layer, snowpack do not deplete from initial water content and inflow is slow down. The First peak is therefore bigger, compared Dischma outflow and lag time is much shorter. The impulses of inflow driven by ice layers suppressed influence of parametrization to each layer. Grains of middle layers are big enough to conduct water efficiently.

In Fig. 16, Fig. 17 and Fig. 18 can be seen paradoxical situation between sim.3 and sim.4. Both of them have bigger grains on the top and bottom layer but while sim. 3 have underestimated outflow, sim. 4 with denser ice layer equals to sim. 2. Sim. 2 have more permeable ice layer and because of slowed down flux two bottom ice layers don't cause water ponding. Their conductivity is big enough to cope with the outflow from less dense and bigger grain ice layers above. Sim. 3 and sim. 4 cause ponding due to inflow from the top layer but as can be seen denser layer reach smaller θ [-] because of restriction from θ_s [-]. Even though sim. 3 conduct water faster than sim. 4 outflow is smaller than the

sim. 4 because of the bigger capacity. More water was held by snowpack while sim. 4 created outflows.

Error criteria will be in this case computed for simulation 2 because there was uncertainty from ice layer description and sim. 1 apparently gives a worse result than sim. 2. Both of simulation had measured input values but different ice layers description.

Tab. 22 - Error criterions for simulation 2.

Parameters	NS	RMSE	MSE
Yam.12	-0.306	4.739	22.461
Yam.10	-0.293	4.716	22.236
Yam.10 - Yam.12	-0.268	4.669	21.804
Yam.10 - Hir.10	-0.279	4.689	21.987
Yam.12 - Yam.10	-0.391	4.889	23.911
Yam.12 - Hir.10	-0.335	4.791	22.954

NS shows best result for Yam.10 – Yam.12, RMSE shows the best result for Yam.10 but all of the parametrizations is really close together. MSE Shows best result for Yam.10 – Yam.12.

6.3 Sertig results

All simulations for Sertig snowpack have at the beginning outflow from initialization that reaches high values. For better visualization of simulation results will be this outflow trimmed. Recapitulation of simulations is as follows:

- Simulation 1 – measured state with ice layers: d = 1.5 mm, ρ =700 kg.m^{-3}
- Simulation 2 – all layers have d reduced by 0.5 mm with ice layers: d = 1.5 mm, ρ =700 kg.m^{-3}
- Simulation 3 – all layers have d enlarged by 0.5 mm with ice layers: d = 1.5 mm, ρ =700 kg.m^{-3}

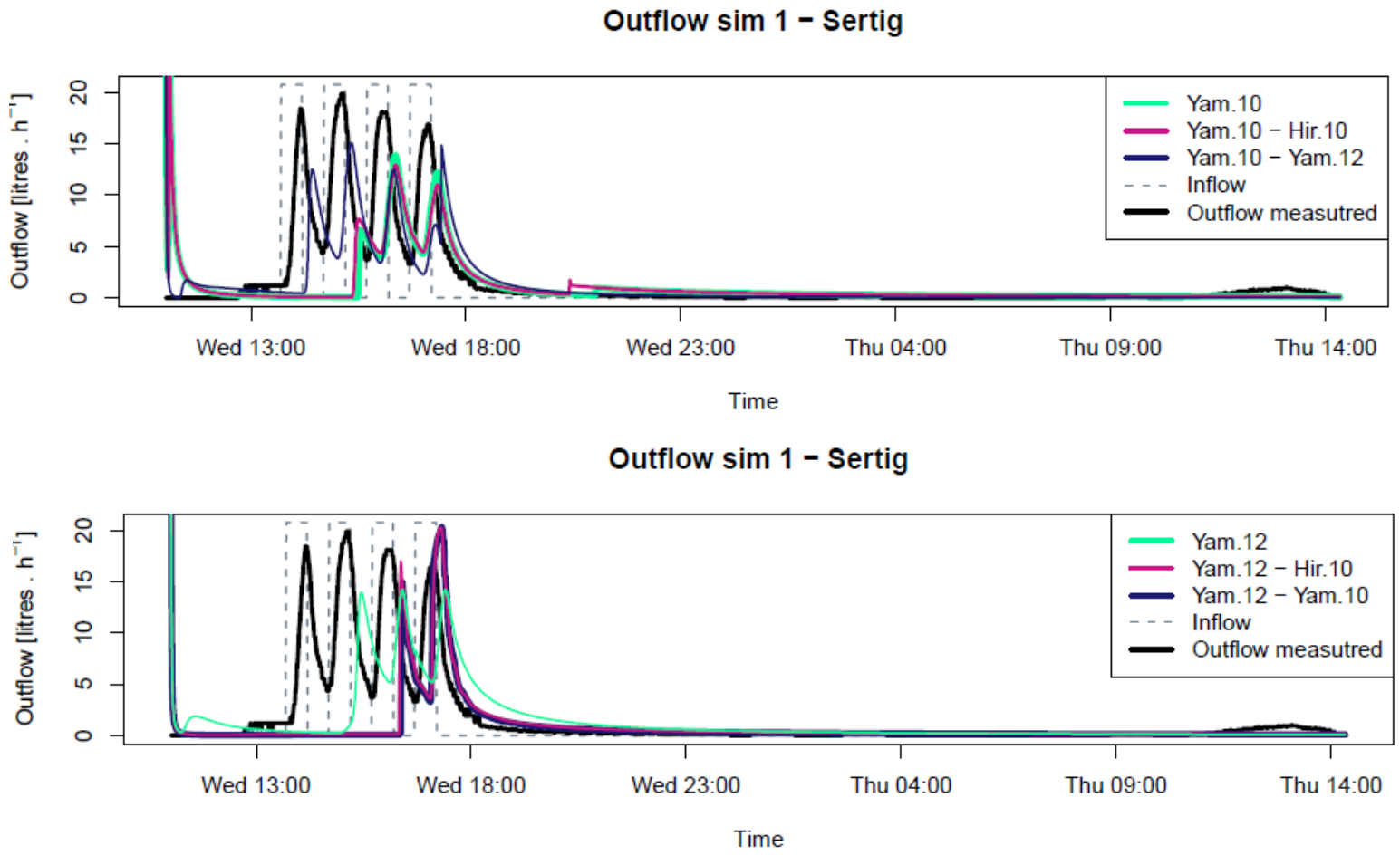

Fig. 19 - Simulated outflow with every parameter combination by DRUtES with profile description that can be seen on Tab. 32 (see appendix) compared to measured inflow and total outflow.

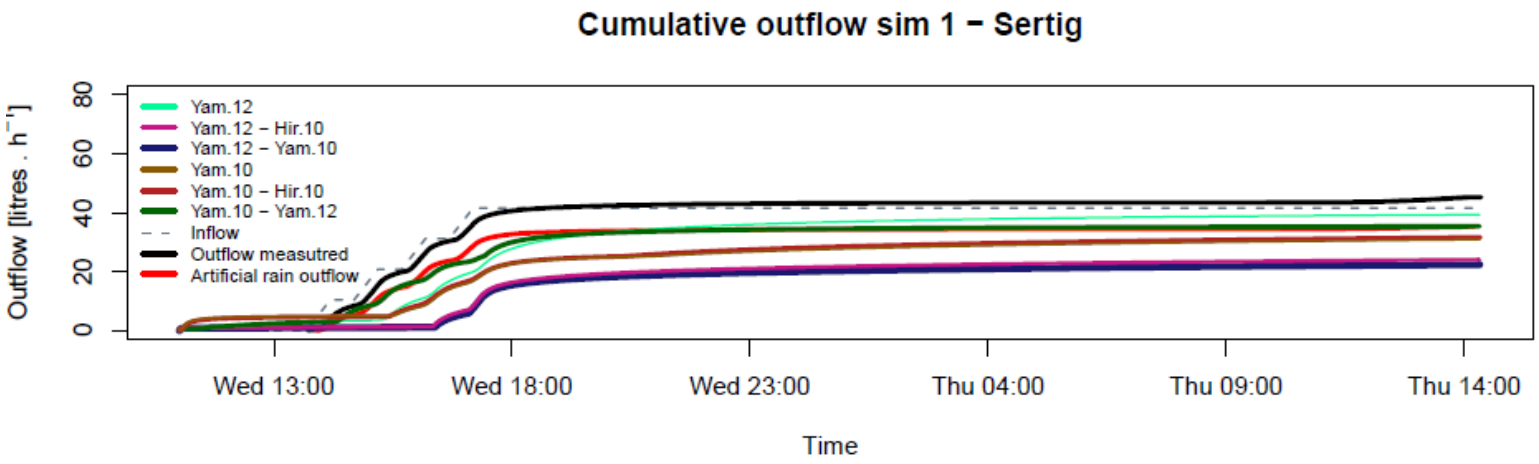

Fig. 20 - Simulated cumulative outflow with every parameter combination by DRUtES with profile description that can be seen on Tab. 32 (see appendix) and compared to measured cumulative inflow, artificial rain that is separated only rain outflow and total outflow that is rain plus non rain water contribution.

Sertig snowpack contained a small initial water content that should help simulation to be more precise because the measured density of snow is closer to bulk dry density than previous profiles. As can be seen in Fig. 19 parameters are not similar as always along α, but differs with Yamaguchi et al., (2012) n. Yam.12 and Yam.10 – Yam.12 gives the biggest outflow from all parametrization and create outflow from initial water content.

Yam.12 have lower initial pressure heads than Yam.10. During sprinkling are values of Yam.12 pressure head closer to zero than Yam.10 values. Yam.12 tends to create big grain distribution with small densities and big grains and it result in a better ability to retain water. Yam.12 reaches sooner saturation and conduct water faster. With previous cases result in this behavior on the significantly smaller outflow but in this case is density lower so, snowpack is not able to retain big volumes of water. This is the reason why Yam.12 – Yam.10 and Yam.12 – Hir.10 showed the worst results. On cumulative outflow result can be seen that Yam.12 is bigger than artificial sprinkling but it is caused by an inability to hold initial water content of the denser bottom layer. Rest of parameter s have a lower volume of cumulative outflow than artificial sprinkling

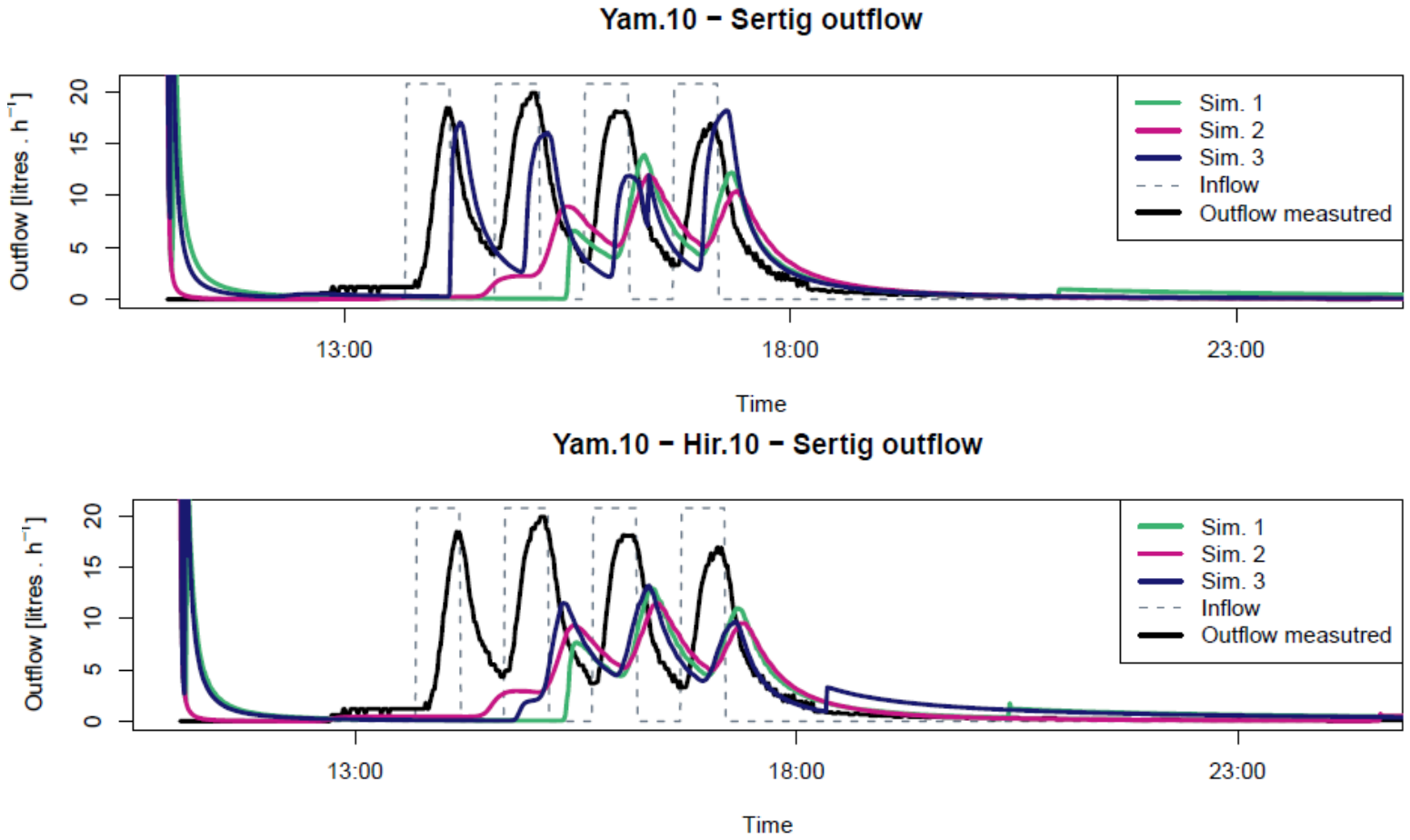

Fig. 21 – Result of sensitivity analysis for Yam.10 and Yam.10 – Hir.10 parameters on Flüela snowpack. Sim. 1 describes the measured state of snowpack and ice layers with *d* 1.5 mm and density of 700 kg.m^{-3}. Sim. 2 is with all grain size reduced by 0.5 mm and ice layers with *d* 1.5 mm and density of 700 kg.m^{-3}. Sim. 3 is with all grain size enlarged by 0.5 mm and ice layers with *d* 1.5 mm and density of 700 kg.m^{-3}. Input values for all sim. can be found in, Tab. 32, Tab. 33 and Tab. 34 (see appendix).

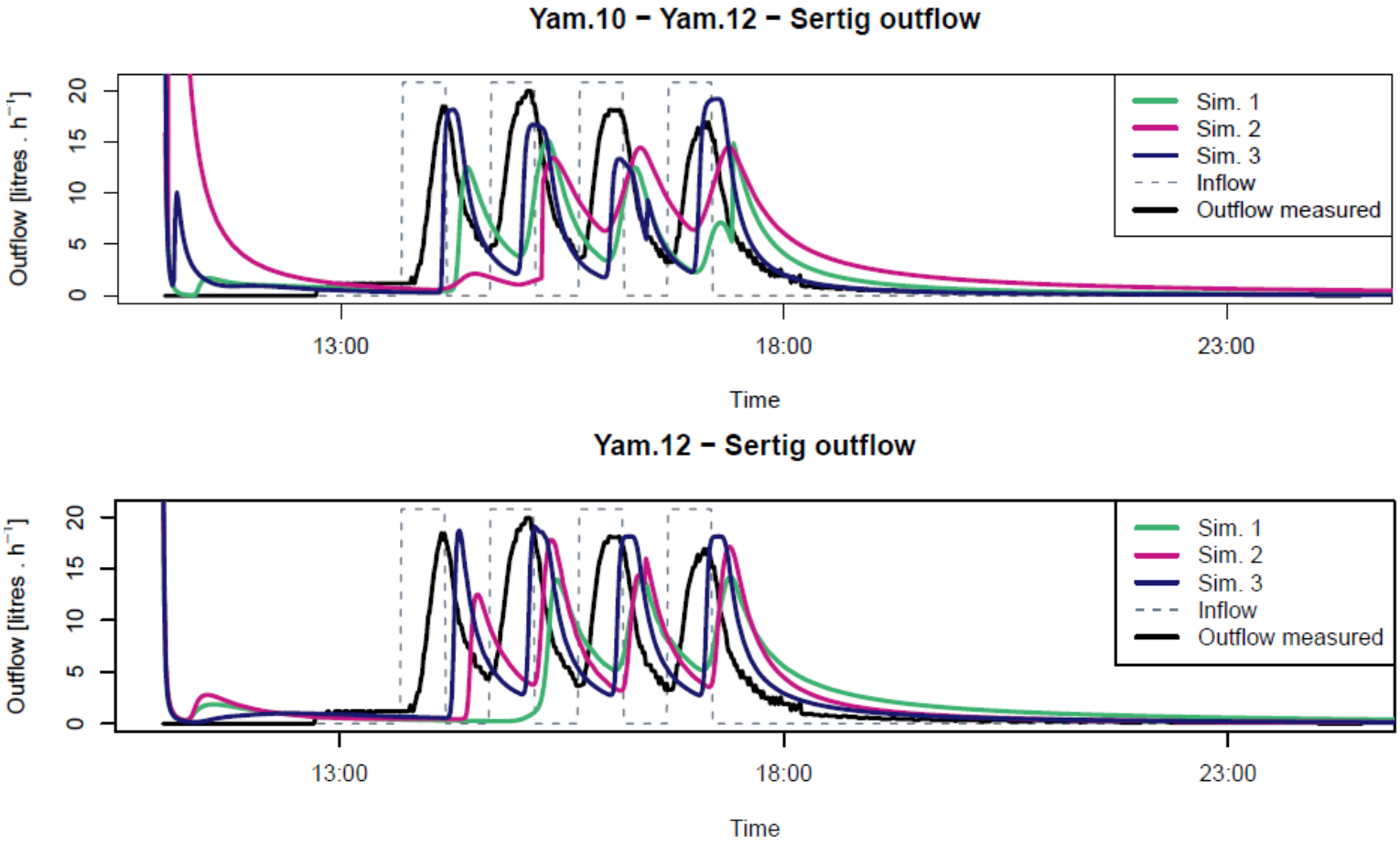

Fig. 22 – Result of sensitivity analysis for Yam.10 and Yam.10 – Hir.10 parameters on Flüela snowpack. Sim. 1 describes the measured state of snowpack and ice layers with *d* 1.5 mm and density of 700 kg.m^{-3}. Sim. 2 is with all grain size reduced by 0.5 mm and ice layers with *d* 1.5 mm and density of 700 kg.m^{-3}. Sim. 3 is with all grain size enlarged by 0.5 mm and ice layers with *d* 1.5 mm and density of 700 kg.m^{-3}. Input values for all sim. can be found in, Tab. 32, Tab. 33 and Tab. 34 (see appendix).

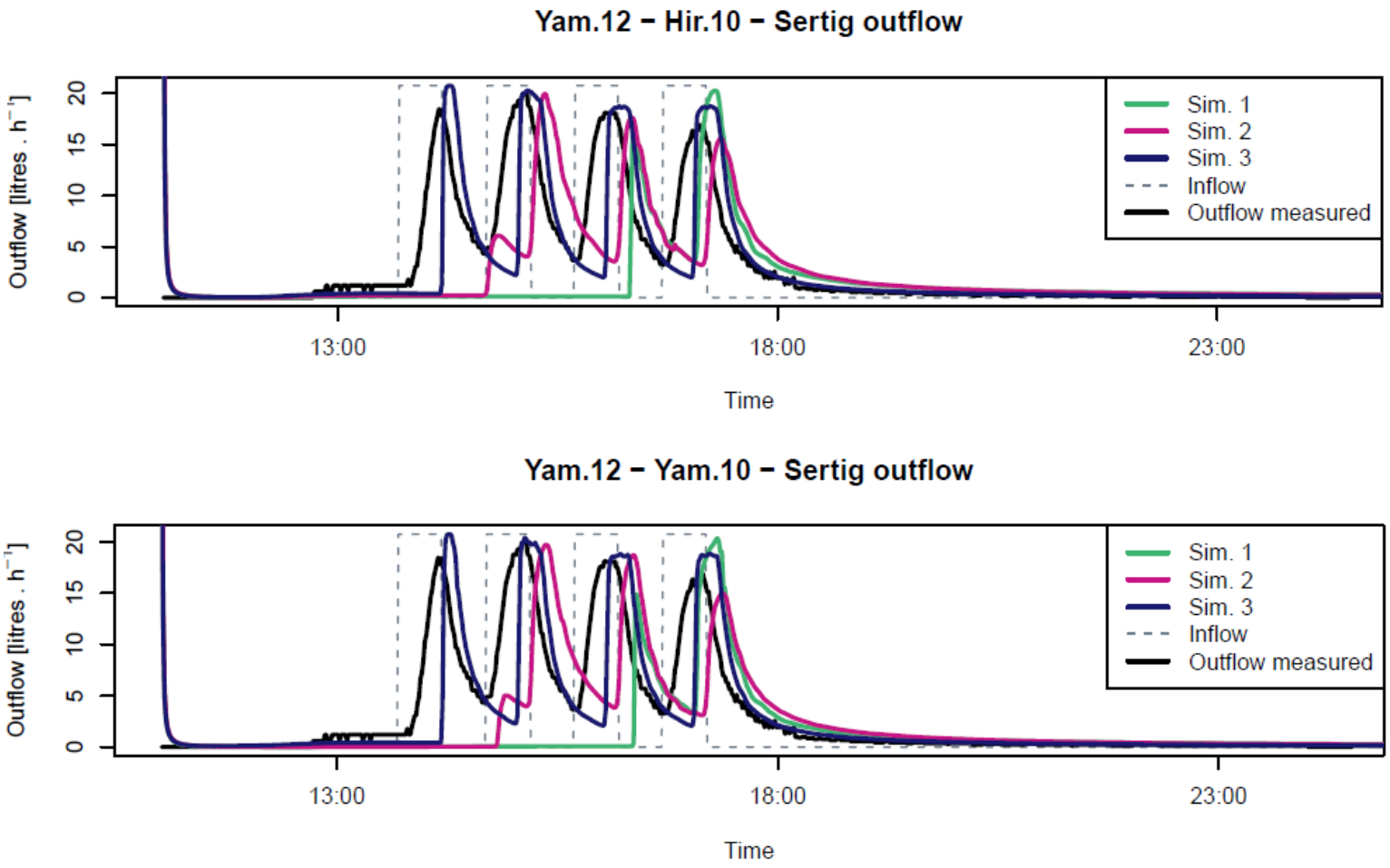

Fig. 23 – Result of sensitivity analysis for Yam.10 and Yam.10 – Hir.10 parameters on Flüela snowpack. Sim. 1 describes the measured state of snowpack and ice layers with *d* 1.5 mm and density of 700 kg.m^{-3}. Sim. 2 is with all grain size reduced by 0.5 mm and ice layers with *d* 1.5 mm and density of 700 kg.m^{-3}. Sim. 3 is with all grain size enlarged by 0.5 mm and ice layers with *d* 1.5 mm and density of 700 kg.m^{-3}. Input values for all sim. can be found in, Tab. 32, Tab. 33 and Tab. 34 (see appendix).

Yam10 and Yam.10-Hir10 reacted differently with coarse grains. While Yam.10 outflow increases, Yam.10 – Hir.10 remain the same as two previous simulations.

Yam.10 – Hir.10 resulted worse conductivity in a denser layer with big grains compared to Yam.10, therefore, ponded water occurs on barriers between two layers. The increase of θ [-] around 30 cm is caused by a change of density in a layer with same initial θ [-] and same grain size. Density increase from 254 kg.m^{-3} to 311 kg.m^{-3}, therefore conductivity decrease, and incoming flux is slow down by layer with 0.5 mm d. Ice layers at the depth of 9.5 and 15.5 cm do not pond water and flow are continuous through them because of unrealistic growth of conductivity with saturation, on the interface of layers with different density arises great flux velocity that saturates ice layers that can cope with the flow. Small grain reduced the difference of conductivity between layers with different densities, so flux is not reaching great values. When water percolates deeper in slower rates it is not able to saturate ice layers anymore, so they remain with low conductivity.

Yam.10 – Yam.12 and Yam.12 show the influence of *n* parameter that overestimated pore distribution. Smaller grains conduct more water due to fast gained water content. On the other hand, this principle is not working anymore with enlarged grains because of sim. 3 creates the biggest outflow volume from all simulation. Bigger grains are more distributed but also have bigger pores and in combination with small density act porous medium like this as coarse sand. Yam.12 – Yam.10 and Yam.12 – Hir.10 that do not overestimate distribution so much creates with the sim. 3 biggest outflow volume from all parameters because of small ability to retain water.

Tab. 23 - Error criterions for simulation 1.

Parameters	NS	RMSE	MSE
Yam.12	0.127	3.776	14.259
Yam.10	-0.076	4.193	17.584
Yam.10 - Yam.12	0.335	3.295	10.857
Yam.10 - Hir.10	-0.002	4.047	16.385
Yam.12 - Yam.10	-0.129	4.296	18.458
Yam.12 - Hir.10	-0.097	4.235	17.939

NS shows best result for Yam.10 – Yam.12, RMSE, and MSE shows the best result for Yam.10 – Yam.12.

6.4 Summary

The main task of this thesis was to try van Genuchten model parametrization for snow on real measured snowpack outflow and test its sensitivity on change of input values. It was proven that simplification is not sufficient to described outflow reliably on different types of the snowpack. Parameters were suggested based on the low variance of samples and especially conductivity gives values that are far from real conditions. Calonne et al., (2012) create an equation for intrinsic permeability based on the higher variation of snow samples than Yamaguchi et al. (2010, 2012) and it gives better results than previous approaches from Shimizu, (1970) and Carman-Kozeny model. Problem is that this approach gives high values of conductivities even with small θ [-]. Uncertainty could arise from an input value of grain radius because Calonne et al., (2012) uses the equivalent spherical radius that is determined from the specific surface area of snow. Data for this thesis does not contain this type of information so as simplification was used measured grain radius. This simplification could play role in simulation precision, but it does not explain big values of conductivities. So, the question is if this is a reliable approach to compute intrinsic permeability for the purpose of van Genuchten model. Calonne et al., (2012) uses averaged intrinsic permeability in three dimensions and states that it is not affected by anisotropy but could be permeability averaged even in time under influence of rain on snow event? Waldner et al., (2004a) states that the uncertainty of models raises from snow hydraulic properties. Colbeck, (1986, 1979, 1983, 1982) describes how snow grains changes under the influence of the environment. With higher temperatures, grains grow and became less bonded and compact. Smaller grains distinguished in coarser grain clusters and with that comes a change of hydraulic properties, especially in the wet snowpack. Based on sensitivity analysis in this thesis could grain size change, have a big impact.

Due to the complicated structure of snowpack, modeled outflow show an unpredictable response. Conductivity causes that values of LWC in snowpack varies from residual water content to full saturation, but these numbers are just suggested in the purpose of model initialization. It is not possible that snowpack could have 60 % water content as can be

seen on Sertig snowpack because it becomes slush with water content up to 40 % (Fierz et al., 2009). The model also causes outflow from initial water content but in the same simulation could cause big ability to retain inflow liquid water. Inflow, therefore, goes into the dry snowpack. Kattelmann and Dozier, (1999) state that increase of liquid water into snowpack have no obvious influence on the rate of densification averaged through snowpack but the result shows that determination of the bulk dry density of snow could improve precision because of parametrization sensitivity especially on snow with lighter densities. Parametrization is not suitable for all types of snow. The important factor is not just density and grain size but even uniformity of grains and pores distribution because the bad interpretation of these factors could result into poorly modeled outflow.

Model neglect preferential flow but when it uses as input wet snowpack with observed matrix flow in real conditions it gives bad result too. This could be credited to the conductivity that creates outflow from initial conditions and subsequently replenishment of water into the snowpack. This approach could give reliable result in total outflow because LWC is pushed out from snowpack and input water took its place (Juras et al., 2017) but it did not happen. Also, Wever et al., (2014) describe that RE models cause lag due to simulating matrix flow instead of preferential flow and suggested that setup of $\theta_r < \theta$ [-] should compensate this issue but due to retention capacity with a combination of high conductivity this approach did not help. Dischma snowpack was not able to release even half of the inflow because of big retention capacity. Flüela snowpack that has bigger density, but smaller grains were able to even with ice layers to deplete bigger outflow than artificial rain volume. Parametrization with smaller grains does not overestimate distribution. Flüela snowpack has the major contribution of melt into outflow that cannot be described by parametrization, but simulated outflow is closer to total outflow than to artificial rain outflow. Only explanations of these result are badly described ice layers that are more permeable, so inflow could deplete in bigger volumes. On the other side, permeable ice layers in conditions of Sertig snowpack do not result in the bigger outflow. Its function as a hardly permeable barrier depends only on the velocity of flux.

7 Conclusion

First question if outflow can be modeled on snowpack properties as density grain size and LWC. Results show that parametrization does not give reliable results whose inaccuracy can be explained by neglected preferential flow or melt. Result underestimate total outflow and create big unrealistic time lag, so modeled outflow is not able to produce first three outflow peaks with all experiment.

The second question was if parametrization working outside of measured samples range on real layered snowpack. The answer is that suggested parametrization have a really good approach to simplification but the snow types that cannot be described by parametrization are common in real conditions. Here should be said that for parametrization improvements is needed to include grain types and its relationship to density and porosity of snow. Because of this uncertainty, modelling of outflow with this approach can gives big errors.

The third question was how big influence has uncertainties of measured input values in the field. This question was answered with sensitivity analysis and it can be said that really depends on snowpack layering. Generally, small densities and bigger grains could case the big difference in outflow even with small changes of input values.

The last question was if LWC and melt water contribution could cause big inaccuracies with a used simple model. This cannot be answered by achieved results of this thesis because outflow simulated with real measured properties of the snowpack was not good enough to be able to draw the conclusion

8 Appendix

```
# amount of soil layers [integer]
0

#van genuchten porous medium parameters, if 1D specify the layer elevation
#      alfa [L-1]  |    n    |    m       | theta_r    | theta_s  |   specific storage    |
#-----------------------------------------1st layer-----------------------------------------------
#     silty clay
 0             0              0              0              0             0

#anisothprophy description
#angle [degrees]  | K_11   |  K_22   | K_33
#-------------------------------------------------
0.0            0


# init. cond [real] | type of init. cond (hpres, H_tot, theta) |  RCZA method [y/n] [char.] |  RCZA method val. [real]
##-------------------------------------------------------------------------------
0                               theta                           n                              0

#################################################################
#################### bc description #############################
#################################################################
# number of boundaries (for 1D problem obviously not more then 2)
2
#list boundaries
# ID starts at 100 (for 1D problem 101 = bottom boundary, 102 = top boundary)
# available boundary types
# 0 - no bc for this domain
# 1 - Dirichlet boundary
# -1 - Dirichlet boundary, the pressure is equal to vertical distance from the defined value
# 2 - Neumann boundary (e.g. rain)
# 3 - Free Drainage
# 4 - Seepage Face
# 5 - atmospheric boundary

# boundary ID       boundary type       use rain.dat [y/n]   value
#-------------------------------------------------------------------------------------------------------------------------------
101                      4                  n                0
102                      2                  y                0
```

Fig. 24 – Example of the configuration file from DRUtES software with dropped parts. This figure only shows parts of the *matrix.conf* file that is mentioned in this chapter. Rows without # are editable. This figure shows DRUtES environment, so every editable value was set to zero except boundary condition because they must be chosen from given options.

```
###------- begin initial mesh configuration -------#####
#problem dimension (1D, 2D, 3D) [integer]
#1 = 1D (drutes.conf/mesh.conf/drumesh1d.conf)
#2 = 2D
#2r = two-dimensional domain for rotational symmetric flow
#3 = 3D
# recently only 1D and 2D is implemented
1

# define mesh generator
# 1 - internal mesh generator (edit drutes.conf/mesh.conf/drumesh2d.conf)
# 2 - t3d mesh generator (provide drutes.conf/mesh.conf/mesh.t3d)
# 3 - gmsh mesh generator (provide drutes.conf/mesh.conf/mesh.msh)
#(if you need different mesh formats contact developers)
1

###------- end initial mesh configuration -------#####
###------- begin error criteria (nonlinear solver) -------#####
# maximum number of iteration of the Picard method [integer]
0

# h tolerance: iteration criterion for the Picard method
0

###------- end error criteria (nonlinear solver) -------####
###-----begin time information------#####
#time units (write what ever you like, will be displayed on your plots) (up to 5 characters)
days

#-----initial dt hod - init dt [real]
0

#-----end time [real]
0

#---minimum time step [real]
0

#-- maximum time step [real]
0

###-----end time information ------###
```

Fig. 25 - Example of the configuration file from DRUtES software with dropped parts. This figure only shows parts of the *global.conf* file that is mentioned in this chapter. Rows without # are editable. This figure is used to show DRUtES environment, so every editable value was set to zero. Mesh configuration was set up according to given options.

```
#############################################################################################
###-------------------------1D geometry information-------------------------------------------
#############################################################################################
# geometry information
0 cm - domain length


#!!!!!!! P O S I T I V E   U P W A R D S !!!!!!!

#amount of intervals with different discretization length [integer]
0

# density  bottom    top    [real]
1       0          0

#number of materials
0

# id    bottom     top
1       0         0
```

Fig. 26- Example of the configuration file from DRUtES software with dropped parts. This figure only shows parts of *drumesh1d.conf* file that are mentioned in this chapter. Rows without # are editable. This figure is used to show DRUtES environment, so every editable value was set to zero.

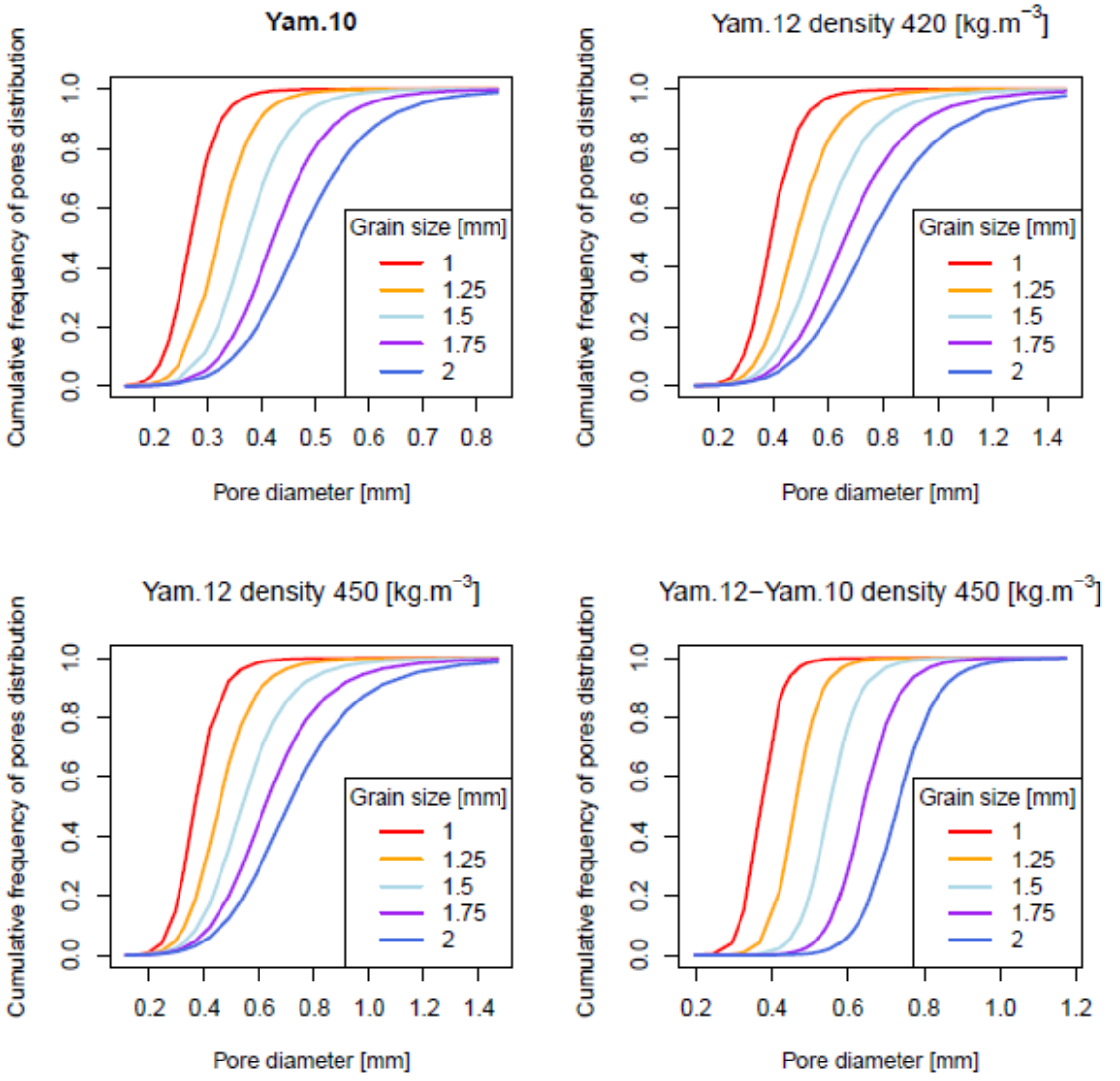

Fig. 27 – The frequency of pore distribution that is computed for Yam.10, Yam.12, Yam.12 - Yam.10. Input for parametrization was measured densities and grain size in Dischma snowpack. Parametrization was computed for 5 values of possible grain size and then substitute to van Genuchten model to obtain θ_e [-]. Pore diameter was computed with neglected contact angle.

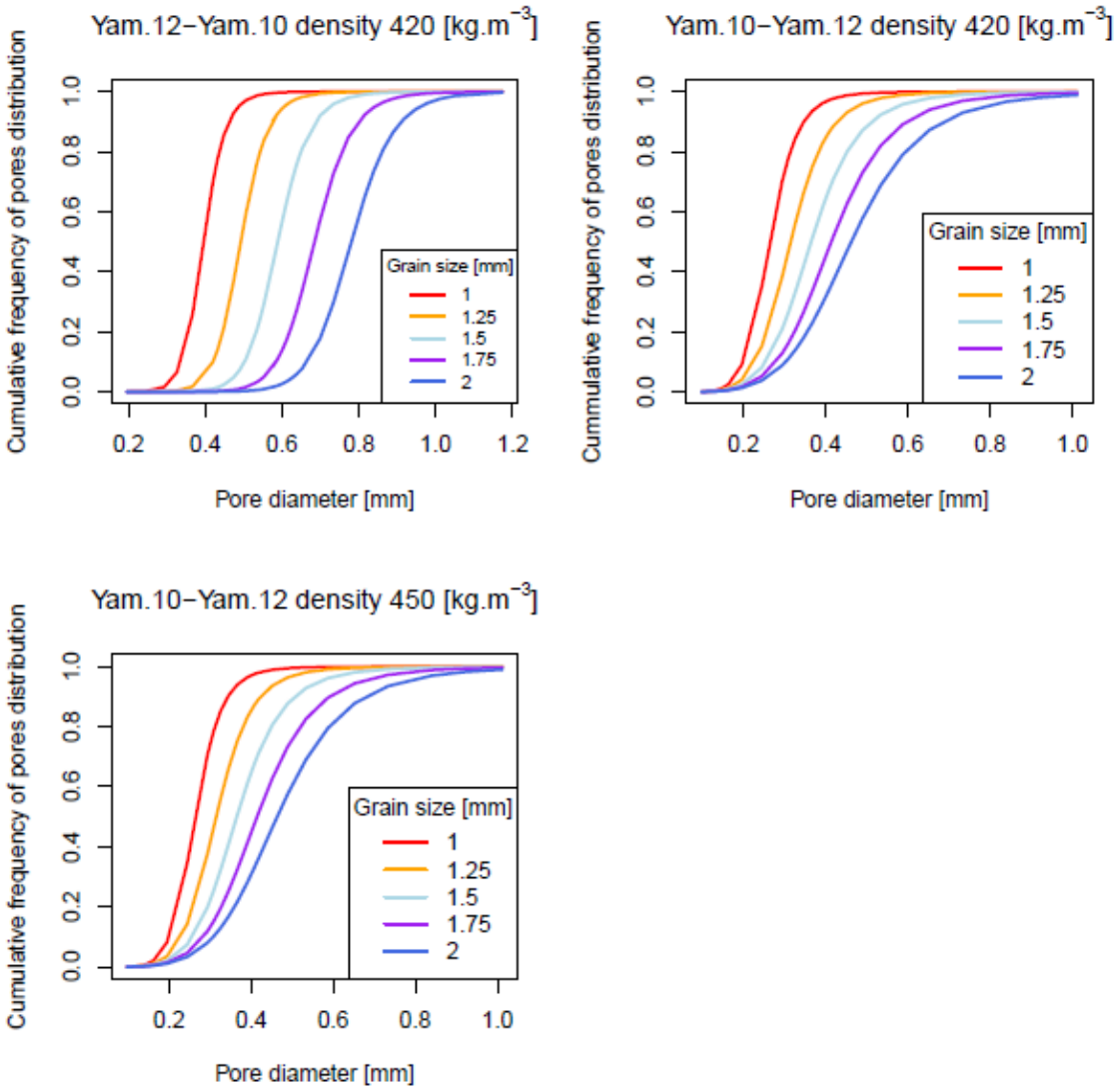

Fig. 28 – The frequency of pore distribution is computed for Yam.12 - Yam.10, Yam.10 - Yam.12. Input for parametrization was measured densities and grain size in Dischma snowpack. Parametrization was computed for 5 values of possible grain size and then substitute to van Genuchten model to obtain θ_e [-]. Pore diameter was computed with neglected contact angle.

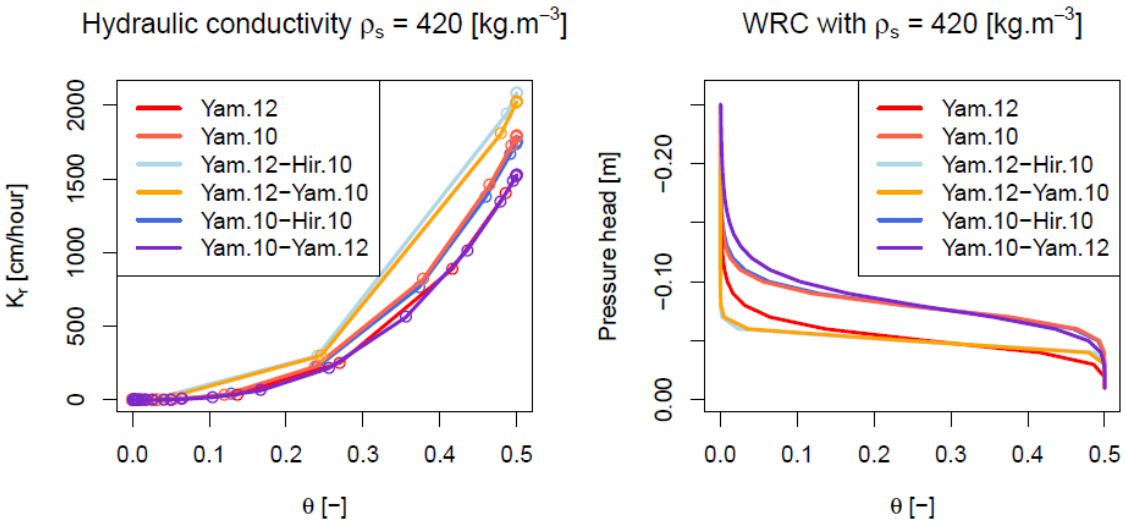

Fig. 29 – WRC and Relative hydraulic conductivity for snow with ρ_s = 420 kg.m^{-3} and *d* 1.5 mm.

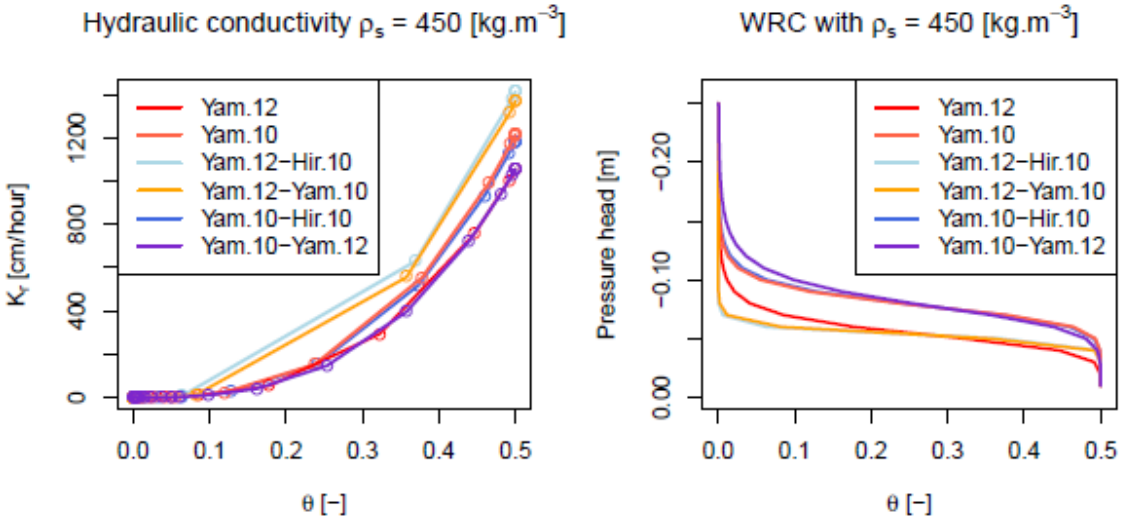

Fig. 30 – WRC and Relative hydraulic conductivity for snow with ρ_s = 450 kg.m^{-3} and *d* 1.5 mm.

Tab. 24 - Input values for DRUtES computed according to methods of this thesis with a mean value grain size that was chosen as first setup (simulation 1).

Layer start [cm]	Layer end [cm]	Initial θ [-]	*d* [mm]	Layer density [kg.m^{-3}]	α Yam.2010 [cm^{-1}]	α Yam.2012 [cm^{-1}]	n Yam.2010 [-]	m Yam.2010 [-]	n Yam.2012 [-]	m Yam.2012 [-]	n Hir.2010 [-]	m Hir.2010 [-]	K Cal.2012 [cm.d^{-1}]	θs [-]
0	5	0.04	1.5	447	0.13	0.19	9.45	0.89	6.90	0.86	8.86	0.89	238205	0.51
5	15	0.03	1.5	420	0.13	0.20	9.45	0.89	6.68	0.85	8.86	0.89	338367	0.54
15	19	0.05	1.5	418	0.13	0.20	9.45	0.89	6.66	0.85	8.86	0.89	347279	0.54
19	30	0.05	1.5	458	0.13	0.19	9.45	0.89	6.99	0.86	8.86	0.89	206465	0.50

Tab. 25 - Input values for DRUtES computed according to methods of this thesis with lowest possible grain size in the purpose of sensitivity analysis (simulation 2).

Layer start [cm]	Layer end [cm]	Initial θ [-]	*d* [mm]	Layer density [kg.m^{-3}]	α Yam.2010 [cm^{-1}]	α Yam.2012 [cm^{-1}]	n Yam.2010 [-]	m Yam.2010 [-]	n Yam.2012 [-]	m Yam.2012 [-]	n Hir.2010 [-]	m Hir.2010 [-]	K Cal.2012 [cm.d^{-1}]	θs [-]
0	5	0,04	1	447	0.09	0.13	11.1	0.91	8.55	0.88	10.90	0.91	105869	0.51
5	15	0.03	1	420	0.09	0.14	11.1	0.91	8.27	0.88	10.90	0.91	150385	0.54
15	19	0.05	1	418	0.09	0.14	11.1	0.91	8.25	0.88	10.90	0.91	154346	0.54
19	30	0.05	1	458	0.09	0.12	11.1	0.91	8.66	0.88	10.90	0.91	91762	0.50

Tab. 26 - Input values for DRUtES computed according to methods of this thesis with the biggest possible grain size in the purpose of sensitivity analysis (simulation 3).

Layer start [cm]	Layer end [cm]	Initial θ [-]	*d* [mm]	Layer density [kg.m^{-3}]	α Yam.2010 [cm^{-1}]	α Yam.2012 [cm^{-1}]	n Yam.2010 [-]	m Yam.2010 [-]	n Yam.2012 [-]	m Yam.2012 [-]	n Hir.2010 [-]	m Hir.2010 [-]	K Cal.2012 [cm.d^{-1}]	θs [-]
0	5	0.04	2	447	0.17	0.25	7.8	0.87	5.95	0.83	7.25	0.86	423475	0.51
5	15	0.03	2	420	0.17	0.27	7.8	0.87	5.76	0.83	7.25	0.86	601541	0.54
15	19	0.05	2	418	0.17	0.27	7.8	0.87	5.75	0.83	7.25	0.86	617386	0.54
19	30	0.05	2	458	0.17	0.25	7.8	0.87	6.02	0.83	7.25	0.86	367049	0.50

Tab. 27 - Input values thesis for DRUtES computed according to methods of this with reduced densities by 20 [kg.m^{-3}] and *d* 1,5 [mm] in the purpose of sensitivity analysis (simulation 4).

Layer start [cm]	Layer end [cm]	Initial θ [-]	*d* [mm]	Layer density [kg.m^{-3}]	α Yam.2010 [cm^{-1}]	α Yam.2012 [cm^{-1}]	n Yam.2010 [-]	m Yam.2010 [-]	n Yam.2012 [-]	m Yam.2012 [-]	n Hir.2010 [-]	m Hir.2010 [-]	K Cal.2012 [cm.d^{-1}]	θs [-]
0	5	0.04	1.5	427	0.13	0.20	9.45	0.89	6.73	0.85	8.86	0.89	308935	0.53
5	15	0.03	1.5	400	0.13	0.21	9.45	0.89	6.51	0.85	8.86	0.89	438838	0.56
15	19	0.05	1.5	398	0.13	0.21	9.45	0.89	6.49	0.85	8.86	0.89	450397	0.57
19	30	0.05	1.5	438	0.13	0.19	9.45	0.89	6.82	0.85	8.86	0.89	267770	0.52

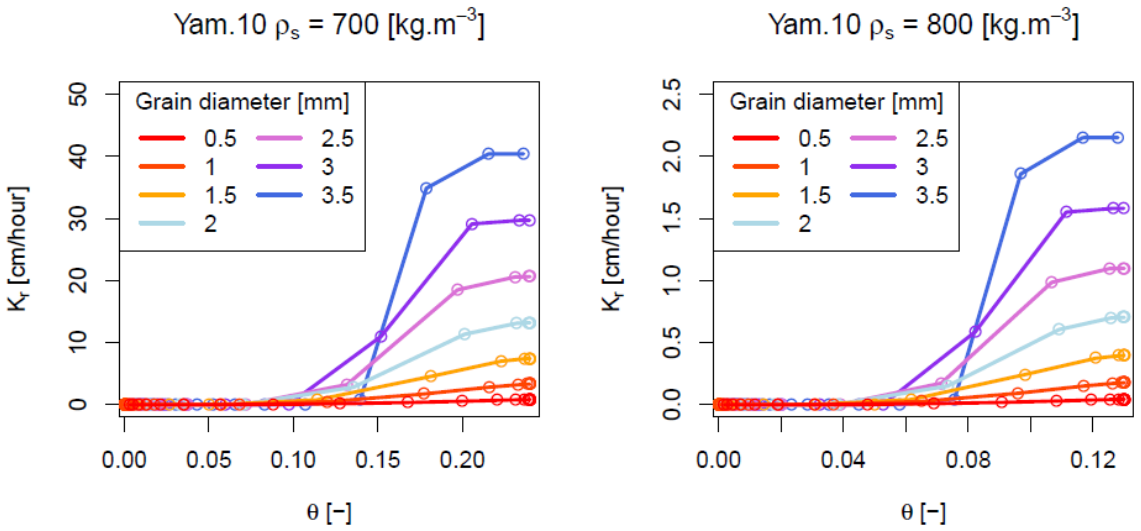

Fig. 31 – Relative hydraulic conductivity for parametrization Yam.10 on two types densities that were proposed as the property of ice layer. According Eq. 1, $\theta_s = 0{,}24$ [-] for snow density ρ_s = 700 kg.m^{-3} and $\theta_s = 0{,}13$ [-] for ρ_s = 800 kg.m^{-3}

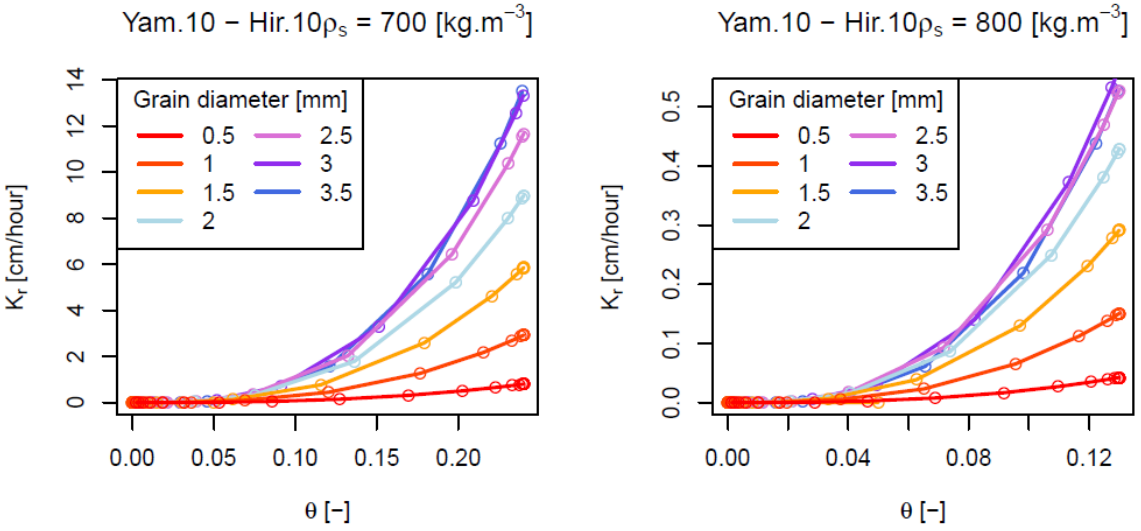

Fig. 32 – Relative hydraulic conductivity for parametrization Yam.10 – Hir.10 computed for two densities that were proposed for the ice layer. According Eq. 1, $\theta_s = 0{,}24$ [-] for snow density ρ_s = 700 kg.m^{-3} and $\theta_s = 0{,}13$ [-] for ρ_s = 800 kg.m^{-3}

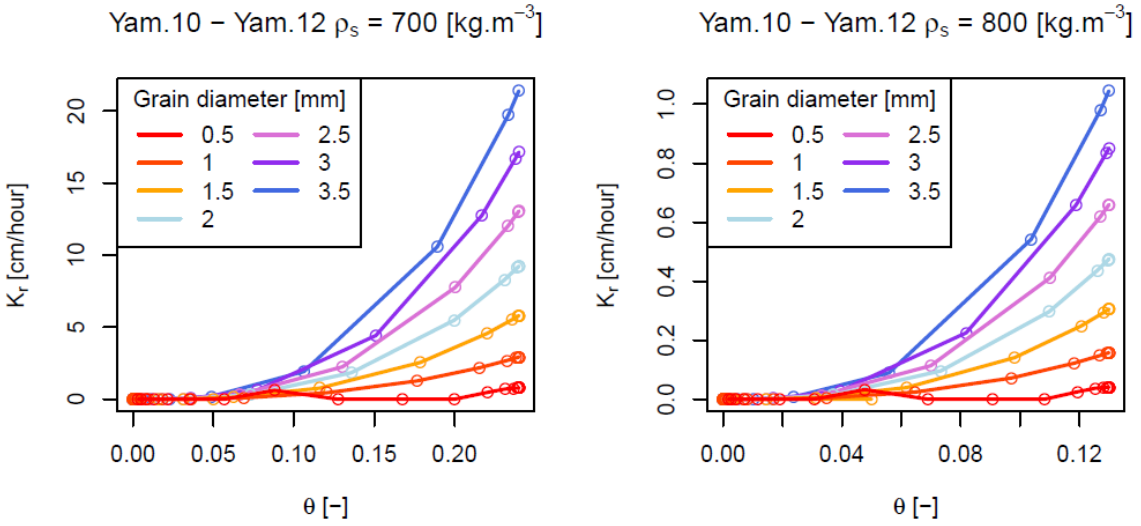

Fig. 33 – Relative hydraulic conductivity for parametrization Yam.10 – Yam.12 10 computed for two densities that were proposed for the ice layer. According Eq. 1, θ_s = 0,24 [-] for snow density ρ_s = 700 kg.m^{-3} and θ_s = 0,13 [-] for ρ_s = 800 kg.m^{-3}

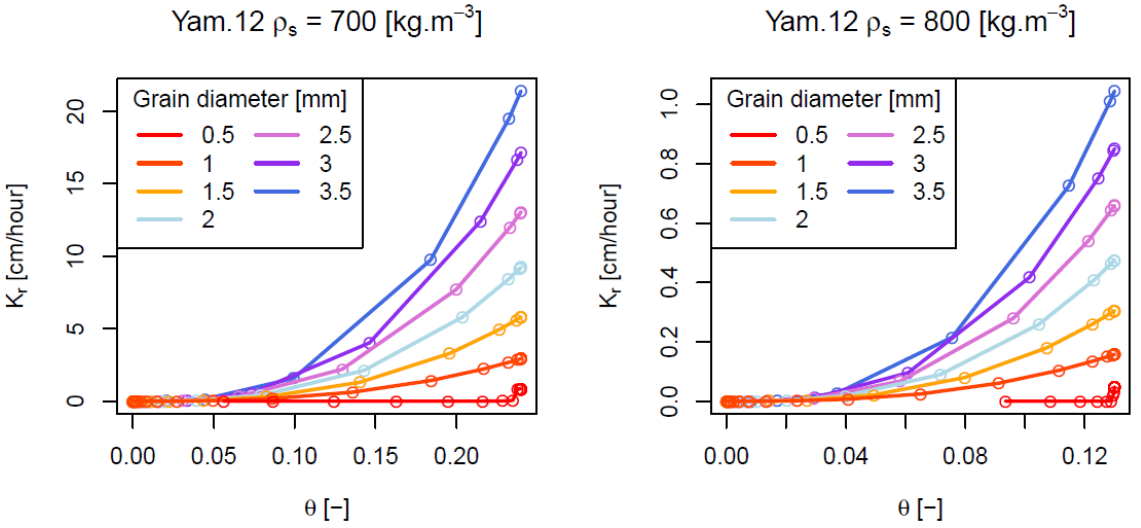

Fig. 34 – Relative hydraulic conductivity for parametrization Yam. 10 computed for two densities that were proposed for the ice layer. According Eq. 1, θ_s = 0,24 [-] for snow density ρ_s = 700 kg.m^{-3} and θ_s = 0,13 [-] for ρ_s = 800 kg.m^{-3}

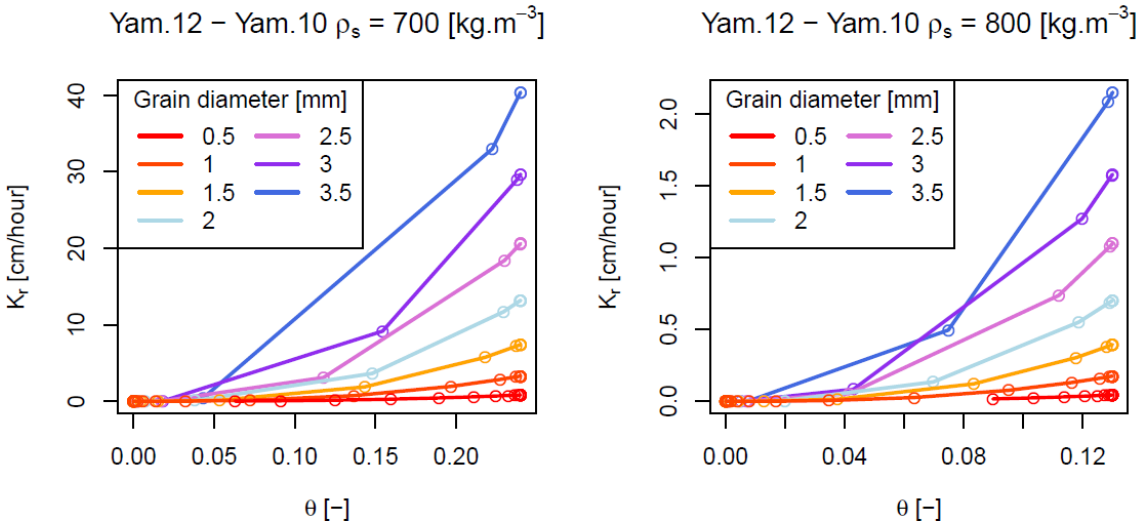

Fig. 35 – Relative hydraulic conductivity for parametrization Yam.12 – Yam. 10 computed for two densities that were proposed for the ice layer. According Eq. 1, $\theta_s = 0{,}24$ [-] for snow density $\rho_s = 700$ kg.m^{-3} and $\theta_s = 0{,}13$ [-] for $\rho_s = 800$ kg.m^{-3}

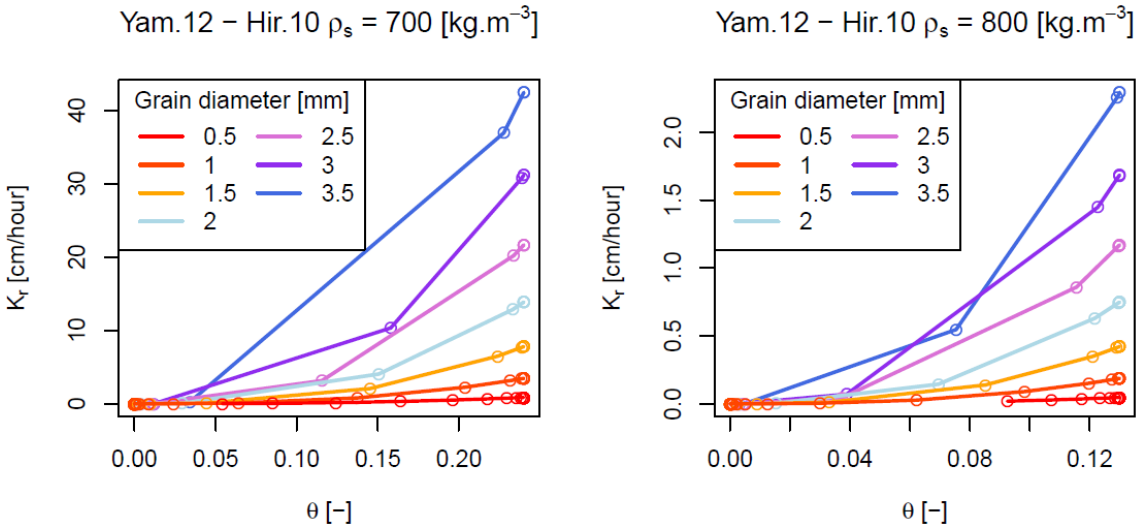

Fig. 36 – Relative hydraulic conductivity for parametrization Yam.12 – Hir.12 10 computed for two densities that were proposed for the ice layer. According Eq. 1, $\theta_s = 0{,}24$ [-] for snow density $\rho_s = 700$ kg.m^{-3} and $\theta_s = 0{,}13$ [-] for $\rho_s = 800$ kg.m^{-3}

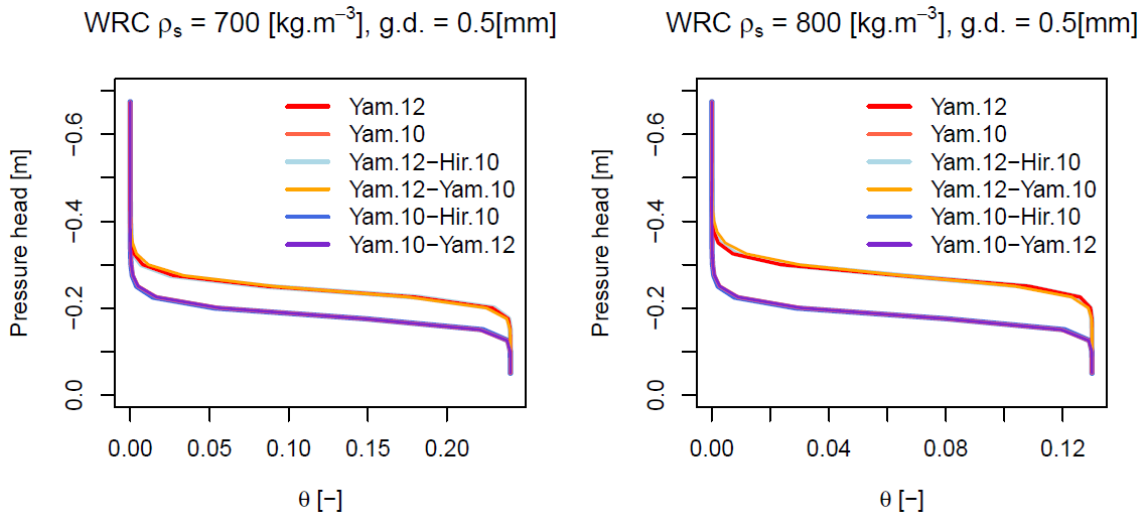

Fig. 37 – WRC for ice layer with *d* = 0.5 mm and density 700 and 800 kg.m^{-3}.

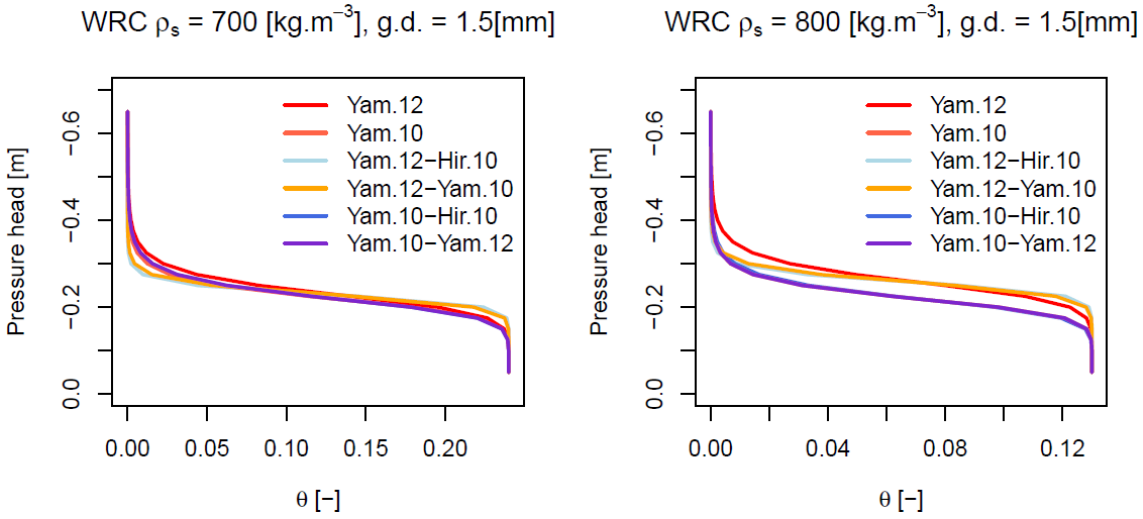

Fig. 38 - WRC for ice layer with *d* of 1.5 mm and density 700 and 800 kg.m^{-3}.

Tab. 28 - Input values for DRUtES computed according to methods of this thesis with ice layers densities set to 700 kg.m^{-3} and *d* of the top and bottom layer 0.5 mm (simulation 1).

Layer start [cm]	Layer end [cm]	Initial θ [-]	*d* [mm]	Layer density [kg.m^{-3}]	α Yam.2010 [cm^{-1}]	α Yam.2012 [cm^{-1}]	n Yam.2010 [-]	m Yam.2010 [-]	n Yam.2012 [-]	m Yam.2012 [-]	n Hir.2010 [-]	m Hir.2010 [-]	K Cal.2012 [cm.d^{-1}]	θs [-]
0	25	0.04	0.5	476	0.06	0.06	12.75	0.92	12.98	0.92	13.46	0.93	18154	0.48
25	26	0.00	0.5	700	0.06	0.04	12.75	0.92	16.15	0.94	13.46	0.93	987	0.24
26	36	0.04	2	522	0.17	0.22	7.80	0.87	6.44	0.84	7.25	0.86	159731	0.43
36	38	0.00	1	700	0.13	0.12	9.45	0.89	8.75	0.89	8.86	0.89	8883	0.24
38	41	0.03	2	521	0.17	0.22	7.80	0.87	6.43	0.84	7.25	0.86	161822	0.43
41	56.7	0.03	2	507	0.17	0.22	7.80	0.87	6.34	0.84	7.25	0.86	194123	0.45
56.7	57	0.00	0.5	700	0.06	0.04	12.75	0.92	16.15	0.94	13.46	0.93	987	0.24
57	75.7	0.04	1	508	0.09	0.11	11.10	0.91	9.16	0.89	10.90	0.91	47904	0.45
75.7	76	0.00	0.5	700	0.06	0.04	12.75	0.92	16.15	0.94	13.46	0.93	987	0.24
76	88	0.03	0.5	471	0.06	0.06	12.75	0.92	12.90	0.92	13.46	0.93	19373	0.49

Tab. 29- Input values for DRUtES computed according to methods of this thesis with ice layers densities set to 700 kg.m^{-3} and *d* 1.5 mm (simulation 2).

Layer start [cm]	Layer end [cm]	Initial θ [-]	*d* [mm]	Layer density [kg.m^{-3}]	α Yam.2010 [cm^{-1}]	α Yam.2012 [cm^{-1}]	n Yam.2010 [-]	m Yam.2010 [-]	n Yam.2012 [-]	m Yam.2012 [-]	n Hir.2010 [-]	m Hir.2010 [-]	K Cal.2012 [cm.d^{-1}]	θs [-]
0	25	0.04	0.5	476	0.06	0.06	12.75	0.92	12.98	0.92	13.46	0.93	18154	0.48
25	26	0.00	1.5	700	0.13	0.12	9.45	0.89	8.75	0.89	8.86	0.89	8883	0.24
26	36	0.04	2	522	0.17	0.22	7.80	0.87	6.44	0.84	7.25	0.86	159731	0.43
36	38	0.00	2	700	0.17	0.16	7.80	0.87	7.50	0.87	7.25	0.86	15792	0.24
38	41	0.03	2	521	0.17	0.22	7.80	0.87	6.43	0.84	7.25	0.86	161822	0.43
41	56.7	0.03	2	507	0.17	0.22	7.80	0.87	6.34	0.84	7.25	0.86	194123	0.45
56.7	57	0.00	1.5	700	0.13	0.12	9.45	0.89	8.75	0.89	8.86	0.89	8883	0.24
57	75.7	0.04	1	508	0.09	0.11	11.10	0.91	9.16	0.89	10.90	0.91	47904	0.45
75.7	76	0.00	1.5	700	0.13	0.12	9.45	0.89	8.75	0.89	8.86	0.89	8883	0.24
76	88	0.03	0.5	471	0.06	0.06	12.75	0.92	12.90	0.92	13.46	0.93	19373	0.49

Tab. 30 - Input values for DRUtES computed according to methods of this thesis with ice layers densities set to 700 kg.m^{-3} with *d* 0.5 mm and *d* of first and top layer set to 1 mm (simulation 3).

Layer start [cm]	Layer end [cm]	Initial θ [-]	*d* [mm]	Layer density [kg.m^{-3}]	α Yam.2010 [cm^{-1}]	α Yam.2012 [cm^{-1}]	n Yam.2010 [-]	m Yam.2010 [-]	n Yam.2012 [-]	m Yam.2012 [-]	n Hir.2010 [-]	m Hir.2010 [-]	K Cal.2012 [cm.d^{-1}]	θs [-]
0	25	0.04	1	476	0.09	0.12	11.10	0.91	8.85	0.89	10.90	0.91	72617	0.48
25	26	0.00	0.5	700	0.06	0.04	12.75	0.92	16.15	0.94	13.46	0.93	987	0.24
26	36	0.04	2	522	0.17	0.22	7.80	0.87	6.44	0.84	7.25	0.86	159731	0.43
36	38	0.00	1	700	0.09	0.08	11.10	0.91	10.93	0.91	10.90	0.91	3948	0.24
38	41	0.03	2	521	0.17	0.22	7.80	0.87	6.43	0.84	7.25	0.86	161822	0.43
41	56.7	0.03	2	507	0.17	0.22	7.80	0.87	6.34	0.84	7.25	0.86	194123	0.45
56.7	57	0.00	0.5	700	0.06	0.04	12.75	0.92	16.15	0.94	13.46	0.93	987	0.24
57	75.7	0.04	1	508	0.09	0.11	11.10	0.91	9.16	0.89	10.90	0.91	47904	0.45
75.7	76	0.00	0.5	700	0.06	0.04	12.75	0.92	16.15	0.94	13.46	0.93	987	0.24
76	88	0.03	1	471	0.09	0.12	11.10	0.91	8.80	0.89	10.90	0.91	77494	0.49

Tab. 31 - Input values for DRUtES computed according to methods of this thesis with ice layers densities set to 800 kg.m^{-3} with *d* 0.5 mm and *d* of first and top layer set to 1 mm (simulation 4).

Layer start [cm]	Layer end [cm]	Initial θ [-]	*d* [mm]	Layer density [kg.m^{-3}]	α Yam.2010 [cm^{-1}]	α Yam.2012 [cm^{-1}]	n Yam.2010 [-]	m Yam.2010 [-]	n Yam.2012 [-]	m Yam.2012 [-]	n Hir.2010 [-]	m Hir.2010 [-]	K Cal.2012 [cm.d^{-1}]	θs [-]
0	25	0.04	1	476	0.09	0.12	11.10	0.91	8.85	0.89	10.90	0.91	72617	0.48
25	26	0.00	0.5	800	0.06	0.04	12.75	0.92	17.44	0.94	13.46	0.93	269	0.13
26	36	0.04	2	522	0.17	0.22	7.80	0.87	6.44	0.84	7.25	0.86	159731	0.43
36	38	0.00	1	800	0.09	0.07	11.10	0.91	11.77	0.92	10.90	0.91	1076	0.13
38	41	0.03	2	521	0.17	0.22	7.80	0.87	6.43	0.84	7.25	0.86	161822	0.43
41	56.7	0.03	2	507	0.17	0.22	7.80	0.87	6.34	0.84	7.25	0.86	194123	0.45
56.7	57	0.00	0.5	800	0.06	0.04	12.75	0.92	17.44	0.94	13.46	0.93	269	0.13
57	75.7	0.04	1	508	0.09	0.11	11.10	0.91	9.16	0.89	10.90	0.91	47904	0.45
75.7	76	0.00	0.5	800	0.06	0.04	12.75	0.92	17.44	0.94	13.46	0.93	269	0.13
76	88	0.03	1	471	0.09	0.12	11.10	0.91	8.80	0.89	10.90	0.91	77494	0.49

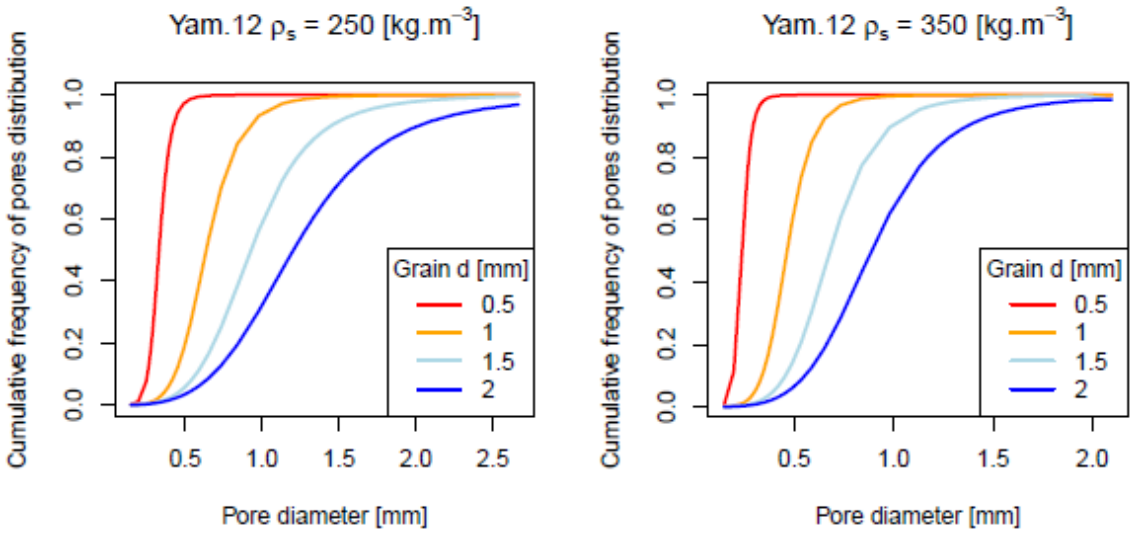

Fig. 39 – Yam.12 curves of frequency pore distribution on densities and grain size that occurs in Sertig snowpack. Parametrization was computed for 5 values of possible grain size and then substitute to van Genuchten model to obtain θ_e [-]. Pore diameter was computed with neglected contact angle.

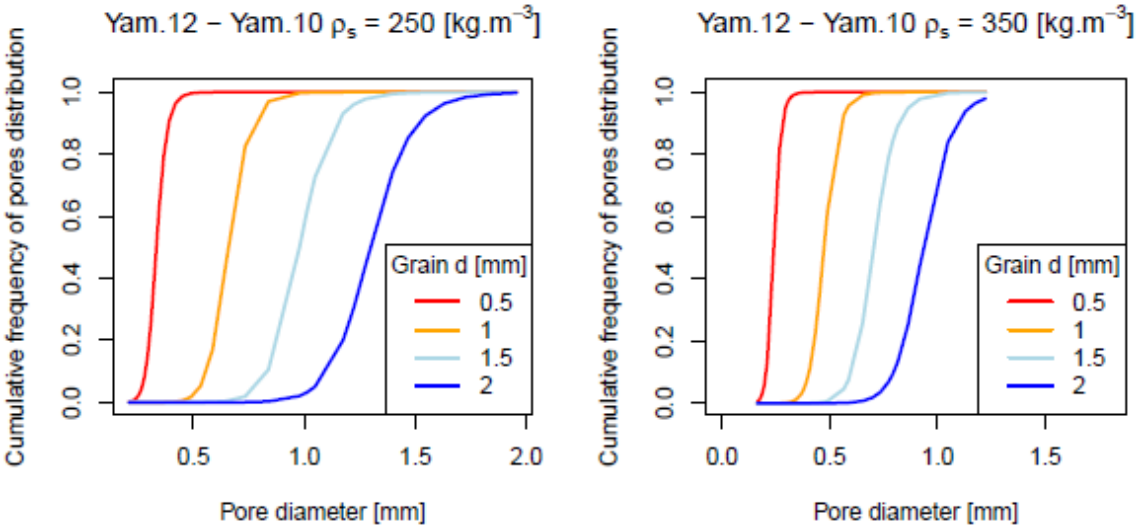

Fig. 40 - Yam.12 – Yam.10 curves of frequency pore distribution on densities and grain size that occurs in Sertig snowpack. Parametrization was computed for 5 values of possible grain size and then substitute to van Genuchten model to obtain θ_e [-]. Pore diameter was computed with neglected contact angle.

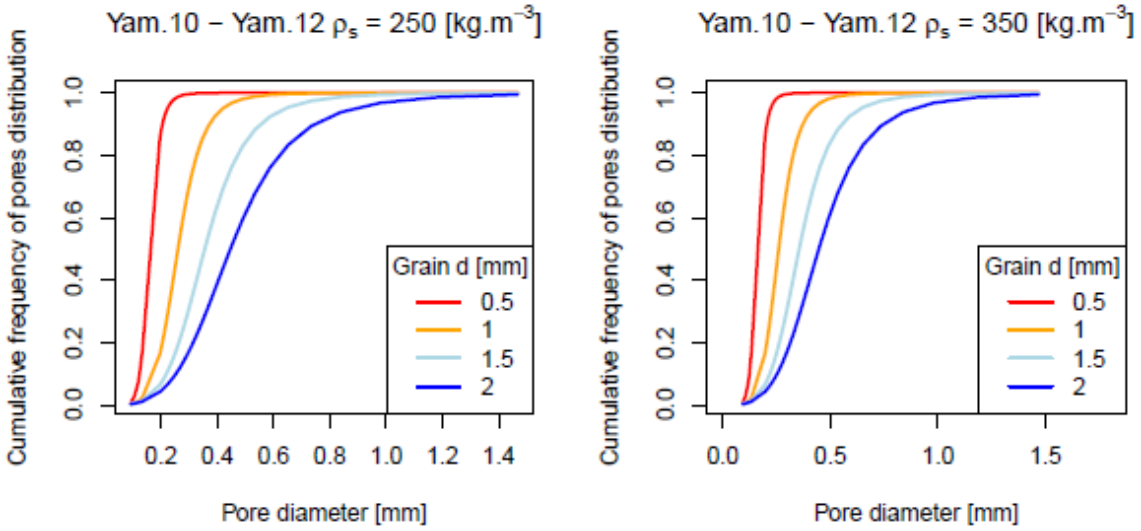

Fig. 41 – Yam.10 – Yam.12 curves of frequency pore distribution on densities and grain size that occurs in Sertig snowpack. Parametrization was computed for 5 values of possible grain size and then substitute to van Genuchten model to obtain θ_e [-]. Pore diameter was computed with neglected contact angle.

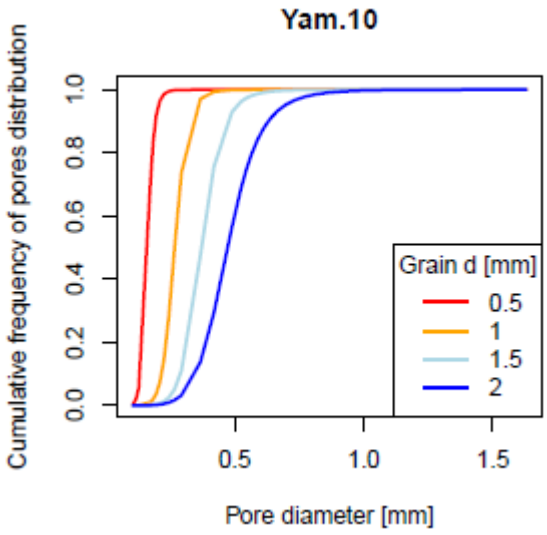

Fig. 42 – Yam.10 curves of frequency pore distribution on densities and grain size that occurs in Sertig snowpack. Parametrization was computed for 5 values of possible grain size and then substitute to van Genuchten model to obtain θ_e [-]. Pore diameter was computed with neglected contact angle.

Tab. 32 - Initial values of simulation 1 for DRUtES. Measured values were used with ice layer setup of 700 kg.m^{-3} and *d* 1.5 mm.

Layer start [cm]	Layer end [cm]	Initial θ [-]	*d* [mm]	Layer density [kg.m^{-3}]	α Yam.2010 [cm^{-1}]	α Yam.2012 [cm^{-1}]	n Yam.2010 [-]	m Yam.2010 [-]	n Yam.2012 [-]	m Yam.2012 [-]	n Hir.2010 [-]	m Hir.2010 [-]	K Cal.2012 [cm.d^{-1}]	θs [-]
0	9.5	0.02	2.25	358	0.18	0.35	6.98	0.86	5.02	0.80	6.57	0.85	1704556	0.61
9.5	11	0.00	1.5	700	0.13	0.12	9.45	0.89	8.75	0.89	8.86	0.89	8883	0.24
11	15.5	0.00	2	358	0.17	0.31	7.80	0.87	5.32	0.81	7.25	0.86	1346810	0.61
15.5	16.5	0.00	1.5	700	0.13	0.12	9.45	0.89	8.75	0.89	8.86	0.89	8883	0.24
16.5	19	0.00	1.5	379	0.13	0.22	9.45	0.89	6.33	0.84	8.86	0.89	576589	0.59
19	29	0.06	1.25	311	0.11	0.23	10.28	0.90	6.28	0.84	9.82	0.90	969215	0.66
29	38	0.00	1.25	254	0.11	0.28	10.28	0.90	5.67	0.82	9.82	0.90	2033445	0.72
38	44	0.00	0.5	258	0.06	0.11	12.75	0.92	9.24	0.89	13.46	0.93	308865	0.72
44	54	0.03	1.25	263	0.11	0.27	10.28	0.90	5.77	0.83	9.82	0.90	1808923	0.71

Tab. 33 - Initial values of simulation 2 for DRUtES. Measured values that were reduced by 0.5 mm in *d* were used with an ice layer setup of 700 kg.m^{-3} and *d* 1.5 mm.

Layer start [cm]	Layer end [cm]	Initial θ [-]	*d* [mm]	Layer density [kg.m^{-3}]	α Yam.2010 [cm^{-1}]	α Yam.2012 [cm^{-1}]	n Yam.2010 [-]	m Yam.2010 [-]	n Yam.2012 [-]	m Yam.2012 [-]	n Hir.2010 [-]	m Hir.2010 [-]	K Cal.2012 [cm.d^{-1}]	θs [-]
0	9.5	0.02	1.75	358	0.15	0.27	8.63	0.88	5.69	0.82	8.01	0.88	1031151	0.61
9.5	11	0.00	1.5	700	0.13	0.12	9.45	0.89	8.75	0.89	8.86	0.89	8883	0.24
11	15.5	0.00	1.5	358	0.13	0.24	9.45	0.89	6.15	0.84	8.86	0.89	757581	0.61
15.5	16.5	0.00	1.5	700	0.13	0.12	9.45	0.89	8.75	0.89	8.86	0.89	8883	0.24
16.5	19	0.00	1	379	0.09	0.15	11.10	0.91	7.83	0.87	10.90	0.91	256262	0.59
19	29	0.06	0.75	311	0.07	0.14	11.93	0.92	8.21	0.88	12.10	0.92	348918	0.66
29	38	0.00	0.75	254	0.07	0.17	11.93	0.92	7.38	0.86	12.10	0.92	732040	0.72
38	44	0.00	0.5	258	0.06	0.11	12.75	0.92	9.24	0.89	13.46	0.93	308865	0.72
44	54	0.03	0.75	263	0.07	0.16	11.93	0.92	7.51	0.87	12.10	0.92	651212	0.71

Tab. 34 - Initial values of simulation 3 for DRUtES. Measured values that were enlarged by 0.5 mm in *d* were used with an ice layer setup of 700 $kg.m^{-3}$ and *d* 1.5 mm.

Layer start [cm]	Layer end [cm]	Initial θ [-]	*d*[mm]	Layer density [$kg.m^{-3}$]	α Yam.2010 [cm^{-1}]	α Yam.2012 [cm^{-1}]	n Yam.2010 [-]	m Yam.2010 [-]	n Yam.2012 [-]	m Yam.2012 [-]	n Hir.2010 [-]	m Hir.2010 [-]	K Cal.2012 [$cm.d^{-1}$]	θs [-]
0	9.5	0.02	2.75	358	0.22	0.43	5.33	0.81	4.56	0.78	5.43	0.82	2546313	0.61
9.5	11	0.00	1.5	700	0.13	0.12	9.45	0.89	8.75	0.89	8.86	0.89	8883	0.24
11	15.5	0.00	2.5	358	0.20	0.39	6.15	0.84	4.77	0.79	5.96	0.83	2104391	0.61
15.5	16.5	0.00	1.5	700	0.13	0.12	9.45	0.89	8.75	0.89	8.86	0.89	8883	0.24
16.5	19	0.00	2	379	0.17	0.30	7.80	0.87	5.47	0.82	7.25	0.86	1025047	0.59
19	29	0.06	1.75	311	0.15	0.32	8.63	0.88	5.30	0.81	8.01	0.88	1899662	0.66
29	38	0.00	1.75	254	0.15	0.38	8.63	0.88	4.80	0.79	8.01	0.88	3985553	0.72
38	44	0.00	1	258	0.09	0.22	11.10	0.91	6.40	0.84	10.90	0.91	1235461	0.72
44	54	0.03	1.75	263	0.15	0.37	8.63	0.88	4.88	0.80	8.01	0.88	3545489	0.71

9 References

Arendt, W., Warma, M., 2003. Dirichlet and Neumann boundary conditions: What is in between? 3, 17.

Avanzi, F., Hirashima, H., Yamaguchi, S., Katsushima, T., Michele, C.D., 2016. Observations of capillary barriers and preferential flow in layered snow during cold laboratory experiments. The Cryosphere 10, 2013–2026. https://doi.org/10.5194/tc-10-2013-2016

Calonne, N., Flin, F., Morin, S., Lesaffre, B., Roscoat, S.R. du, Geindreau, C., 2011. Numerical and experimental investigations of the effective thermal conductivity of snow. Geophysical Research Letters 38. https://doi.org/10.1029/2011GL049234

Calonne, N., Geindreau, C., Flin, F., Morin, S., Lesaffre, B., Rolland du Roscoat, S., Charrier, P., 2012. 3-D image-based numerical computations of snow permeability: links to specific surface area, density, and microstructural anisotropy. The Cryosphere 6, 939–951. https://doi.org/10.5194/tc-6-939-2012

Celia, M.A., Bouloutas, E.T., Zarba, R.L., 1990. A general mass-conservative numerical solution for the unsaturated flow equation. Water Resources Research 26, 1483–1496. https://doi.org/10.1029/WR026i007p01483

Chai, T., Draxler, R.R., 2014. Root mean square error (RMSE) or mean absolute error (MAE)? – Arguments against avoiding RMSE in the literature. Geoscientific Model Development 7, 1247–1250. https://doi.org/10.5194/gmd-7-1247-2014

Colbeck, S.C., 1986. Classification of seasonal snow cover crystals. Water Resources Research 22, 59S-70S. https://doi.org/10.1029/WR022i09Sp0059S

Colbeck, S.C., 1979. Water flow through heterogeneous snow. Cold Regions Science and Technology 1, 37–45. https://doi.org/10.1016/0165-232X(79)90017-X

Colbeck, S.C., 1972. A Theory of Water Percolation in Snow. Journal of Glaciology 11, 369–385. https://doi.org/10.3189/S0022143000022346

Coléou, C., Lesaffre, B., 1998. Irreducible water saturation in snow: experimental results in a cold laboratory. Annals of Glaciology 26, 64–68. https://doi.org/10.3189/1998AoG26-1-64-68

Conway, H., Abrahamson, J., 1984. Air Permeability as a Textural Indicator of Snow. Journal of Glaciology 30, 328–333. https://doi.org/10.3189/S0022143000006171

De Michele, C., Avanzi, F., Ghezzi, A., Jommi, C., 2013. Investigating the dynamics of bulk snow density in dry and wet conditions using a one-dimensional model. The Cryosphere 7, 433–444. https://doi.org/10.5194/tc-7-433-2013

Denoth, A., 1994. An electronic device for long-term snow wetness recording. Annals of Glaciology 19, 104–106. https://doi.org/10.3189/S0260305500011058

Farthing, M.W., Ogden, F.L., 2017. Numerical Solution of Richards' Equation: A Review of Advances and Challenges. Soil Science Society of America Journal 81, 1257. https://doi.org/10.2136/sssaj2017.02.0058

Feng, X., Kirchner, J.W., Renshaw, C.E., Osterhuber, R.S., Klaue, B., Taylor, S., 2001. A study of solute transport mechanisms using rare earth element tracers and artificial rainstorms on snow. Water Resources Research 37, 1425–1435. https://doi.org/10.1029/2000WR900376

Fierz, C., R.L, A., Y, D., P, E., Greene, E., Mcclung, D., Nishimura, K., Satyawali, P., Sokratov, S., 2009. The international classification for seasonal snow on the ground (UNESCO, IHP (International Hydrological Programme)–VII, Technical Documents in Hydrology, No 83; IACS (International Association of Cryospheric Sciences) contribution No 1).

Ginting, V., 2012. Time Integration Techniques for Richards Equation. Procedia Computer Science, Proceedings of the International Conference on Computational Science, ICCS 2012 9, 670–678. https://doi.org/10.1016/j.procs.2012.04.072

Hirashima, H., Yamaguchi, S., Sato, A., Lehning, M., 2010. Numerical modeling of liquid water movement through layered snow based on new measurements of the water retention curve. Cold Regions Science and Technology, International Snow Science Workshop 2009 Davos 64, 94–103. https://doi.org/10.1016/j.coldregions.2010.09.003

Ho-Le, K., 1988. Finite element mesh generation methods: a review and classification. Computer-Aided Design 20, 27–38. https://doi.org/10.1016/0010-4485(88)90138-8

Jaedicke, C., Kern, M.A., Gauer, P., Baillifard, M.-A., Platzer, K., 2008. Chute experiments on slushflow dynamics. Cold Regions Science and Technology, International Snow Science Workshop (ISSW) 2006 51, 156–167. https://doi.org/10.1016/j.coldregions.2007.03.011

Juras, R., Würzer, S., Pavlásek, J., Vitvar, T., Jonas, T., 2017. Rainwater propagation through snowpack during rain-on-snow sprinkling experiments under different snow conditions. Hydrology and Earth System Sciences 21, 4973–4987. https://doi.org/10.5194/hess-21-4973-2017

Kattelmann, R., Berg, N., Pack, M., 1985. Estimating Regional Snow Water Equivalent with a Simple Simulation-Model. Water Resour. Bull. 21, 273–280.

Kattelmann, R., Dozier, J., 1999. Observations of snowpack ripening in the Sierra Nevada, California, U.S.A. Journal of Glaciology 45, 409–416. https://doi.org/10.3189/S002214300000126X

Kinar, N.J., Pomeroy, J.W., 2015. Measurement of the physical properties of the snowpack. Rev. Geophys. 53, 481–544. https://doi.org/10.1002/2015RG000481

Kuráž, M., Česká zemědělská univerzita v Praze, Katedra vodního hospodářství a environmentálního modelování, 2011. Numerical solution of the flow and transport equations in porous media with the dual permeability conceptual approach. VeRBuM, Zlín.

Kuraz, M., Mayer, P., Havlicek, V., Pech, P., 2013. Domain decomposition adaptivity for the Richards equation model. Computing 95, 501–519. https://doi.org/10.1007/s00607-012-0279-8

Kuráž, M., Mayer, P., Havlíček, V., Pech, P., Pavlásek, J., 2013. Dual permeability variably saturated flow and contaminant transport modeling of a nuclear waste repository with capillary barrier protection. Applied Mathematics and Computation 219, 7127–7138. https://doi.org/10.1016/j.amc.2011.08.109

Kuráž, M., Mayer, P., Holub, J., Bloecher, J.R., n.d. DRUtES © [WWW Document]. drutes.org. URL http://drutes.org/public/?core=account (accessed 3.8.19).

Liston, G.E., Elder, K., 2006. A distributed snow-evolution modeling system (SnowModel). J. Hydrometeorol. 7, 1259–1276. https://doi.org/10.1175/JHM548.1

Máca, P., 2015. Hydrologické modely a automatická optimalizace parametrů.

Mualem, Y., 1976. A new model for predicting the hydraulic conductivity of unsaturated porous media. Water Resources Research 12, 513–522. https://doi.org/10.1029/WR012i003p00513

Richards, L.A., 1931. Capillary conduction of liquids through porous mediums. Physics 1, 318–333. https://doi.org/10.1063/1.1745010

Schneebeli, M., 1995. Development and stability of preferential flow paths in a layered snowpack. Biogeochemistry of seasonality snow-covered catchments 8.

Shimizu, H., 1970. Air Permeability of Deposited Snow 33.

Singh, A.K., 2011. Snow Ripening, in: Singh, V.P., Singh, P., Haritashya, U.K. (Eds.), Encyclopedia of Snow, Ice and Glaciers. Springer Netherlands, Dordrecht, pp. 1064–1064. https://doi.org/10.1007/978-90-481-2642-2_676

Singh, P., Spitzbart, G., Hübl, H., Weinmeister, H.W., 1997b. Hydrological response of snowpack under rain-on-snow events: a field study. Journal of Hydrology 202, 1–20. https://doi.org/10.1016/S0022-1694(97)00004-8

Smart, C.C., Owens, I.F., Lawson, W., Morris, A.L., 2000. Exceptional ablation arising from rainfall- induced slushflows: Brewster Glacier, New Zealand. Hydrological Processes 14, 1045–1052. https://doi.org/10.1002/(SICI)1099-1085(20000430)14:6<1045::AID-HYP995>3.0.CO;2-9

Sturm, M., Taras, B., Liston, G.E., Derksen, C., Jonas, T., Lea, J., 2010. Estimating Snow Water Equivalent Using Snow Depth Data and Climate Classes. Journal of Hydrometeorology 11, 1380–1394. https://doi.org/10.1175/2010JHM1202.1

Tessin, A.-K., 2016. Biochar in soil: Effect on physical, chemical and hydrological properties in differently textured soils. [WWW Document]. URL https://docplayer.net/37841698-Biochar-in-soil-effect-on-physical-chemical-and-hydrological-properties-in-differently-textured-soils-master-thesis-ann-kathrin-tevin.html (accessed 4.15.19).

van Genuchten, M.Th., 1980. A Closed-form Equation for Predicting the Hydraulic Conductivity of Unsaturated Soils1. Soil Science Society of America Journal 44, 892. https://doi.org/10.2136/sssaj1980.03615995004400050002x

Waldner, P.A., Schneebeli, M., Schultze-Zimmermann, U., Flühler, H., 2004a. Effect of snow structure on water flow and solute transport. Hydrological Processes 18, 1271–1290. https://doi.org/10.1002/hyp.1401

Wever, N., Fierz, C., Mitterer, C., Hirashima, H., Lehning, M., 2014. Solving Richards Equation for snow improves snowpack meltwater runoff estimations in detailed multi-layer snowpack model. The Cryosphere 8, 257–274. https://doi.org/10.5194/tc-8-257-2014

Wever, N., Würzer, S., Fierz, C., Lehning, M., 2016. Simulating ice layer formation under the presence of preferential flow in layered snowpacks. The Cryosphere 14.

Würzer, S., Jonas, T., Wever, N., Lehning, M., 2016. Influence of Initial Snowpack Properties on Runoff Formation during Rain-on-Snow Events. J. Hydrometeor. 17, 1801–1815. https://doi.org/10.1175/JHM-D-15-0181.1

Yamaguchi, S., Katsushima, T., Sato, A., Kumakura, T., 2010. Water retention curve of snow with different grain sizes. Cold Regions Science and Technology 64, 87–93. https://doi.org/10.1016/j.coldregions.2010.05.008

Yamaguchi, S., Watanabe, K., Katsushima, T., Sato, A., Kumakura, T., 2012. Dependence of the water retention curve of snow on snow characteristics. Annals of Glaciology 53, 6–12. https://doi.org/10.3189/2012AoG61A001